Alma Mater Studiorum - Università di Bologna

DOTTORATO DI RICERCA IN

BENI CULTURALI E AMBIENTALI

Ciclo 34

Settore Concorsuale: 03/A1 - CHIMICA ANALITICA

Settore Scientifico Disciplinare: CHIM/12 - CHIMICA DELL'AMBIENTE E DEI BENI CULTURALI

DEVELOPMENT OF NEW IMMUNOCHEMICAL AND SPECTROSCOPIC ANALYTICAL METHODS FOR THE CHARACTERIZATION AND CONSERVATION OF WORKS OF ART

Presentata da: Lucrezia Gatti

Coordinatore Dottorato

Roberto Pasini

Supervisore

Rocco Mazzeo

Co-supervisore

Silvia Prati

Giorgia Sciutto

Esame finale anno 2022

Alla mia famiglia

Abstract

Cultural heritage is constituted by complex and heterogenous materials, such as paintings but also ancient remains, that contribute to reconstruct the past. However, all ancient materials are exposed to external environment and their interaction produces different changes due to chemical, physical and biological phenomena. The organic fraction, especially the proteinaceous one, has a crucial role in all these materials: in archaeology proteins reveal human habits, in artworks they disclose technics and help for a correct restoration. However, protein investigation is an issue due to its low amount, its interaction with the mineral fraction and the degradation phenomena. For these reasons the development of methods that allow the preservation of the sample as much as possible and a deeper knowledge of the deterioration processes is fundamental.

The research activities presented in this PhD thesis have been focused on the development of new immunochemical and spectroscopic approaches in order to detect and identify organic substances in artistic and archaeological samples. Organic components could be present in different cultural heritage materials as constituent element (*e.g.*, binders in paintings, collagen in bones) and their knowledge is fundamental for a complete understanding of past life, degradation processes and appropriate restauration approaches.

The combination of immunological approach with a chemiluminescence detection and Laser Ablation-Inductively Coupled Plasma-Mass Spectrometry allowed a sensitive and selective localization of collagen and elements in ancient bones and teeth. Near-infrared spectrometer and hyper spectral imaging have been applied in combination with chemometric data analysis as non-destructive methods for bones prescreening for the localization of collagen. Moreover, an investigation of amino acids in enamel has been proposed, in order to clarify teeth biomolecules survival overtime through the optimization and application of High-Performance Liquid Chromatography on modern and ancient enamel powder. New portable biosensors were developed for ovalbumin identification in paintings, thanks to the combination between biocompatible Gellan gel and electro-immunochemical sensors, to extract and identify painting binders with the contact only between gel and painting and between gel and electrodes.

Contents

List of figures

List of tables

List of abbreviations

FTIR Fourier transform infrared

XRF X-Ray fluorescence

ATR attenuated total reflection

AAs amino acids

NCPs non collagenous proteins

TC tropocollagen

HA hydroxyapatite

DEJ dentin-enamel junction

EOM enamel organic matrix

OES outer enamel surface

AAR amino acid racemization

XRD X-ray diffraction

SEM scanning electron microscopy

ZooMS Zooarchaeology by mass spectrometry

LC-MS/MS liquid chromatography–mass spectrometry coupled mass spectrometry

HPLC high-performance liquid chromatography

GC gas chromatography

MS mass spectrometry

CL chemiluminescence

HRP horseradish peroxidase

Ab antibody

Ag antigen

LA-ICP-MS Laser Ablation-Inductively Coupled Plasma-Mass Spectrometry

OVA ovalbumin

LOD limit of detection

NIR near infrared

PCA principal component analysis

HSI hyperspectral imaging

NDI Normalized Difference Images

LV latent variables

EAA essential amino acids

NEAA non-essential amino acids

SDEC standard deviation of the error of calibration

SDEP standard deviation of the error of prediction

ROI regions of interest

MSC multiplicative scatter correction

SPEs screen printed electrodes

SWV scan rate square wave voltammetry

RSD relative standard deviation

CHAPTER 1

INTRODUCTION

Science and cultural heritage have been strongly connected to each other and, in recent years, the Conservation Scientist professional figure has been officially recognized in Italy too. Nowadays, a multidisciplinary approach based on the collaboration between archaeologists, art historians, conservators and scientists, permits a deeper and more precise investigation and preservation of cultural heritage. In particular, chemical analyses allow the characterization of the artworks original and current composition and the understanding of their deterioration processes.

Cultural heritage consists in a complex group of different materials fundamental for human history reconstruction. Therefore, cultural heritage preservation not only concerns paintings and sculptures, but it also includes archaeological remnants, such as human and animal bones and teeth. Among organic substances, proteins have a crucial role in all these materials: in archaeology proteins reveal human habits, in artworks they disclose technics and help for a correct restoration.

However, all ancient materials are exposed to external environment and their interaction produces different changes in the artworks. Some parameters, such as humidity, temperature, light, pH, pollutants, microorganisms and human manipulation, are responsible for deterioration processes [1], [2]. For these reasons, the analytical investigation of materials could be fundamental not only for the identification of the components, but also for the understanding of the alteration due to chemical, physical and biological factors.

In painting, proteinaceous binders such as ovalbumin or collagen, are one of the main classes of organic components applied as binders and the preference for one of them was usually connected to the artistic technique, the environment or the period. The main interest of conservation scientists is the diagnosis of the composition and alteration state of the complex multilayered structure of paintings in order to preserve cultural heritage integrity. For this purpose, non-invasive methods are commonly used as pre-screening investigation of paintings surface without damaging, in order to select sampling area for further destructive techniques. These methods include for example portable Fourier Transform Infrared (FTIR) and Raman spectrometers, multispectral imaging, X-Ray Fluorescence (XRF) [1], [3]–[5]. However, destructive analysis, such as FTIR in

attenuated total reflection (ATR) and high-performance liquid chromatography (HPLC), have still been used, especially for binders and degradation products identification [1], [6]. In the last few years, immunochemical approaches were also developed for the identification of binders, thanks to the high specificity of the reaction antigen-antibody, which allows the identification of a target protein [7]–[9].

In archaeological field, the analysis of both mineral and organic fractions is an issue due to the diagenetic changes. Indeed, they could both be modified due to ground waters penetration during diagenesis. It is known that there is a mutual protection between mineral fraction and proteins, but the understanding of the correlation between elements variations and presence of collagen in the same specimen is still unclear. In addition to this, the majority of traditional investigations on mineral and organic components useful for dating, diet, environment and usages reconstruction, such as carbon dating, DNA identification or isotopes analysis, are destructive and require a large amount of samples [10]–[14]. However, proteins are unevenly distributed not only in different bones and teeth, but also in the same specimen according to the age and the environment. In order to select samples with enough proteins for further destructive analyses, new non-destructive methods for bones pre-screening for the localization of collagen are needed. Moreover, the exact composition and distribution of some proteins and their diagenetic processes are partially unknown, especially in teeth.

On one hand, the developing of non-invasive methods is a main goal in conservation science in order to preserve cultural heritage integrity, both for painting and archaeological remains investigation. On the other hand, the development of new imaging system, albeit invasive, is fundamental to overturn actual knowledge and to open the way to new information on human history.

Based on the previous considerations, the research activities here presented were focused on the development of immunochemical and spectroscopic methods for proteins detection and characterization in different materials: ancient remains (bones and teeth) and paintings.

Regarding proteinaceous binders, the research presents a new biosensor based on the combination between biocompatible Gellan gel and electro-immunochemical sensors in

order to extract and identify painting binders through the contact between gel and painting and between gel and electrodes. The developed method is portable, less invasive and faster than the others and it could be used *in situ* by restorers. Moreover, it ensures the security of the operators, artworks and environment.

Regarding bones and teeth, the combination between immunochemical chemiluminescence (CL) imaging and Laser Ablation-Inductively Coupled Plasma-Mass Spectrometry (LA-ICP-MS) has been presented as a new approach with the aim to characterize the diagenetic pathways in ancient bones and teeth, mapping both collagen and elements distribution and clarifying their correlation. Moreover, two non-destructive methods for bones pre-screening to localize collagen were developed. The first one is a portable non-invasive microNIR spectrometer with an acquisition range between 1100 nm and 2200 nm. The second one is based on the use of a Hyper Spectral camera working in the NIR spectral range, for the evaluation of the collagen distribution in bone samples. The developed methodologies present several advantages: they are fast and non-invasive, ensuring the extensive acquisition of data from a large number of precious samples. Moreover, no sample pre-treatment and reagents are required.

Due to the uncertain distribution of teeth proteins, teeth have also been studied in this PhD thesis. In detail, a CL protocol for amelogenin X detection and localization has been developed on teeth cross-sections and on powder, to demonstrate the encapsulation of amelogenin X in hydroxyapatite. This research helped to clarify the distribution of this protein in tooth tissues, contributing towards further investigation for sex determination. Moreover, an investigation of amino acids in teeth has been proposed, clarifying where and for how long the peptides and the amino acids (AA) could survive entrapped in the tooth enamel.

1.1. Organic substances in artworks and archaeological remnants

Paintings and archeological remains are complex heterogenous materials, consisting in a combination of inorganic and organic components. A complete knowledge of their composition is fundamental for a correct evaluation of their changes over time and for a subsequent adequate restoration and conservation.

Organic fraction can have different chemical composition with different properties and different degradation, not only between disparate objects of study but also within the same one, especially in archaeological specimens. The present thesis will be focused on protein materials, in detail collagen and amelogenin in ancient remains and ovalbumin in paintings.

Proteins are polymers composed by subunits, called amino acids (AAs). Amino acids show a common structure, based on a central carbon atom bound to a hydrogen atom, a carboxyl group ($-COO^-$), an amino group ($-NH_3^+$) and R group, which is peculiar for each amino acid. The carboxyl and the amino groups of amino acids react forming peptide bonds, that allow having a polymeric structure. After polypeptide formation, it has one end with a free amino group (N terminus) and the other one with a free carboxyl group (C terminus) [11].

Proteins present four structure levels. The primary structure is described as a linear sequence of amino acids, while the secondary one is referred to the conformations, mainly α-helix and β-sheet. The tertiary structure is the result of a three-dimensional configuration of secondary structure and it present different chemical forces, such as electrostatic interaction between R groups. Finally, the quaternary structure is an association of more polypeptides, creating a multi-subunit protein [11], [15].

Both in artworks and in ancient remains, protein investigation is an issue due to its low amount, to its interaction with the mineral fraction and to the degradation phenomena. For these reasons the development of methods that allow the preservation of the sample as much as possible and a deeper knowledge of the deterioration are fundamental.

1.1.1. Archaeological remnants

Archaeological remains are traces of ancient life, which have the potential to survive for centuries preserving information about the past. Fossil biominerals can reveal past diet, environmental and species evolution, human migrations, age. Both mineral and organic phases are fundamental for past reconstruction. Indeed, mineral phase contains information about some isotopes useful for diagenesis and it also protects organic phase from degradation. The organic fraction holds helpful information for dating (C^{14}), diet (N

and C) and evolution (DNA, proteins). In particular, proteins importance has been recently recognized with the developing of paleoproteomic, thanks to the better resistance of collagen as compared to DNA [11].

Bone structure

Bone is an heterogenous biomaterial composed by a mineral and an organic fraction.

The first one is made up of bioapatite and it is responsible for bones rigidity and durability. Bioapatite is carbonate-substituted hydroxyapatite, described as:

$Ca_{10}(PO_4)_{6-x}(OH)_{2-y}(CO_3^{2-})_{x+y}$

During life, carbonate (CO_3^{2-}) can substitute phosphate group (PO_4^{2-}) or hydroxyl group (OH^-) in mineral structure. These two different types of substitution produce two different types of bioapatite, defined as Type B (less common) and Type A (more common) respectively [16]–[18]. Carbonate substitutions reduce bioapatite crystallinity compared to hydroxyapatite, causing a high structural strain, surface area and solubility in water. Moreover, bioapatite presents water and different ions, such as calcium (Ca^{2+}), magnesium (Mg^{2+}) or potassium (K^+), according to different factors, for instance diet, ages and health [16], [17].

The second one, organic fraction, is composed for the 90% by collagen, mainly type I, and for the remainder by 'non collagenous proteins' (NCPs), among which osteocalcin, osteopontin, immunoglobulin, proteoglycans and matrix extracellular phosphoglycoprotein [11].

Collagen is composed of three left-handed helices of α-chains bound together to form a right-handed triple helix, known as tropocollagen (TC). It consists in a repeated sequence, where glycine is present every three AAs, followed by other two AAs Xaa-Yaa, typically proline and hydroxyproline. Intra and interchains disulphide bonds are formed when the α-chains are bended, forming the triple helix and creating the initial procollagen molecule. After secretion of procollagen from fibroblasts (development and fracture healing) or osteoblasts, the N- and C- propeptides are splitted by specific N- and C-protenases. Finally, collagen self-assembles into fibrils and a complex series of cross-links is formed

[18], [19]. The polypeptide chains (two α1 and one α2) are arranged as superhelix flanked by N- and C- terminal non triple-helical regions (Figure 1.1.) [15], [18]–[20]. Collagen creates cross-links with the adjacent molecules too. Collagen cross-links are the by-product of collagenic lysine and hydroxylysine ε-amino group conversion into aldehydes, which through a reaction with lysyl oxidase, bind the adjacent collagen molecules that are easily reducible. However, in mature bones these reducible cross-links decrease and make way for pyridinoline cross-links. Pyridinoline crosslinks are characterized by a stabilization process accomplished after the intermolecular bonds of younger collagen fibrils and cross-links become reduced. There are two types of pyridinoline cross-links, hydroxylysyl-pyridinoline and lysylpyridinoline, where the first one is found predominantly in internal connective tissue and the second one is typical of bone and dentin [2], [17], [20].

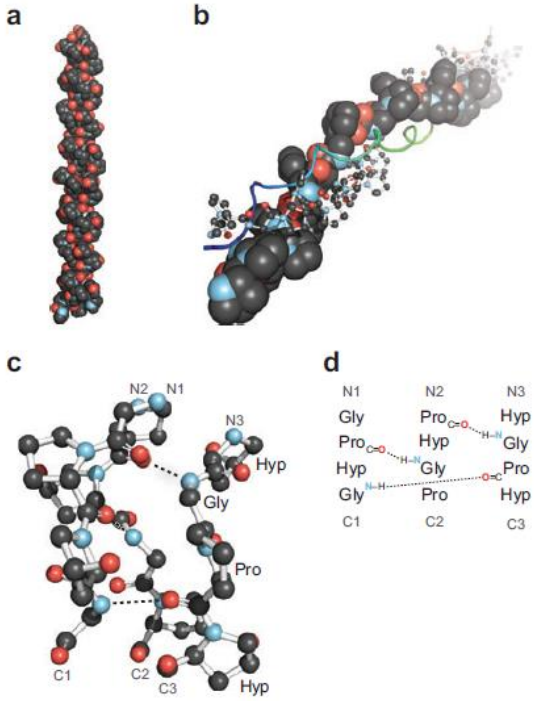

Figure 1.1. Collagen triple-helix structure formed by $(ProHypGly)_4$-(ProHypAla)-$(ProHypGly)_5$ [20].

Intermolecular bonds occur creating lacunae between collagen fibrils, these gaps represent primary sites of mineral deposition. Complete mineralization is achieved by

replacing water, within and among collagen, with small hydroxyapatite (HA) crystals. Therefore, as the volume of the mineral in bone increases, the volume of water decreases accordingly. Moreover, it has been known that the mechanical properties of the bone strongly depend on its state of hydration. Mineralized tissues swell and shrink with adsorption and desorption of water, mainly due to water entering the collagen fibril [2], [20].

Formation and maintenance of bones occur thanks to three types of cells: osteoblasts, osteocytes and osteoclasts. Osteoblasts are responsible for the production of the mineral structure and of osteoides, which are an uncalcified matrix rich in collagen, besides other non-collagenous proteins.

Osteoid tissue calcifies after a time of 10 days, when HA crystals are dropped into the matrix, and once this happens, 15% of the mature osteoblasts remain encapsuled in the mineralized matrix becoming osteocytes, with the function of maintaining bone tissue, while some cells remain on the bone surface becoming flat lining cells. Osteocytes, derived from the osteoblasts, produce matrix proteins which can subsequently calcify and they are located in bone lacunae. Finally, osteoclasts are responsible for the resorption of bone tissue; they are usually found in contact with a calcified bone surface and within a lacuna [15], [17], [21], [22].

Tooth structure

Teeth are a complex material, constituted through a long development process called odontogenesis. Teeth growth starts thanks to the interaction between oral epithelium and mesenchymal tissue, an embryonic tissue. Teeth principal components are three hard calcified tissues: dentin, enamel and cementum (Figure 1.2.).

The first one is produced by odontoblasts, which are the results of mesenchymal cells cytodifferentiation. Odontoblasts secrete pre-dentin under epithelial inner layer with a subsequent development of HA crystals. Dentin is composed by 70% of HA, 20% of organic fraction, mainly collagenous proteins, and 10% of water. Moreover, in the inner part of dentin, close to dental pulp, odontoblasts remain for life and they continue to produce dentin [2], [11], [23]–[27]. Dentin can be distinguished in three different types:

primary dentin, which is in contact with enamel; secondary dentin, which is closed to cementum and it is slowly produced during life; tertiary dentin, which can be secreted as a reaction to stressful events (*e.g.*, carious).

Pre-dentin deposition induces a cytodifferentiation of inner epithelial cell in ameloblast, responsible for enamel crystals production. Enamel is a highly mineralized tissue (ca. 95-99 % wt), mostly composed by HA, and it contains only a small portion of organic material. Enamel formation is called amelogenesis and it consists in three different phases: presecretory stage, with cytodifferentiation of ameloblasts; secretory stage, with enamel matrix formation; maturation stage, with mineralization of enamel [11], [23], [24], [26]–[28]. Unlike odontoblasts, ameloblasts disappear after enamel production, so that enamel cannot be secreted again during life. During enamel growth, a lot of proteins are secreted by ameloblasts and the most abundant is amelogenin group, which are proteins rich in proline and expressed by both X and Y chromosomes [29], [30].

Lastly, cementum is secreted by cementoblasts and consists in about 45–50% inorganic mineral (mainly apatite) and 50–55% organic matter (mainly collagen and glycoproteins) and water. Its thickness increases with the age and, thanks to its similarity to bone structure, it could be a good source for DNA extraction [2].

Dentin-enamel junction (DEJ) is the interface between the first two tissues, dentin and enamel, and it could represent the original position of ameloblasts and odontoblasts in first phases of odontogenesis. Along DEJ interface, a layer of residual enamel proteins constitutes enamel organic matrix (EOM), a post eruptive tissue [23].

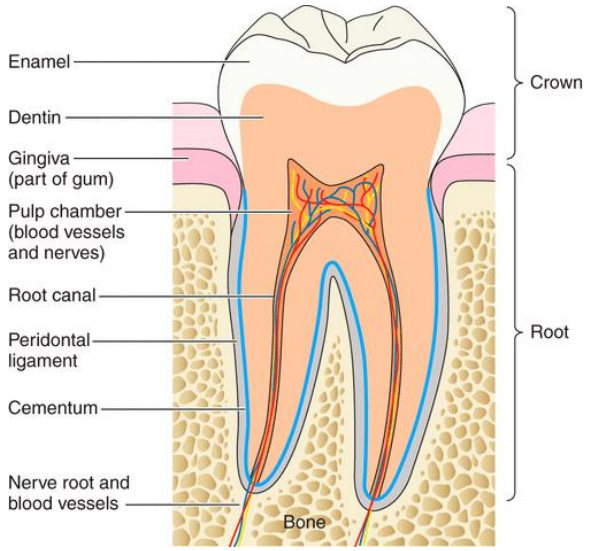

Figure 1.2. Structure of human tooth [28].

Bones and teeth diagenesis

Skeletal tissues preserve history of life, but they all undergo diagenesis processes, according to their composition [31]. After death, human remains are exposed to environment, that represents an "open system" in terms of chemical, physical and microbiological alteration. Material composition and burial environment (e.g. sediment pH, temperature, presence of water) both contribute to their alteration, with consequent microstructural changes and loss of achievable information [2], [32].

A deeper knowledge of post-mortem modification is fundamental in order to understand how humans and animals remains are altered. After death, environmental parameters can quickly change over time, resulting in a different type of diagenetic change [32]. Post-mortem damages can be induced by physical and biological factors; all these are strictly correlated, and they reinforce each other.

Physical agents, such as soil acidity, temperature, permeability and hydrology can dramatically affect the rate of skeletal deterioration [2], [32]. A soil with neutral or slightly alkaline pH, in a temperate area, is better for the skeletal integrity; otherwise, it would be dissolved in a short time [2]. Archaeological bones have a higher porosity than living ones, thus they adsorb more water through their pores. Fluctuating environments

are the most dangerous for bones preservation, producing cracks with a subsequent higher exposure to water penetration and microbial growth. Moreover, redistribution of elements can occur due to groundwater penetration within the sample [2], [32].

Biological agents are represented by both macroscopic and microscopic agents. The first group is composed by animals, able to produce punctures and scratches, and plants, able to create a reticulate network of grooves, cutting bones and secreting acids that lead to decalcification and whitening of the affected area [2]. The second group is composed by microorganisms, both fungi and bacteria, which attack physical and chemical stability. Indeed, bacteria and fungi penetrate in bone matrix producing a spongy porosity, especially due to fungal hyphae. Bacterial degradation occurs deeper inside the sample, leading to reprecipitation of dissolved mineral within the tunnels [2].

This combination of phenomena induces a chemical change in bones and teeth structure.

Collagen deterioration and loss are the result of the combination of three main reactions: hydrolysis of the peptides bonds, which causes a progressive break-up of collagen peptide bonds in the α- chain and requires one molecule of water for each peptide bond; racemization of the individual amino acids, that consists in the post-mortem interconversion from L enantiomers to D enantiomers of the same amino acids; decomposition of amino acids in simpler constituents [2], [11], [32], [33].

Collagen deterioration could also occur due to microorganisms, which are able to secrete collagen-degraded enzymes. Initially, they are only able to attack the collagen bone surface, thanks to the mineral protection. However, the presence of cracks increases the risk for collagen loss, because they allow exogenous material penetration with a consequent alteration of structure. Once the association between HA and collagen is disrupted, the bone tissues are inevitably more susceptible to diagenesis [2].

It is important to remind that mineral and organic fractions protect each other and the alteration of one of them after burial affects the other one. Collagen decomposition and loss exposes mineral fraction to water penetration, promoting dissolution and reprecipitation of phosphate within pores and elemental changes. Mineral disruption promotes the water penetration with higher risk for collagen hydrolysis and

decomposition [2], [34], [35]. Therefore, bones and teeth that present a limited diagenetic decay usually have a better conservation even of the organic fraction [2], [36], [37].

Due to its instability, biogenic apatite survival after burial depends on reorganization and growth through dissolution and recrystallization, increasing crystallinity and forming a new and more stable structure characterized by a decrease in carbonate fraction [2]. According to previous researches, mineral recrystallization occurs with pH under 6 or over 9, while in neutral conditions there is a higher stability of bioapatite [2], [38], [39]. Moreover, collagen loss exposes mineral fraction to water penetration, promoting dissolution and reprecipitation within pores. This phenomenon allows ionic exchange through the incorporation of reactive ions, such as HPO_4^{2-}, PO_4^{3-}, CO_3^{2-}, Ca^{2+}, Mg^{2+} [2], [40], [41]. Recrystallization can also produce reduction of microporosity combined with an increase of microporosity [2], [38]. However, porosity alteration can be caused by microbial tunnelling too; indeed, they can advance mineral dissolution and redistribution of phosphate, in order to get to the collagen [2], [40].

Teeth, compared to bone and soft tissues, are abundant in the archaeological and paleontological record, due to their resistance to the diagenesis processes. Despite their better endurance, teeth could undergo diagenetic changes. Their matrix can be modified by microbiological enzymes production, promoting secondary mineral precipitation. Moreover, a chemical alteration of biogenic apatite can occur with an increase of Fe, Mn, Si, Al and Ba [42].

Due to the possible largely organic fraction loss during diagenesis, the organic fraction of enamel and dentin received little attention by the paleoscience community until recently [43].

Detection of proteins in bones and teeth

Ancient bones are a fundamental material for archaeological reconstruction, because of the information obtainable from both mineral and organic fractions. There are five principal diagenetic parameters to evaluate: bone histology, crystallinity, porosity, carbonate and collagen content [36], [44]–[46].

These can be investigated through different approaches, for instance isotopes investigations, amino acid racemization (AAR), X-ray diffraction (XRD), scanning electron microscopy (SEM) coupled with energy dispersive X-ray diffraction [11], [47], [48], vibrational spectroscopy (FTIR and Raman) [33], [44], [49]–[53].

Several protocols have been developed to extract collagen from bones remains, to be submitted to more specific investigation such as radiocarbon dating, based on ^{14}C decay after death [54], [55], Zooarchaeology by Mass Spectrometry (ZooMS), able to provide more taxonomic information based on peptide fingerprint [56]–[58], or AAR, based on the ratio between D/L enantiomers [11], [59].

These sophisticated, destructive and expensive analyses conduct to a positive outcome only if the amount of collagen is enough. However, collagen preservation varies according to the site of provenance and also within the same contest or the same bone. For these reasons, there is the necessity to develop prescreening methods in order to preserve remains integrity as much as possible and to evaluate their possible collagen content.

In this context, FTIR is a powerful technique for the assessment of materials, evaluating collagen presence and crystallinity changes after diagenesis. Conservation state of remains has been evaluated both in diffuse reflection and in attenuated total reflection (ATR) with non-portable instruments. Even if the last one is highly sensitive, it has the disadvantage of requiring a laboratory and the contact between sample and the instrument [44], [50]. In recent years, portable FTIR in total reflection allows in situ analysis without a direct contact with the sample with a high perspective in archaeological field, but only few works used it until now [60].

Teeth are fundamental to carry out phylogenetic and diagenetic studies, yielding crucial information on evolution, sexual dimorphism, pathogens, diet, gestation and perinatal life, physiological stresses [32], [61]–[64]. In order to obtain these information, different techniques have been applied on ancient teeth, such as DNA, elemental and isotopic analyses, proteomics, radiocarbon dating, morphological and micro-textural investigation [32], [61], [62], [65], [66]. Because of the lower amount of the organic fraction, proteins of enamel and dentin received little attention by the paleoscience community until

recently [43]. Moreover, proteins and protein-residuals localization in enamel is still unclear. Some scholars analyzed teeth protein distribution using liquid chromatography–mass spectrometry coupled mass spectrometry (LC-MS/MS) showing that the amelogenin in enamel is presumably localized close to the DEJ and at the outer enamel surface [67], [68].

In odontology, immunochemical methods, such as immunofluorescence, gold-immuno cytochemistry and in situ hybridization, have been used to clarify amelogenin localization, but researchers disagree about it. Some of them have identified it only in ameloblast [69], [70], but other researchers have showed its presence in association with odontoblast and in dentin before mineralization, not only in first stages of teeth growth but also in injured teeth as a reaction to caries [24]–[26].

1.1.2. Painting binders

Easel paintings include all type of painting, except for mural painting. Movable paintings have a complex stratigraphy composed by [71] (Figure 1.3.):

1. Support: it could be constituted of wood, canvas, paper, metal panels, glass.
2. Preparation layer: it is composed by a binder and an inert fraction. The first one is usually animal glue, divided in hard glue (with impurities) and gelatin (pure collagen). The second one is mainly gypsum, but there are also preparations made with earth, lead white.
3. Painting layers: they are characterized by a mixture of pigments (organic or inorganic) and binders (glue, ovalbumin, casein, gums).
4. Varnish: it is not always present and it is a mixture of natural resins, mainly vegetal ones.

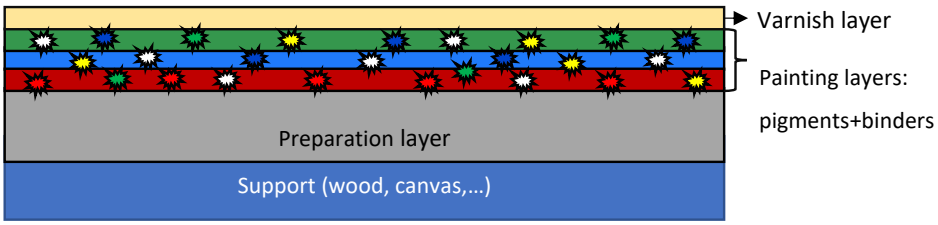

Figure 1.3. Schematic structure of painting.

Binders are proteins with different properties according to their amino acids sequences.

Glue is obtained from animal skin and cartilages and its chemical and physical properties depend on their origin and treatments. Glue solutions were usually prepared solubilizing glue in water by gradual heating. Its reversibility is the main advantage, allowing a redissolution in water, making it reusable. Three main degradation phenomena can occur: swelling and shrinkage due to humidity; chemical reactions with consequent loss of binding and mechanical properties; microbiological degradation [71], [72].

Egg is the second fundamental binder in artworks. It is an emulsion of a colloidal aqueous solution of proteins; egg white is mainly composed by proteins, especially ovalbumin, while egg yolk also presents a high content of fats and fatty substances. Unlike glue, egg is irreversible, thus it cannot be solubilized again in water [71], [72].

Casein is the main protein of milk and it is not naturally soluble in water. However, it was not very common due to its fast degradation process. In particular, it loses its mechanical properties, causing painting cracks and brittles [71], [72].

Gums are natural polysaccharides obtained from plants. They are composed by a simple sequence of sugar monomers and they are soluble in water. They were used for watercolors, inks and pastels [71], [72].

Identification of binders

Identification of binding media is fundamental for art history reconstruction and for appropriate restauration. However, it is challenging for researchers because of their tendency to undergo degradation processes over time [3], [73]–[75]. These chemical

changes depend on the protein structure and they are mainly due to oxidation reactions promoted especially by temperature and light [73], [74].

Spectroscopic techniques have been widely used, especially FTIR-ATR, thanks to its ability to give a complete investigation of both organic and inorganic fractions despite the necessity of sample, and non-invasive methods in reflection mode, such as portable FTIR [5], [76]. However, the spectroscopic signals due to protein presence could be covered by some mineral peaks (*e.g.* calcium carbonate) [72].

Proteomic approaches, as high-performance liquid chromatography (HPLC) and gas chromatography (GC) combined with mass spectrometry (MS), have been also commonly applied to distinguish among binders [77]. However, they have shown several problems in case of protein mixture and alterations. Thus, immunological techniques with different detection methods have been developed on cultural heritage, thanks to their highly specific and sensitive identification of the target protein. The most recent works have developed a chemiluminescence detection method able to identify not only which protein is present but also its localization in the stratigraphy [7], [9], [78].

The main issue in paintings investigation is the development of non-invasive methods, which allow a complete analysis of the artwork without damaging it and without the transport in a laboratory. For this reason, new non-destructive and portable methods have been recently developed in order to extract binders for further investigation (such as MS) without damaging the painting or to obtain a portable kit for a fast in situ analysis [79]–[81].

1.2. Aim of the thesis

The research activities here presented have been focused on the development of new immunochemical and spectroscopic approaches in order to detect and identify organic substances in artistic and archaeological samples. Organic components could be present in different cultural heritage materials as constituent element (*e.g.*, binders in paintings, collagen in bones) and their knowledge is fundamental for a complete understanding of past life, degradation processes and appropriate restauration approaches.

To overcome the limits of traditional methods and to fill the gap in present knowledge, the present work has the aim to propose new innovative approaches combining high sensitivity, ease of use and as little sampling as possible.

In Chapter 2 a combination between immunochemical chemiluminescence (CL) imaging and Laser Ablation-Inductively Coupled Plasma-Mass Spectrometry (LA-ICP-MS) has been presented as a new approach for the characterization of diagenetic pathways in ancient bones and teeth. Immunochemistry is widely applied in different fields, due to the high selectivity of antigen-antibody reaction. The protocol here presented was developed on ancient bone and tooth fragments, from different period and archaeological sites, thanks to the collaboration with the Bones Laboratory (University of Bologna, Ravenna Campus). It relies on the binding to the target protein (*i.e.*, collagen) of a specific anti-collagen primary antibody, which is then detected by a horseradish peroxidase (HRP)-labeled secondary antibody specie-specific and a HRP CL enzyme substrate. The light emission produced by the HRP-catalyzed reaction is detected using an optical microscope equipped with a cooled ultrasensitive CCD camera allowing easy collagen localization. The combination of CL data with LA-ICP-MS maps on the same samples has shown a high potential in bones diagenetic process clarification. Indeed, isotopes and rare earth elements content variation are considered as a reflection of the interaction between the matrices and the pore water of the surrounding environment [37], [82]–[85]. They are also considered as collagen preservation indices, due to the mutual relation between mineral fraction and biomolecules [36]. However, this theoretical correlation has never been proved before on so many samples and with a complete mapping of both collagen and elements. The results of the combination between CL method and LA-ICP-MS allow

a significant increment of the useful information achievable for the description of the degree of diagenetic alteration in bones and teeth. Moreover, a CL protocol for amelogenin X detection and localization has been developed on teeth cross-sections. The results contributed to clarify the distribution of this protein in tooth tissues. Due to the encapsulation of amelX in HA crystals, an approach on enamel powder has been proposed through the combination of an extraction protocol from enamel powder and a CL protocol on nitrocellulose membranes. Despite the loss of the spatial information, the method could be the starting point for a multiplex portable and fast system for sex determination that need only a low amount of sample.

In Chapter 3 a new portable microNIR prototype has been proposed as a prescreening method on bone, in order to select samples with enough collagen content for further investigations. Specific investigations such as radiocarbon dating, taxonomic determination and amino acid racemization (AAR), provide essential information, but they are time consuming, expensive and they require a lot of sample and an enough amount of protein for a positive result. For these reasons, in this chapter a non-invasive, fast, low cost and easy to use portable instrument has been presented with the aim to select samples according to their collagen content. The method is based on the acquisition of data through a microNIR spectrometer in region 1208–2160.5 nm. Spectra acquired were then elaborated through multivariate data processing in Matlab. To evaluate the method potential, it was firstly applied on standard samples prepared in laboratory with known percentage of collagen. Then it was applied on real bones samples from different period and provenance. In both cases, the Principal Component Analysis (PCA) allowed a good separation among samples according to the band attributed to collagen.

In Chapter 4 an innovative and highly efficient near-infrared hyperspectral imaging (NIR-HSI) method has been presented to provide spectral maps able to reveal collagen distribution in large-size bones, also offering semi-quantitative estimations. NIR-HSI allows a prescreening to select not only the best samples, but also sampling points for subsequent specific analysis. The method is based on Normalized Difference Image (NDI), which allows to create false color images. NDI approach was implemented for this study exploiting the NDI values extracted from each pixel of the HSI and comparing the computed median values among reference and unknown samples. The work was

conducted in collaboration with the Bones Lab (University of Bologna, Ravenna Campus) and the University of Genova.

In Chapter 5 an investigation of amino acids in teeth has been proposed, in order to clarify teeth biomolecules survival overtime. Teeth are less studied than bones, but they are particularly important for archaeologists and paleontologists, thanks to their better resistance than bones to diagenetic processes. The present chapter is focused on the development of an advanced analytical approach for the comprehensive characterization of organic remains in archaeological and fossil teeth, overturning the current knowledge about protein-residual preservation in deep-time fossil materials and opening the way to new information in paleontology and archaeology research field. In more detail, the research has been based on the optimization and application of High-Performance Liquid Chromatography (HPLC) for amino acid identification. The research was conducted at the Max Planck Institute for Chemistry (Mainz, Germany), thanks to the collaboration with the research group of Dr. Alfredo Martínez García.

Chapter 6 presents a new biosensor based on the combination between biocompatible Gellan gel and electro-immunochemical sensors in order to extract and identify painting binders through the contact between gel and painting and between gel and electrodes. Gellan gel was preferred thanks to its physical and chemical properties. An electro-immunoassay was chosen due to antigen-antibody high specific reaction and higher sensitive detection through electrochemical revelation than traditional immunochemical methods. The proposed biosensor is faster than traditional extractive methods and less invasive, because it is based on the migration of protein through the gel impacting electrodes. Moreover, protein digestion is not necessary, because an electro-immunochemical protocol has been developed blocking specific antibody on electrodes surface. Therefore, this new biosensor provides binder identification with a single analysis replicable on different artwork points and directly *in situ* without laboratories analysis. The analyses were performed firstly on paper in order to develop a standard protocol on a simpler substratum and then on mock-ups painting with different layers prepared in laboratory, in order to evaluate the gel ability to extract protein without painting damages. The present research was possible thanks to the collaboration with the University of Roma Tor Vergata (Prof.ssa Laura Micheli and Prof.ssa Claudia Mazzuca).

1.3. References

[1] S. Dallongeville, N. Garnier, C. Rolando, and C. Tokarski, “Proteins in Art , Archaeology , and Paleontology : From Detection to Identi fi cation,” 2016, doi: 10.1021/acs.chemrev.5b00037.

[2] C. Kendall *et al.*, “Diagenesis of archaeological bone and tooth,” *Palaeogeogr. Palaeoclimatol. Palaeoecol.*, vol. 491, no. November 2017, pp. 21–37, 2018, doi: 10.1016/j.palaeo.2017.11.041.

[3] L. Cartechini *et al.*, “Immunodetection of proteins in ancient paint media,” *Acc. Chem. Res.*, vol. 43, no. 6, pp. 867–876, 2010, doi: 10.1021/ar900279d.

[4] M. G. Giuffrida, R. Mazzoli, and E. Pessione, “Back to the past: deciphering cultural heritage secrets by protein identification,” pp. 5445–5455, 2018.

[5] E. Joseph, S. Prati, G. Sciutto, M. Ioele, P. Santopadre, and R. Mazzeo, “Performance evaluation of mapping and linear imaging FTIR microspectroscopy for the characterisation of paint cross sections,” *Anal. Bioanal. Chem.*, vol. 396, no. 2, pp. 899–910, 2010, doi: 10.1007/s00216-009-3269-8.

[6] R. Mazzeo, *Analytical chemistry for cultural heritage*. 2017.

[7] L. S. Dolci *et al.*, “Ultrasensitive chemiluminescent immunochemical identification and localization of protein components in painting cross-sections by microscope low-light imaging,” *Anal. Bioanal. Chem.*, vol. 392, no. 1–2, pp. 29–35, 2008, doi: 10.1007/s00216-008-2023-y.

[8] G. Sciutto, “Development of advanced analytical approaches for the characterization of organic substances in artistic and archaeological samples,” University of Bologna, 2011.

[9] G. Sciutto *et al.*, “Single and multiplexed immunoassays for the chemiluminescent imaging detection of animal glues in historical paint cross-sections,” *Anal. Bioanal. Chem.*, vol. 405, no. 2–3, pp. 933–940, 2013, doi: 10.1007/s00216-012-6463-z.

[10] G. Scorrano *et al.*, "Methodological strategies to assess the degree of bone preservation for ancient DNA studies," *Ann. Hum. Biol.*, vol. 42, no. 1, pp. 10–19, 2015, doi: 10.3109/03014460.2014.954614.

[11] B. Demarchi, *Amino Acids and Proteins in fossil Biominerals*. 2020.

[12] M. Vašinová Galiová *et al.*, "Elemental mapping in fossil tooth root section of Ursus arctos by laser ablation inductively coupled plasma mass spectrometry (LA-ICP-MS)," *Talanta*, vol. 105, pp. 235–243, 2013, doi: 10.1016/j.talanta.2012.12.037.

[13] R. Simpson and R. Simpson, "Historical overview and new directions in bioarchaeological trace element analysis : a review," 2021.

[14] C. Wadsworth *et al.*, "Comparing ancient DNA survival and proteome content in 69 archaeological cattle tooth and bone samples from multiple European sites," *J. Proteomics*, vol. 158, pp. 1–8, 2017, doi: 10.1016/j.jprot.2017.01.004.

[15] T. Brown and K. Brown, *Biomolecular Archaeology*. Wiley-Blackwell, 2011.

[16] N. J. De Winter, C. Snoeck, R. Schulting, T. Fernández-crespo, and P. Claeys, "High-resolution trace element distributions and models of trace element diffusion in enamel of Late Neolithic / Early Chalcolithic human molars from the Rioja Alavesa region (north-central Spain) help to separate biogenic from diagenetic trends," *Palaeogeogr. Palaeoclimatol. Palaeoecol.*, vol. 532, no. June, p. 109260, 2019, doi: 10.1016/j.palaeo.2019.109260.

[17] A. P. Mamede, D. Gonçalves, M. P. M. Marques, and L. A. E. Batista de Carvalho, "Burned bones tell their own stories: A review of methodological approaches to assess heat-induced diagenesis," *Appl. Spectrosc. Rev.*, vol. 53, no. 8, pp. 603–635, 2018, doi: 10.1080/05704928.2017.1400442.

[18] K. A. Hing, "Bone repair in the twenty-first century: Biology, chemistry or engineering?," *Philos. Trans. R. Soc. A Math. Phys. Eng. Sci.*, vol. 362, no. 1825, pp. 2821–2850, 2004, doi: 10.1098/rsta.2004.1466.

[19] J. Anné *et al.*, "Advances in bone preservation: Identifying possible collagen preservation using sulfur speciation mapping," *Palaeogeogr. Palaeoclimatol. Palaeoecol.*, vol. 520, no. May 2018, pp. 181–187, 2019, doi: 10.1016/j.palaeo.2019.01.030.

[20] M. D. Shoulders and R. T. Raines, "Collagen structure and stability," *Annu. Rev. Biochem.*, vol. 78, pp. 929–958, 2009, doi: 10.1146/annurev.biochem.77.032207.120833.

[21] S. Mays, *The archaeology in human bones*. London and New York, 1998.

[22] A. L. Boskey and R. Coleman, "Critical reviews in oral biology & medicine: Aging and bone," *J. Dent. Res.*, vol. 89, no. 12, pp. 1333–1348, 2010, doi: 10.1177/0022034510377791.

[23] M. Jágr, P. Ergang, S. Pataridis, M. Kolrosová, M. Bartoš, and I. Mikšík, "Proteomic analysis of dentin–enamel junction and adjacent protein-containing enamel matrix layer of healthy human molar teeth," *Eur. J. Oral Sci.*, vol. 127, no. 2, pp. 112–121, 2019, doi: 10.1111/eos.12594.

[24] P. Papagerakis, M. MacDougall, D. Hotton, I. Bailleul-Forestier, M. Oboeuf, and A. Berdal, "Expression of amelogenin in odontoblasts," *Bone*, vol. 32, no. 3, pp. 228–240, 2003, doi: 10.1016/S8756-3282(02)00978-X.

[25] A. L. J. J. Bronckers *et al.*, "Dentin sialoprotein: biosynthesis and developmental appearance in rat tooth germs in comparison with amelogenins, osteocalcin and colagen type-I," *Cell Tissue Res.*, vol. 272, no. 2, pp. 237–247, 1993, doi: 10.1007/BF00302729.

[26] T. A. Mitsiadis, A. Filatova, G. Papaccio, M. Goldberg, I. About, and P. Papagerakis, "Distribution of the amelogenin protein in developing, injured and carious human teeth," *Front. Physiol.*, vol. 5, no. Nov, 2014, doi: 10.3389/fphys.2014.00477.

[27] P. Papagerakis and T. Mitsiadis, "Development and structure of teeth and periodontal teeth," *Prim. Metab. Bone Dis. Disord. Miner. Metab.*, pp. 901–910,

2018, doi: 10.1002/9781119266594.ch117.

[28] R. S. Lacruz, S. Habelitz, J. T. Wright, and M. L. Paine, “Dental enamel formation and implications for oral health and disease,” *Physiol. Rev.*, vol. 97, no. 3, pp. 939–993, 2017, doi: 10.1152/physrev.00030.2016.

[29] G. A. Castiblanco, D. Rutishauser, L. L. Ilag, S. Martignon, J. E. Castellanos, and W. Mejía, “Identification of proteins from human permanent erupted enamel,” *Eur. J. Oral Sci.*, vol. 123, no. 6, pp. 390–395, 2015, doi: 10.1111/eos.12214.

[30] M. Zeichner-David, “Is there more to enamel matrix proteins than biomineralization?,” *Matrix Biol.*, vol. 20, no. 5–6, pp. 307–316, 2001, doi: 10.1016/S0945-053X(01)00155-X.

[31] T. Tütken, T. W. Vennemann, and H. U. Pfretzschner, “Early diagenesis of bone and tooth apatite in fluvial and marine settings: Constraints from combined oxygen isotope, nitrogen and REE analysis,” *Palaeogeogr. Palaeoclimatol. Palaeoecol.*, vol. 266, no. 3–4, pp. 254–268, 2008, doi: 10.1016/j.palaeo.2008.03.037.

[32] R. E. M. Hedges, “Bone diagenesis : an overview of processes,” vol. 3, pp. 319–328, 2002.

[33] G. Dal Sasso, M. Lebon, I. Angelini, L. Maritan, D. Usai, and G. Artioli, “Bone diagenesis variability among multiple burial phases at Al Khiday (Sudan) investigated by ATR-FTIR spectroscopy,” *Palaeogeogr. Palaeoclimatol. Palaeoecol.*, vol. 463, pp. 168–179, 2016, doi: 10.1016/j.palaeo.2016.10.005.

[34] M. H. Schweitzer, R. Avci, T. Collier, and M. B. Goodwin, “Microscopic, chemical and molecular methods for examining fossil preservation,” *Comptes Rendus - Palevol*, vol. 7, no. 2–3, pp. 159–184, 2008, doi: 10.1016/j.crpv.2008.02.005.

[35] C. N. Trueman *et al.*, “Comparing rates of recrystallisation and the potential for preservation of biomolecules from the distribution of trace elements in fossil bones,” *Comptes Rendus Palevol*, vol. 7, no. 2–3, pp. 145–158, 2008, doi: 10.1016/j.crpv.2008.02.006.

[36] C. N. Trueman, K. Privat, and J. Field, “Why do crystallinity values fail to predict the extent of diagenetic alteration of bone mineral?,” *Palaeogeogr. Palaeoclimatol. Palaeoecol.*, vol. 266, no. 3–4, pp. 160–167, 2008, doi: 10.1016/j.palaeo.2008.03.038.

[37] P. V. Ullmann *et al.*, “Molecular tests support the viability of rare earth elements as proxies for fossil biomolecule preservation,” *Sci. Rep.*, vol. 10, no. 1, pp. 1–11, 2020, doi: 10.1038/s41598-020-72648-6.

[38] F. Berna, A. Matthews, and S. Weiner, “Solubilities of bone mineral from archaeological sites: The recrystallization window,” *J. Archaeol. Sci.*, vol. 31, no. 7, pp. 867–882, 2004, doi: 10.1016/j.jas.2003.12.003.

[39] S. W. Keenan and A. S. Engel, “Early diagenesis and recrystallization of bone,” *Geochim. Cosmochim. Acta*, vol. 196, pp. 209–223, 2017, doi: 10.1016/j.gca.2016.09.033.

[40] C. N. G. Trueman, A. K. Behrensmeyer, N. Tuross, and S. Weiner, “Mineralogical and compositional changes in bones exposed on soil surfaces in Amboseli National Park, Kenya: Diagenetic mechanisms and the role of sediment pore fluids,” *J. Archaeol. Sci.*, vol. 31, no. 6, pp. 721–739, 2004, doi: 10.1016/j.jas.2003.11.003.

[41] C. I. Smith, C. M. Nielsen-Marsh, M. M. E. Jans, and M. J. Collins, “Bone diagenesis in the European Holocene I: patterns and mechanisms,” *J. Archaeol. Sci.*, vol. 34, no. 9, pp. 1485–1493, 2007, doi: 10.1016/j.jas.2006.11.006.

[42] F. Lugli *et al.*, “Enamel peptides reveal the sex of the Late Antique ‘Lovers of Modena,’” *Sci. Rep.*, vol. 9, no. 1, pp. 1–8, 2019, doi: 10.1038/s41598-019-49562-7.

[43] E. Cappellini *et al.*, “Early Pleistocene enamel proteome sequences from Dmanisi resolve Stephanorhinus phylogeny performed analyses and data interpretation,” *Bienvenido Martínez-Navarro*, vol. 574, no. 7776, pp. 103–107, 2020, doi: 10.6084/m9.figshare.7212746.

[44] S. H. Bayarı, K. Özdemir, E. H. Sen, C. Araujo-Andrade, and Y. S. Erdal,

"Application of ATR-FTIR spectroscopy and chemometrics for the discrimination of human bone remains from different archaeological sites in Turkey," *Spectrochim. Acta - Part A Mol. Biomol. Spectrosc.*, vol. 237, 2020, doi: 10.1016/j.saa.2020.118311.

[45] A. Grunenwald, C. Keyser, A. M. Sautereau, E. Crubézy, B. Ludes, and C. Drouet, "Novel contribution on the diagenetic physicochemical features of bone and teeth minerals, as substrates for ancient DNA typing," *Anal. Bioanal. Chem.*, vol. 406, no. 19, pp. 4691–4704, 2014, doi: 10.1007/s00216-014-7863-z.

[46] G. J. van Klinken and R. E. M. Hedges, "Experiments on collagen-humic interactions: speed of humic uptake, and effects of diverse chemical treatments," *J. Archaeol. Sci.*, vol. 22, no. 2, pp. 263–270, 1995, doi: 10.1006/jasc.1995.0028.

[47] O. López-Costas, Ó. Lantes-Suárez, and A. Martínez Cortizas, "Chemical compositional changes in archaeological human bones due to diagenesis: Type of bone vs soil environment," *J. Archaeol. Sci.*, vol. 67, pp. 43–51, 2016, doi: 10.1016/j.jas.2016.02.001.

[48] L. E. Munro, F. J. Longstaffe, and C. D. White, "Burning and boiling of modern deer bone: Effects on crystallinity and oxygen isotope composition of bioapatite phosphate," *Palaeogeogr. Palaeoclimatol. Palaeoecol.*, vol. 249, no. 1–2, pp. 90–102, 2007, doi: 10.1016/j.palaeo.2007.01.011.

[49] D. Baykal, O. Irrechukwu, P. C. Lin, K. Fritton, R. G. Spencer, and N. Pleshko, "Nondestructive assessment of engineered cartilage constructs using near-infrared spectroscopy," *Appl. Spectrosc.*, vol. 64, no. 10, pp. 1160–1166, 2010, doi: 10.1366/000370210792973604.

[50] M. G. Bridelli, C. Stani, and R. Bedotti, "Fourier transform infrared conformational investigation of type I collagen aged by in vitro induced dehydration and non-enzymatic glycation treatments," *J. Biol. Res. - Boll. della Soc. Ital. di Biol. Sper.*, vol. 90, no. 1, 2017, doi: 10.4081/jbr.2017.6254.

[51] C. Chadefaux, A. Le Hô, L. Bellot-Gurlet, and I. Reiche, "Curve-fitting micro-atr-

ftir studies of the amide I and II bands of type i collagen in archaeological bone material," *e-PRESERVATIONScience*, vol. 6, pp. 129–137, 2009.

[52] H. Kimura-Suda and T. Ito, "Bone quality characteristics obtained by Fourier transform infrared and Raman spectroscopic imaging," *J. Oral Biosci.*, vol. 59, no. 3, pp. 142–145, 2017, doi: 10.1016/j.job.2017.04.002.

[53] I. Kontopoulos, S. Presslee, K. Penkman, and M. J. Collins, "Preparation of bone powder for FTIR-ATR analysis: The particle size effect," *Vib. Spectrosc.*, vol. 99, no. September, pp. 167–177, 2018, doi: 10.1016/j.vibspec.2018.09.004.

[54] C. Wadsworth and M. Buckley, "Characterization of proteomes extracted through collagen-based stable isotope and radiocarbon dating methods," 2018, doi: 10.1021/acs.jproteome.7b00624.

[55] A. Zazzo, J. S. Matthieu, L. Sébastien, and C. Moreau, "Radiocarbon dating of calcined bones: insights from combustion experiments under natural conditions," vol. 54, no. 3, 2012.

[56] F. Welker, M. Soressi, W. Rendu, J. Hublin, and M. Collins, "Using ZooMS to identify fragmentary bone from the Late Middle / Early Upper Palaeolithic sequence of Les Cottés, France," *J. Archaeol. Sci.*, vol. 54, pp. 279–286, 2015, doi: 10.1016/j.jas.2014.12.010.

[57] K. Mcgrath *et al.*, "Identifying archaeological bone via non-destructive ZooMS and the materiality of symbolic expression : Examples from iroquoian bone points," *Sci. Rep.*, no. January, pp. 1–10, 2019, doi: 10.1038/s41598-019-47299-x.

[58] M. Collins, M. Buckley, H. H. Grundy, and J. Thomas-oates, "ZooMS : the collagen barcode and fingerprints," *Spectrosc. Eur.*, vol. 22, no. 2, 2010.

[59] M. R. Dickinson, A. M. Lister, and K. E. H. Penkman, "A new method for enamel amino acid racemization dating: A closed system approach," *Quat. Geochronol.*, vol. 50, pp. 29–46, 2019, doi: 10.1016/j.quageo.2018.11.005.

[60] L. Legan, T. Leskovar, M. Črešnar, F. Cavalli, D. Innocenti, and P. Ropret, "Non-

invasive reflection FTIR characterization of archaeological burnt bones: Reference database and case studies," *J. Cult. Herit.*, vol. 41, pp. 13–26, 2020, doi: 10.1016/j.culher.2019.07.006.

[61] C. Froment *et al.*, "Analysis of 5000 year-old human teeth using optimized large-scale and targeted proteomics approaches for detection of sex-specific peptides," *J. Proteomics*, 2020, doi: 10.1016/j.jprot.2019.103548.

[62] A. Gismondi *et al.*, "A multidisciplinary approach for investigating dietary and medicinal habits of the Medieval population of Santa Severa (7th-15th centuries, Rome, Italy)," *PLoS One*, vol. 15, no. 1, pp. 1–30, 2020, doi: 10.1371/journal.pone.0227433.

[63] J. A. Lueders-Dumont, X. T. Wang, O. P. Jensen, D. M. Sigman, and B. B. Ward, "Nitrogen isotopic analysis of carbonate-bound organic matter in modern and fossil fish otoliths," *Geochim. Cosmochim. Acta*, vol. 224, pp. 200–222, 2018, doi: 10.1016/j.gca.2018.01.001.

[64] M. Buckley, M. Collins, J. Thomas-Oates, and J. C. Wilson, "Species identification by analysis of bone collagen using matrix-assisted laser desorption/ionisation time-of-flight mass spectrometry," *Rapid Commun. Mass Spectrom.*, vol. 23, pp. 3843–3854, 2009, doi: 10.1002/rcm.4316.

[65] P. Dąbrowski *et al.*, "Assessing weaning stress – Relations between enamel hypoplasia, δ18O and δ13C values in human teeth obtained from early modern cemeteries in Wroclaw, Poland," *Ann. Anat.*, vol. 232, 2020, doi: 10.1016/j.aanat.2020.151546.

[66] K. Jaouen *et al.*, "Zinc isotope variations in archeological human teeth (Lapa do Santo, Brazil) reveal dietary transitions in childhood and no contamination from gloves," *PLoS One*, vol. 15, no. 5, pp. 1–23, 2020, doi: 10.1371/journal.pone.0232379.

[67] M. Jágr, A. Eckhardt, S. Pataridis, and I. Mikšík, "Comprehensive proteomic analysis of human dentin," *Eur. J. Oral Sci.*, vol. 120, no. 4, pp. 259–268, 2012,

doi: 10.1111/j.1600-0722.2012.00977.x.

[68] D. R. Green, F. Schulte, K. H. Lee, M. K. Pugach, M. Hardt, and F. B. Bidlack, "Mapping the tooth enamel proteome and amelogenin phosphorylation onto mineralizing porcine tooth crowns," *Front. Physiol.*, vol. 10, no. JUL, pp. 1–16, 2019, doi: 10.3389/fphys.2019.00925.

[69] A. Nanci *et al.*, "Comparative immunochemical analyses of the developmental expression and distribution of ameloblastin and amelogenin in rat incisors," *J. Histochem. Cytochem.*, vol. 46, no. 8, pp. 911–934, 1998, doi: 10.1177/002215549804600806.

[70] M. Nakamura, P. Bringas, A. Nanci, M. Zeichner-David, B. Ashdown, and H. C. Slavkin, "Translocation of enamel proteins from inner enamel epithelia to odontoblasts during mouse tooth development," *Anat. Rec.*, vol. 238, no. 3, pp. 383–396, 1994, doi: 10.1002/ar.1092380313.

[71] M. Matteini, R. Mazzeo, and A. Moles, *Chemistry for restoration: painting and restoration material*.2016.

[72] J. Arslanoglu, J. Schultz, J. Loike, and K. Peterson, "Immunology and art: Using antibody-based techniques to identify proteins and gums in artworks," *J. Biosci.*, vol. 35, no. 1, pp. 3–10, 2010, doi: 10.1007/s12038-010-0001-y.

[73] M. González-Cabrera, A. Domínguez-Vidal, and M. J. Ayora-Cañada, "Monitoring UV-accelerated alteration processes of paintings by means of hyperspectral micro-FTIR imaging and chemometrics," *Spectrochim. Acta - Part A Mol. Biomol. Spectrosc.*, vol. 253, 2021, doi: 10.1016/j.saa.2021.119568.

[74] Y. M. Issa, G. Abdel-Maksoud, M. Ibrahim, and M. Magdy, "A combination of analytical methods to evaluate the effect of humidity aging on the painting materials of icon models," *Vib. Spectrosc.*, vol. 107, no. September 2019, p. 103010, 2020, doi: 10.1016/j.vibspec.2019.103010.

[75] M. P. Colombini, F. Modugno, R. Fuoco, and A. Tognazzi, "A GC-MS study on the deterioration of lipidic paint binders," *Microchem. J.*, vol. 73, no. 1–2, pp. 175–

185, 2002, doi: 10.1016/S0026-265X(02)00062-0.

[76] D. Mancini, A. Percot, L. Bellot-Gurlet, P. Colomban, and P. Carnazza, "On-site contactless surface analysis of modern paintings from Galleria Nazionale (Rome) by reflectance FTIR and Raman spectroscopies," *Talanta*, vol. 227, no. January, p. 122159, 2021, doi: 10.1016/j.talanta.2021.122159.

[77] W. Fremout, J. Sanyova, S. Saverwyns, P. Vandenabeele, and L. Moens, "Identification of protein binders in works of art by high-performance liquid chromatography-diode array detector analysis of their tryptic digests," *Anal. Bioanal. Chem.*, vol. 393, no. 8, pp. 1991–1999, 2009, doi: 10.1007/s00216-009-2686-z.

[78] G. Sciutto *et al.*, "Development of a multiplexed chemiluminescent immunochemical imaging technique for the simultaneous localization of different proteins in painting micro cross-sections," *Anal. Bioanal. Chem.*, vol. 399, no. 9, pp. 2889–2897, 2011, doi: 10.1007/s00216-010-4258-7.

[79] M. Zangheri *et al.*, "A portable device for on site detection of chicken ovalbumin in artworks by chemiluminescent immunochemical contact imaging," *Microchem. J.*, vol. 124, pp. 247–255, 2016, doi: 10.1016/j.microc.2015.08.026.

[80] M. Manfredi *et al.*, "Method for Noninvasive Analysis of Proteins and Small Molecules from Ancient Objects," *Anal. Chem.*, vol. 89, no. 6, pp. 3310–3317, 2017, doi: 10.1021/acs.analchem.6b03722.

[81] P. Cicatiello, G. Ntasi, M. Rossi, G. Marino, P. Giardina, and L. Birolo, "Minimally Invasive and Portable Method for the Identification of Proteins in Ancient Paintings," *Anal. Chem.*, vol. 90, no. 17, pp. 10128–10133, 2018, doi: 10.1021/acs.analchem.8b01718.

[82] C. Argentino, F. Lugli, A. Cipriani, S. Conti, and D. Fontana, "A deep fluid source of radiogenic Sr and highly dynamic seepage conditions recorded in Miocene seep carbonates of the northern Apennines (Italy)," *Chem. Geol.*, vol. 522, no. May, pp. 135–147, 2019, doi: 10.1016/j.chemgeo.2019.05.029.

[83] D. N. Grimstead, A. E. Clark, and A. Rezac, “Uranium and vanadium concentrations as a trace element method for identifying diagenetically altered bone in the inorganic phase,” *J. Archaeol. Method Theory*, vol. 25, no. 3, pp. 689–704, 2018, doi: 10.1007/s10816-017-9353-z.

[84] D. Herwartz, T. Tütken, K. P. Jochum, and P. M. Sander, “Rare earth element systematics of fossil bone revealed by LA-ICPMS analysis,” *Geochim. Cosmochim. Acta*, vol. 103, pp. 161–183, 2013, doi: 10.1016/j.gca.2012.10.038.

[85] C. N. Trueman, L. Kocsis, M. R. Palmer, and C. Dewdney, “Fractionation of rare earth elements within bone mineral: A natural cation exchange system,” *Palaeogeogr. Palaeoclimatol. Palaeoecol.*, vol. 310, no. 1–2, pp. 124–132, 2011, doi: 10.1016/j.palaeo.2011.01.002.

CHAPTER 2

CHEMILUMINESCENCE IMMUNOASSAY FOR PROTEINS DETECTION IN ANCIENT REMAINS

Part of the chapter is reproduced from: "Combining elemental and immunochemical analyses to characterize diagenetic alteration patterns in ancient skeletal remains"

L. Gatti, F. Lugli, G. Sciutto, M. Zangheri, S. Prati, M. Mirasoli, S. Silvestrini, S. Benazzi, T. Tütken, K. Douka, C. Collina, F. Boschin, M. Romandini, P. Iacumin, M. Guardigli, A. Roda, R. Mazzeo

Scientific Reports, 2022

2.1. Chemiluminescence

Luminescence can be defined as the radiation emitted by a molecule or an atom, due to its return to the ground state from the excited one, and it can be classified based on the excitation source [1].

Chemiluminescence consists in a light-emitting reaction, namely a reaction which occurs in presence of a strongly oxidant specie and compounds. In these reactions electron-excited molecules are produces and, when they returned to the ground state, they emit a photon [1]–[5].

CL reaction can be divided in direct and indirect reactions. The first one produces an excited-state molecule, responsible for light emission. In the second one the excited product is not able to be directly involved in the reaction and it transfers its energy to a highly fluorescent energy acceptor, which then emits increasing signal [1].

A chemical reaction should satisfy some requirements to produce light [4]:

1. In order to occupy an excited state, the reaction has to be adequately exothermic. The free energy requirement can be calculated with this equation:

$$-\Delta G \geq \frac{hc}{\lambda_{ex}} = \frac{28600}{\lambda_{ex}} \qquad (1.1)$$

   Therefore, photons are produced in the visible range (400-750nm) requiring approximately 40-70 kcal mol^{-1}.
2. This electronically excited state has to be accessible on the reaction coordinate.
3. The emission of photons from the excited state has to be a favorable energy emission process. For this reason, the reaction product has to be a fluorescent molecule.

The CL quantum yield, defined as the number of photons emitted for reacting molecule, can be expressed as:

$$\Phi_{CL} = \Phi_R \times \Phi_{ES} \times \Phi_F \qquad (1.2)$$

where Φ_R reflects the chemical yield of the reaction, Φ_{ES} is the fraction of the product due to entering in an excited state and Φ_F is the fluorescent quantum yield [4], [6].

Employing simple reagents, CL reaction has a flash-type kinetics, which means a few seconds emission. Therefore, some enzymes can be used in presence of an excess of a proper CL enzyme substrate to obtain a more intense and longer CL signal. Moreover, suitable enhancers can be added to the substrate to have a prolonged emission of some minutes, improving the detection and the reproducibility [1], [6], [7].

Luminol derivates are the best-known available substrates. The final product of the luminol oxidation reaction is a 3-aminophtalate ion in the excited state that decays by emitting photons at a wavelength of about 425 nm. The reaction occurs in alkaline environment in presence of an oxidizing agent as H_2O_2 [2], [6], [8]. The luminol enhanced reaction is very slow, thus it can be catalyzed by various enzymes as horseradish peroxidase (HRP), one of the most used enzymes to promote the CL reaction (Figure 2.1) [2], [9]. The use of an enzyme amplify the signal with a consequent detectability improvement [2], [9]. The kinetic of the reaction is quite fast, thus some enhancers, such as substituted phenols, naphthols, phenylboronic acids, and phenothiazine derivatives, can be used to stabilize and increase the intensity of the CL signal [2], [6], [8].

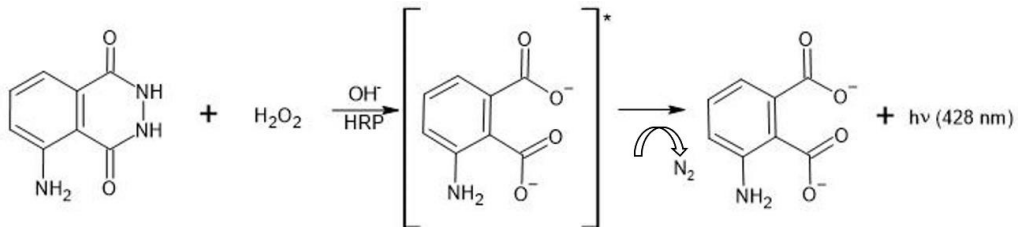

Figure 2.1. HRP-catalyzed luminol oxidation.

2.2. Chemiluminescent immunochemical system

Immunochemical methods are based on the specific binding between antibody (Ab) and antigen (Ag). Antibodies are glycoproteins obtained by the immune system in response to a specific antigen in organisms [5], [7]. They are structurally designed as y-molecules, which present two identical and constant polypeptides, called heavy chains, and other two

variable polypeptides, called light chains. They can be divided in 5 groups according to their different structures and functions: IgM, IgA, IgE, IgD and IgG, the most abundant one. The latter presents two variable regions in the y "arms", at the end of which there is the antigen binding site called paratope, and a constant region specific for the specie in which it has been isolated (Figure 2.2.). The antigen epitope is the portion where Ag interacts with the paratope [7].

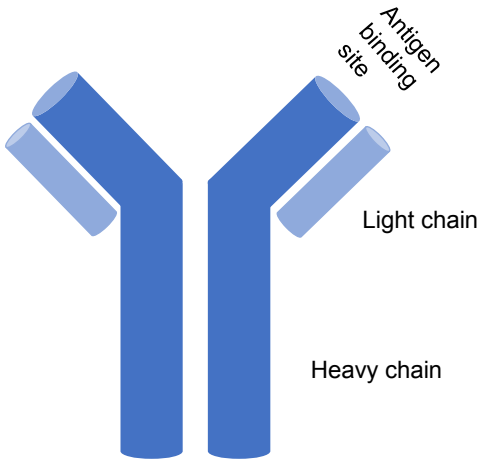

Figure 2.2. Antibody structure.

The two parameters used to characterize Ab-Ag reaction are affinity and avidity. The first one defines the strength of the binding as Ab and Ag concentration at the equilibrium. On the contrary, the second one represents the overall stability of the complex, defining all factors involved in the reaction [5], [7].

Monoclonal and polyclonal antibody can be produced and used for immunoassays. Monoclonal antibodies contain a single immunoglobulin allowing highly specific interaction with the antigen, because they recognize only one epitope. However, their disadvantage is the lower possibility of interaction. In order to increase possibility of interaction between Ag and Ab, polyclonal antibodies are employed due to their ability to recognize different antigenic sites [7].

In order to detect Ab-Ag binding, there are two possible methods for antibodies labeling with a suitable marker: direct and indirect. In the direct method, there is only one antibody, which is directly conjugated with the enzyme. In the indirect one, there is a

primary antibody, which is not conjugated to the enzyme and specific for the target protein. After this first reaction, a secondary antibody, labeled with the enzyme, is added to recognize the primary antibody according to animal source (Figure 2.3.) [7], [10].

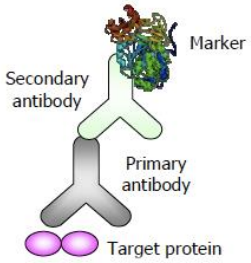

Figure 2.3. Schematic representation of indirect method [11].

In chemiluminescence immunoassay the marker is an enzyme detectable by the appropriate CL substrate, HRP is one of the most commonly used.

CL imaging methods allow the localization of antigens in the sample surface at microscopic levels. They have been developed thanks to the combination of optical microscopes and high-resolution cameras, such as cooled charged-coupled device (CCD) cameras [4], [9].

Luminographs, used for the acquisition of images, employ ultrasensitive CCD cameras and optical systems enclosed in a light-tight box to prevent interference from ambient light. To reduce the background signal, mainly ascribable to the thermal noise, the detectors are cooled to low temperatures by means of thermoelectric or cryogenic systems. This allows for accumulation of the CL signal over long times and therefore increases the sensitivity. When connected to an optical microscope, imaging devices permit measurement and localization of the emission on the sample with a resolution of the order of micrometers. Due to the low light intensity characteristic of the CL emissions, it is necessary to minimize the loss of signal in the optical system. Thus, suitable lens systems and objectives with high numerical aperture should be used to increase the efficiency of collection of the CL signal. The obtained CL gray scale images allow the localization of protein according to the intensity and location of lighter areas [4], [12].

2.3. Chemiluminescent immunochemical detection of proteins

Immunochemical methods exploit the high specificity of the antigen–antibody recognition reaction, which allows to distinguish between different proteins and to determine the biological source of a given protein. Immunochemical techniques are widely used in biomedical field for identification of specific proteins. In last decades, cultural heritage researchers have shown a growing interest for enzyme-linked immunosorbent assay (ELISA), testing it especially on paintings in order to identify binders clarifying pictorial technique and simplifying restauration choices. This growing interest allow the development of both portable instruments for *in situ* determination of binders and immunochemical imaging methods for proteins localization in cross-sections [13]–[19]. The detection could be done through different methods, such as immunofluorescence which is the most used detection method in conservation science. However, it presents some problems due to the sample autofluorescence and light scattering on the sample surface. In order to overcome these problems, chemiluminescence (CL) detection approach has been developed. It is preferred because it ensures higher sensitivity in comparison to colorimetric and fluorescence detection, also providing good spatial resolution and low background signal, due to the absence of autofluorescence [20]–[22]. Moreover, it requires a reduced instrumentation and sample preparation allowing different analytical methods. The only disadvantage could be the signal inhibition by sample matrix [2].

A lower interest has been shown for the application of these methods on archaeological remains, probably due to the high deterioration of ancient proteins. Only few applications on archaeological samples have been reported, employing for instance ELISA for ovalbumin and casein detection and for diseases identification [10], [23], [24] or *in situ* immunofluorescence for collagen evaluation [25], [26].

In order to develop a highly sensitive and quite fast detection and localization of proteins in ancient bones and teeth a CL-immunochemical protocol has been developed during this PhD thesis in order to localize collagen in bone and tooth fragments. Moreover, due to the higher resistance of enamel, a protocol for amelogenin X detection has been

developed and it is the starting point for further perspectives in teeth proteins investigation.

2.4. Combining elemental and immunochemical analyses to characterize diagenetic alteration patterns in ancient skeletal remains

Bones and teeth are complex biomineralized tissues composed by a mineral fraction, mainly carbonate-substituted bioapatite, and an organic fraction, mainly collagen type I protein in bones and dentin [27]–[34].

After burial, bone structure and composition are subjected to diagenesis, which is the alteration induced by physical, biological, and chemical degradation [35]–[39]. Similarly, tooth dentin can be subjected to post-burial biological and chemical degradation [35], [40]–[43]. Despite the lower resistance of bone and dentin to diagenesis than the highly mineralized enamel, their analysis provides chemical and isotopic information on diet and provenance. Moreover, they also contain DNA and proteins, from which information on gender, taxonomy and evolution. can be obtained for past reconstructions of human and faunal life histories. Yet, the preservation of the organic fraction is pivotal to obtain such information by archeometric investigations.

During diagenesis, the mineral fraction may be affected by the penetration of ground waters into the bone structure, inducing apatite recrystallization, changes in the elemental composition and adsorptions onto the surface of bioapatite crystals [44]–[46]. Some essential trace elements, abundant during life, decrease after burial while others, such as rare earth elements (REE) and uranium (U), are incorporated during diagenesis. Moreover, hydrolysis may induce the breakage of the peptide bonds, leading to the decomposition of proteinaceous materials [35], [47]–[52]. These phenomena could result in a heterogeneous preservation of the organic fraction within the same specimen.

Among the investigated elements, strontium (Sr) and barium (Ba) have been considered as specific biomarkers for trophic level and diet [53]. Indeed, they are widely used in dietary reconstruction, thus their physiological constraints are relatively well-known and provide a solid reference for studies on bone chemistry [53]. Yet, due to diagenetic processes that promote post-burial substitution of lattice Ca^{2+} by alkali elements, Sr^{2+} and Ba^{2+} are commonly enriched in fossil bones compared to fresh bones (~ 10 µg/g and ~

200 µg/g respectively in human fresh bones) [50], [54], [55]. Uranium (U) and REE are widely used as diagenetic proxies monitor the alteration degree of bones (and teeth) due to their remarkably low levels in fresh bones (<1 µg/g). However, their effective correlation with the amount of preserved collagen has not yet been adequately assessed. During diagenesis, U and REE migrate from the soil to the bone tissues, mostly through groundwaters (*i.e.*, pore fluid interaction). Particularly, being highly water soluble as uranyl (UO_2^{2+}), uranium is readily incorporated in fossil bones and represents a strong marker for post-depositional chemical alteration of the bone mineral portion [54], [56]–[58]. Similarly, due to the high adsorption capacity of bone crystallites for REE^{3+} [33], their adsorption began immediately with the exposure of bone to pore water, yielding high REE content in fossil specimens (ΣREE up to several 1000 µg/g) [59].

The enrichment of abovementioned elements may be theoretically correlated to diagenetic and degradation effects on both inorganic and organic fraction of ancient bones. Indeed, bones and teeth that were affected only by a limited degree by diagenetic decay of the mineral component, usually show a better conservation of the organic fraction [52]. In contrast, when a strong diagenetic alteration of the mineral structure is observed, also the organic component shows a worse conservation status. This suggests a possible mutual protection between mineral and organic fractions, since the degradation of collagen expose the mineral fraction to water penetration (due to the increased porosity) promoting diagenetic processes and, simultaneously, the degradation of the mineral structure facilitates the water penetration with higher risk for collagen hydrolysis [35], [52], [56], [60].

According to this correlation, specific elements such as U and Sr, that are commonly used as diagenetic markers for the assessment of the state of conservation of the mineral components of bone and teeth, have also been used as markers for the evaluation of the organic fraction preservation in the same specimens [52], [54], [57], [58], [61]–[63]. Indeed, the low abundance of diagenetic elemental markers reflects a limited/no bioapatite alteration and thus should correspond to collagen preservation as both biomineral and the protein phase are tightly intergrown and mutually protected each other. In contrast, a high content of these elements indicates a stronger alteration and *postmortem* should also lead to a greater collagen loss.

To date, the relationship between the variation of the diagenetic markers and the presence of collagen in the same sample is still unclear and not adequately studied.

Elemental and isotope analyses, based on the use of different analytical techniques such as synchrotron-based X-ray fluorescence [64], [65] and Laser Ablation-Inductively Coupled Plasma-Mass Spectrometry (LA-ICP-MS) [55], [63], [66]–[70], have been applied to identify well-preserved areas (possible rich in collagen) to be sampled for studies concerning, *e.g.*, dating, paleodiet reconstruction and taxonomic discrimination. Fourier Transform Infrared (FTIR) has also been applied to assess the degradation state of bone. In particular, amide-to-phosphate ratio and crystallinity index were used to evaluate the preservation of the organic fraction [38], [71]–[75].

Nevertheless, to date, no investigations have been conducted to evaluate the effective correlation between collagen distribution (irrefutably identified with high selective techniques) and elemental composition of the diagenetic markers in different areas of the same samples. Only recently, a study reported the parallel investigation of REE distribution and collagen on a single sample (a well-preserved dinosaur fibula). Collagen has been detected by combining enzyme-linked immunosorbent assay (ELISA) applied on protein extracts, and *in situ* immunofluorescence applied on bone fragments [52]. The results suggested the correlation between the low REE content with the presence of collagen.

The present study proposes a new analytical strategy for the characterization of diagenetic pathways in ancient bones and teeth, combining elemental and collagen distribution investigations obtained with LA-ICP-MS and chemiluminescence (CL) immunochemical microscopy imaging, respectively. In particular, CL immunochemical analysis was applied for the first time on archaeological and fossil bones and tooth to sensitively localize collagen protein in complex biomineralized matrices, providing a new tool to screen for the presence of proteins, since the characterization of proteins in ancient skeletal remains may address research questions concerning diet and genetic relations.

Immunochemical methods exploit the high specificity of the antigen–antibody recognition reaction, ensuring the direct and specific detection of collagen [14], [17], [18], [76]. These methods have been widely applied in bioanalysis and clinical chemistry and,

over the past decade, have proven to be efficient methods for the selective identification of proteins in cultural heritage objects [14], [17], [18], [23]–[26], [76]–[78].

The new approach proposed herein presents specific advantages that permits to overcome several limitations of previous research studies: (i) a higher number of samples from various archeological excavation sites and characterized by different chronological periods and collagen content have been considered; (ii) the distribution of collagen was determined using CL immunochemical detection, which has proved to be more sensitive than immunofluorescence and highly selective in the specific identification of proteins in complex matrices [78], also providing good spatial resolution and low background signal; (iii) several diagenetic marker elements were quantified by LA-ICP-MS analysis, exploiting the combined use of single-spots and laser ablation imaging [79]. The latter permitted to obtain a distribution map of the element of interest, directly comparable with the CL collagen images, which further on could enable the identification of diagenetic marker elements (*i.e.*, REEs and U) correlated with collagen preservation. The investigation of samples, from different period/age and excavation sites, allowed to assess the influence of different variables, which could affect diagenetic phenomena and thus collagen preservation, identifying elements that can be used as representative diagenesis extent markers. Age was the first variable considered in order to identify independent marker (*i.e.*, from the Early Middle Ages to the Middle-Upper Paleolithic). In addition, samples from the same period but from different sites were considered to evaluate the impact of diagenesis on bones from different ecogeographical regions (*i.e.*, Northern and Southern Italy).

Exploring the correlation between collagen and the distribution of diagenetic markers could be useful to deeper understand the phenomena promoting post-burial elemental uptake/leaching and biomolecule degradation/preservation. This, in turn, can help future works identifying and retrieving non-altered biogenic chemical signals from (fossil) bones.

The present work was possible thanks to the collaboration with the Bones Lab, supervised by the professor Stefano Benazzi. Indeed, LA-ICP-MS analyses were conducted by Dr.

Federico Lugli, member of Bones Lab group, at the University of Modena and Reggio-Emilia.

2.4.1. Materials and methods

2.4.1.1. Samples preparation

Small fragments were obtained from each bone sample, while the tooth has been cut in half. The fragments were then embedded in Implex® polyester resin (Remet S.A.S., Bologna, Italy) and polished with abrasive paper Micromesh™ from 120 to 12000 grit to obtain a smooth surface [13]. Visible images of the smaller cross-sections were acquired with an Olympus BX51M optical microscope (Olympus Corporation, Tokio, Japan) connected to an Olympus DP70 digital camera and processed through Autopano Giga 4.2 and Adobe Photoshop 2020. Visible images of the sample with a larger dimension (bison and tooth) were acquired with a stereo-microscope Leica® MZ6 connected to a Canon® power shot 550 digital camera.

2.4.1.2. Assay procedure

Samples were first incubated at room temperature under stirring for 1 h with a phosphate buffered saline (PBS)/milk5 blocking solution (PBS containing c = 5 % (g/L) non-fat dried milk (Sigma-Aldrich)). PBS for preparation of blocking solution and antibody solutions contained 10 mmol/L phosphate buffer and 137 mmol/L NaCl, with pH adjusted to 8.1. After washing for 5 min with PBS under stirring, they were incubated overnight at 4°C with the rabbit anti-type I collagen polyclonal antibody (primary antibody, 0.90 mg/mL stock concentration, ab34710, AbCam, Cambridge, UK) diluted 1000 times in PBS/milk1 (PBS containing c = 1 % (g/L) non-fat dried milk). Afterwards, the samples were washed (4x) with PBS under stirring and incubated for 4 h at 4°C with the polyclonal horseradish peroxidase (HRP)-labeled anti-rabbit IgG antibody produced in goat (secondary antibody, 0.68 mg/mL stock concentration, 12-348, Sigma-Aldrich Co., St. Louis, MO) diluted 500 times in PBS/milk1. Negative control tests for assessing the specificity were instead performed by using the polyclonal anti-chicken ovalbumin rabbit antibody (1.0 mg/mL stock concentration, ab181688, AbCam, Cambridge, UK) diluted 1000 times in PBS/milk1 as primary antibody [14]. After incubation with the

immunoreagents, samples were washed again (4x) with PBS, then 50 µL - 100 µL of the SuperSignal ELISA Femto CL substrate for HRP (ThermoFisher Scientific, Inc., Rockford, IL) was added to completely cover the cross-section. Finally, a sequence of CL images (image integration time 30 s) was acquired using Olympus BX51M optical microscope (Olympus Corporation, Tokio, Japan) connected to a cooled ultrasensitive monochromatic Retiga Lumo™ CCD camera (Teledyne, Photometrics, Tucson, AZ). The microscope was enclosed in a homemade dark box to exclude any interference from ambient light. Live images of the samples were also acquired to assess the localization of the CL signals. To directly compare elemental and CL data of samples BI RS 1, semi-quantitative intensities of the light signal were interpolated from the CL image along the laser ablation profile area using Icy 2.1.2.0 (icy.bioimageanalysis.org) and reported as relative intensities (*i.e.*, scaled to the maximum value). To obtain a representative averaged signal of the area of interest, data from six equidistant lines were collected. Finally, a LOWESS smoothing filter (span 0.1) was applied to the resulting averaged signal using Origin 2020. The protocol is schematically described in Figure 2.4.

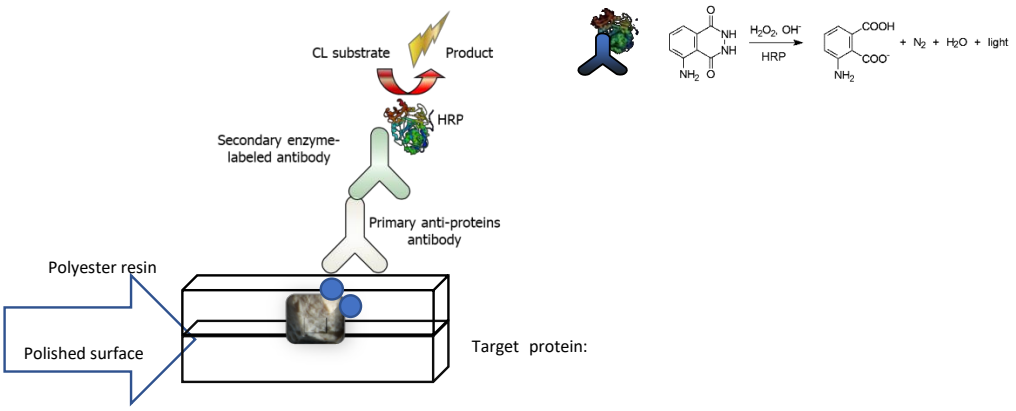

Figure 2.4. Schematic representation of the CL-protocol on ancient bones and teeth.

2.4.1.3. Laser ablation ICP-MS analyses

The LA-ICP-MS elemental analysis was conducted using a 213-nm laser ablation system (New Wave Research Inc., Fremont, CA) coupled to an X-SeriesII quadrupole ICP-MS (Thermo Scientific) housed at the Centro Interdipartimentale Grandi Strumenti of the University of Modena and Reggio Emilia. A circular spot size of 80 µm, an energy density

of about 5 J/cm^2 and a repetition rate of 10 Hz were employed. Helium (0.6 L/min) was used as carrier gas. To avoid external contaminations, sample surface was carefully pre-ablated before each analysis. The following masses were collected to possibly detect post-depositional diagenetic modifications: ^{44}Ca, ^{88}Sr, ^{137}Ba, ^{139}La, ^{140}Ce, ^{141}Pr, ^{146}Nd, ^{147}Sm, ^{153}Eu, ^{157}Gd, ^{159}Tb, ^{163}Dy, ^{165}Ho, ^{166}Er, ^{169}Tm, ^{172}Yb, ^{175}Lu and ^{238}U. Backgrounds were corrected by subtracting the on-peak baseline signals collected during 45 s acquisition with laser off. Data were then internally calibrated using ^{44}Ca (ω = 26.9 % for dentin and ω = 26.5 % for bone) and externally through NIST SRM 612 (trace elements in glass), following [80]. Relative standard deviations measured on NIST SRM 612 are better than 10 %. Results of NIST SRM 1400 (bone ash pressed pellet, quality control) are reported in Table 2.1 and compared with reference values from the GeoReM database [81]. Limits of detection were calculated as three standard deviations of the blank signal, following [80]. A two-tailed *t*-test was performed on elemental data of low vs. high collagen areas, using a MATLAB script. Only data above the LOD were considered. Laser ablation imaging was performed with the same instrument, following the protocol described in Sforna and Lugli (2017) [79]. Specifically, the bone sample was mapped using unspaced line scans with a spot size of 50 µm, covering the whole sample surface. Maps were then built in a MATLAB environment, using MapIT! (see [79]).

Table 2.1. Compositional data of the quality control reference material NIST SRM 1400 bone ash. Average and confidence interval (C.I.) are calculated based on 9 spot analyses (*i.e.*, replicas). Limit of detections (LOD) are reported as 3σ of the blank.

Element	**Average mass fraction (µg/g)**	**C.I. 95 % (µg/g)**	**Reference values in µg/g (from GeoReM)**	**LOD (µg/g)**
Sr	241	237-245	210 - 274 (compiled: 249)	0.1
Ba	243	223-262	240 - 308 (compiled: 240)	0.01
La	0.407	0.223-0.592	0.01 - 0.46 (compiled: 0.386)	0.005
Ce	0.710	0.446-0.974	0.009 - 0.94 (compiled: 0.821)	0.001
Pr	0.077	0.046-0.108	0.008 - 0.094 (compiled: 0.086)	0.001

Nd	0.293	0.170-0.415	0.009 - 0.342 (compiled: 0.316)	0.003
Sm	0.059	0.028-0.090	0.008 - 0.0664 (compiled: 0.0595)	0.002
Eu	0.013	0.004-0.021	0.0136	0.001
Gd	0.050	0.034-0.066	0.006 - 0.071 (compiled: 0.064)	0.004
Tb	0.006	0.004-0.008	0.00885 - 0.01 (compiled: 0.0096)	0.0006
Dy	0.058	0.040-0.076	0.009 - 0.0524 (compiled: 0.0479)	0.004
Ho	0.010	0.006-0.014	0.009 - 0.012	0.001
Er	0.023	0.018-0.028	0.008 - 0.0276 (compiled: 0.0254)	0.003
Tm	0.005	0.002-0.007	0.003 - 0.009 (compiled: 0.0034)	0.002
Yb	0.022	0.014-0.029	0.006 - 0.0237 (compiled: 0.0183)	0.005
Lu	0.005	0.001-0.010	0.0034 - 0.009	0.002
U	0.060	0.038-0.082	0.062 - 0.076 (compiled: 0.066)	0.0007

2.4.2. Results and discussion

2.4.2.1. Results

In this study, seven archaeological bone fragments and one tooth have been analyzed by means of CL immunochemical microscopy imaging and LA-ICP-MS (Table 2.2 and Figure 2.5). Samples come from different ages and sites. Samples from the Middle-Upper Paleolithic were from caves, but from different ecogeographical of Italy with a different climate (*i.e.*, RB38 from the Northern Italy, RSS1 and RSS2 from Southern Italy). Samples RSS1 and RSS2 were obtained from the same bone but they were considered

separately, since diagenesis could affect heterogeneously different areas of the same bone.

Table 2.2. Bone and tooth samples analyzed in this study with relevant details.

Sample	Skeletal tissue	Provenance	Burial setting	Age	Taxonomy
FK BI RS 1	Bone	Rhine gravels (Upper Rhine Valley, Germany)	Fluvial sediment	Late Pleistocene	Mammal (*Bison* sp.)
S2	Bone	Grotta della Cala (Salerno, Campania, Italy)	Cave	Middle-Upper Paleolithic	Mammal
S37	Bone	Castello della Motta of Savorgnano (Udine, Friuli-Venezia Giulia, Italy)	Open-air site	Early Middle Ages	Aves
S40	Bone	Castello della Motta of Savorgnano (Udine, Friuli-Venezia Giulia, Italy)	Open-air site	Early Middle Ages	Aves
RB38	Bone	Riparo del Broion (Vicenza, Veneto, Italy)	Cave	Middle Paleolithic	Mammal
RSS1	Bone	Roccia San Sebastiano cave, Mondragone (Caserta, Campania, Italy)	Cave	Middle Paleolithic	Mammal
RSS2	Bone	Roccia San Sebastiano cave, Mondragone (Caserta, Campania, Italy)	Cave	Middle Paleolithic	Mammal

Velia_T440	Tooth	Velia (Salerno, Campania, Italy)	Open-air coastal site	Roman Ages	Mammal (*Homo sapiens*)

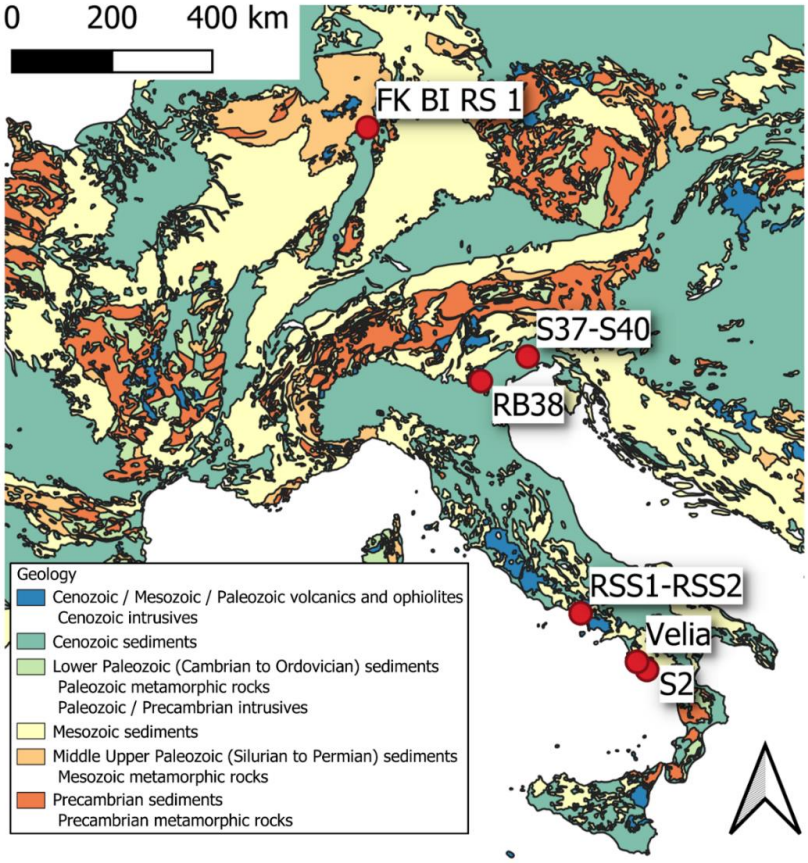

Figure 2.5. Excavation sites of the skeletal samples considered in this study. The simplified geological map has been drawn using QGIS 3.18 (https://www.qgis.org/) by F.L., based on the geological map from [82].

Bone samples

A Late Pleistocene bison bone (FK BI RS 1), which had been investigated in a previous study [83], [84], was submitted to the analytical protocol proposed. This bone fragment is a cross section of a Bison sp. tibia, exposing the entire cortical thickness (Figure 2.6a). The sample was chosen due to its peculiar preservation features having an outer rim (2-3 mm) where, macroscopically, collagen is apparently highly degraded. Yet, the inner cortex portion is better preserved. Such a zonation is also evident from microchemical analyses performed previously on the bone itself [83]. Specifically, the trend of

decreasing C/N atomic ratio from 16.6 at the outer rim to 3.2 towards the center of the bone compacta reflects the strong incorporation of soil-derived humic matter in the outer bone area, also highlighted by the typical dark-brownish coloration [85]. The immunochemical analysis showed indeed the presence of the CL signal mainly localized within the internal part of the bone cortex (Figure 2.6b), with a lower content of collagen in the outer part of the specimen.

This agrees with the expected preservation patterns, where collagen is likely to be better preserved in the inner part of bones, namely those areas less affected by alteration processes from the environment and microbial attack [35], [61], [86].

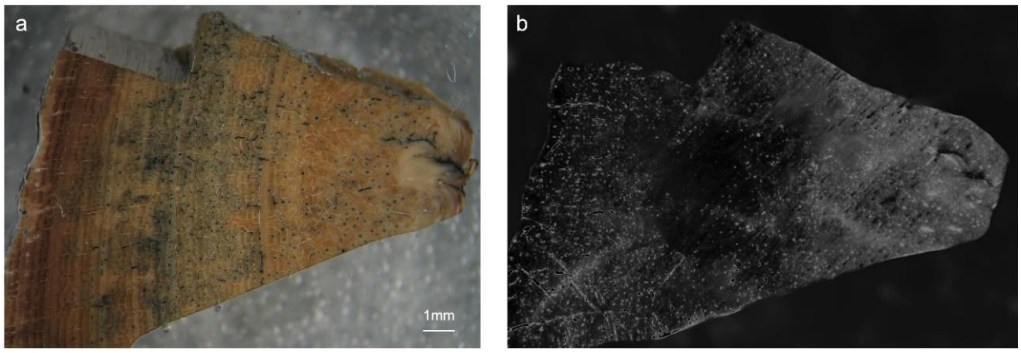

Figure 2.6. Stereomicroscope (left) and CL (right) images of the investigated sample FK BI RS 1 (1.25x magnification). Outer surface is on the left and the inner part is on the right.

Subsequently, line-scan LA-ICP-MS analyses were performed on the sample to quantify its elemental content and cross-monitor the presence of potential elemental gradients linked to the differences in organic matter distribution observed through CL imaging.

Our analysis indicated a well-recognizable gradient (Figure 2.7a) from the outside towards the inside of the bone fragment with a significant decrease in the mass fraction of Ba and Sr in the innermost better-preserved areas (from 1000 µg/g down to 300 µg/g for Ba and from 600 µg/g down to 375 µg/g for Sr). REE (expressed here as the sum of the REE content, *i.e.*, ΣREE) and U were also measured to better investigate the elemental behavior in well-preserved and altered areas (Figure 2.7b). Despite the high variance in mass fraction values along the sample, ΣREE and U clearly decrease several orders of magnitude towards the inner part of the bone (from 200 µg/g down to 0.01 µg/g for U

and from 5 µg/g down to 0.01 µg/g for ΣREE). The innermost part of the compacta of FK BI RS 1, close to the medullar cavity, displays a slight enrichment in ΣREE and U. This latter, specifically, shows an increasing mass fraction from ca. 10000 µm (less than 0.1 µg/g) to the right edge of the sample (up to 20 µg/g). It should be noted that this enrichment is approximately 10 times lower in terms of absolute mass fraction, compared with the outermost bones surface (Figure 2.7). Therefore, a different, though less prominent, diagenetic elemental uptake from the medullar cavity ─ left empty after the decomposition and commonly infilled post-depositional by local soil ─ occurred.

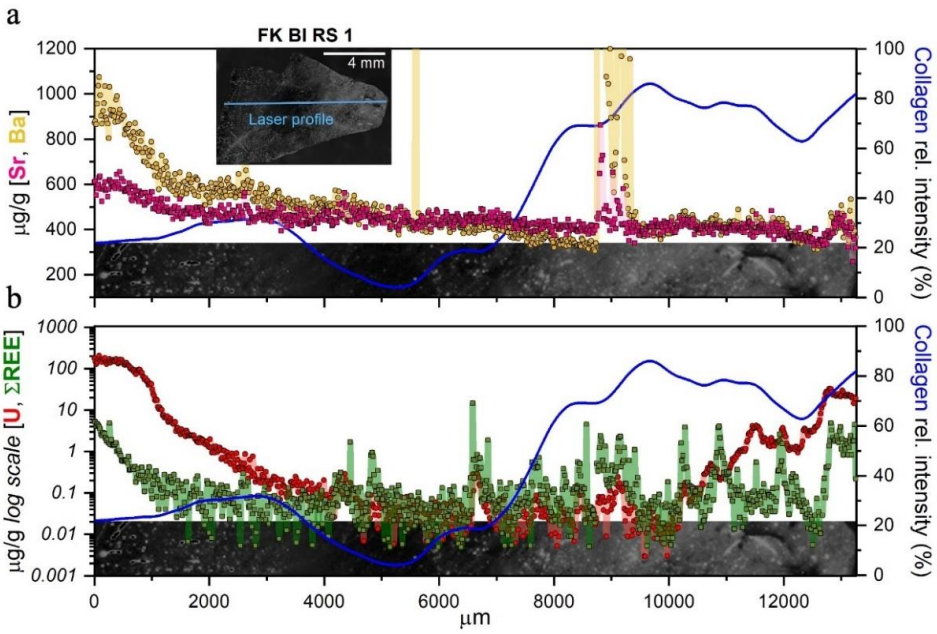

Figure 2.7. Elemental (Sr, Ba, U and ΣREE) profiles are compared with the CL collagen signal of FK BI RS 1 bone. Outer surface is on the left and the inner part is on the right. Spikes in Sr and Ba profiles at ca. 5600 µm and 9000 µm possibly reflect the presence of post-depositional secondary bone porosity infills by diagenetic minerals or sediment. Note that U and ΣREE are reported in log-scale. Semi-quantitative intensities of the light signal were interpolated from the CL image itself along the LA profile using Icy 2.1.2.0 (icy.bioimageanalysis.org [87]) and reported as relative intensities (scaled to the maximum value). To obtain a representative averaged signal of the area of interest, data from six equidistant lines were collected. Finally, a LOWESS smoothing filter (span 0.1) was applied to the resulting averaged signal.

Several other bones (Table 2.2) were analyzed by the integrated CL and LA-ICP-MS approach to better elucidate the possible correlation between collagen loss and elemental uptake after burial.

The use of the CL immunoassay on the selected samples allow to obtain well detectable CL signals for almost all the samples, even though with different spatial distributions (Figure 2.8).

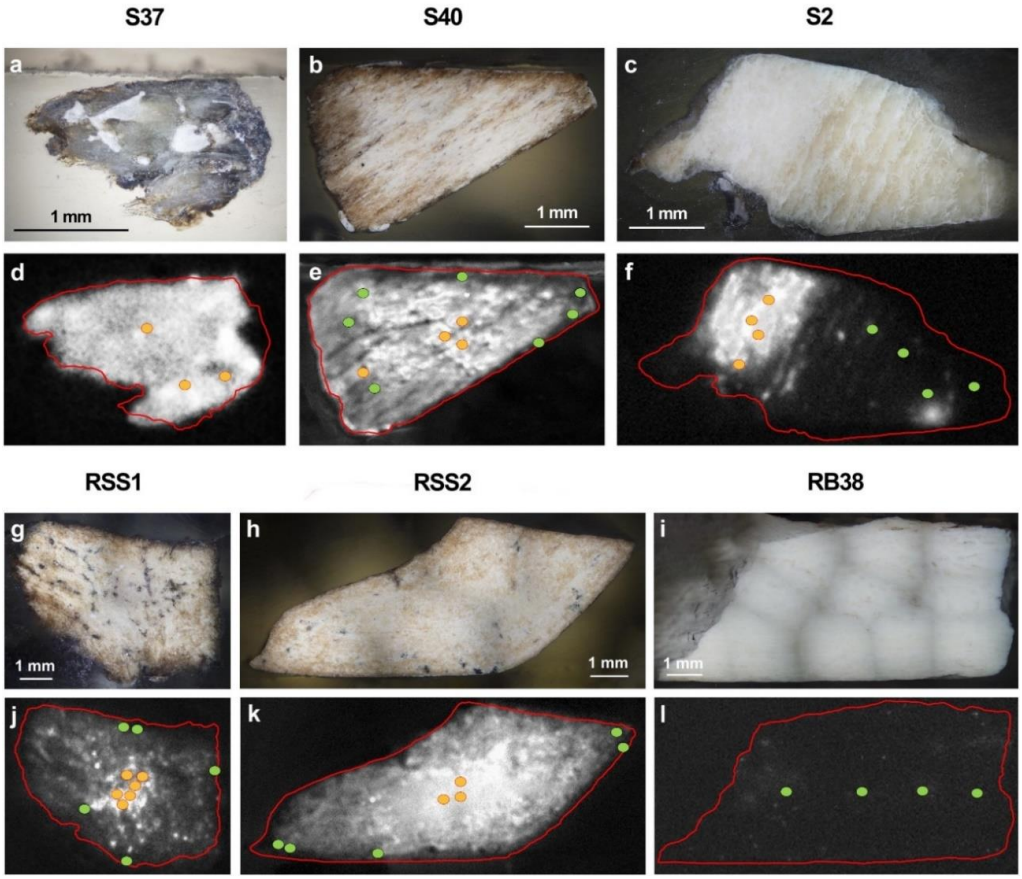

Figure 2.8. Optical microscope (top) and CL (bottom) images of investigated archeological faunal bone samples with known age and provenance (Table 1): (a, d) sample S37 (5x magnification, outer surface is on the top and the inner part is down), (b, e) sample S40 (1.25x magnification, outer surface is on the top and the inner part is down), (c, f) sample S2 (1.25x magnification, inner surface is on the top and the outer part is down), (g, j) sample RSS1 (1.25x magnification, inner surface is on the top and the outer part is down), (h, k) sample RSS2 (1.25x magnification, inner surface is on the top and the outer is down), (i, l)

sample RB38 (1.25x magnification, inner surface is on the top and the outer is down). LA-ICP-MS points of analysis are showed in CL images placed in "high" (orange) and "low" (green) collagen content areas.

Sample S37 (Figures 2.8a and 2.8d) showed an intense CL signal spread all over the sample surface, as expected for a relatively modern bone specimen (Middle Ages). On the other hand, sample S40, coming from the same archeological context of S37, shows a more heterogeneous collagen preservation and distribution (Figure 2.8b and 2.8e). Sample S2 (Figures 2.8c and 2.8f) pertains to the Middle-Upper Paleolithic (>50 ka) and displays two distinct areas with different collagen contents. Specifically, the low-collagen area seems macroscopically characterized by the precipitation of secondary calcium carbonate minerals, as suggested by the yellowish coloration. Bone fragment RSS1 (Figures 2.8g and 2.8j) and RSS2 (Figures 2.8h and 2.8k), which were collected from different areas of the same bone specimen, both exhibited stronger CL signals in the central area of the fragment. Sample RB38 (Figures 2.8i and 2.8l) did not show any significant CL signal, hence the signal was lower than the LOD [76].

CL immunochemical investigations were integrated with LA-ICP-MS micro-chemical analyses. Ablation spots were selected based on areas with different collagen content based on CL images, aiming to obtain at least three LA spots per area (low vs. high collagen content). This allowed to gather specific information for the areas with differentiated collagen content. For each bone sample, areas characterized by "high" and "low" collagen contents were identified according to the CL results. The identification of areas with high or low collagen content is related to the presence or absence of the CL signal in the investigated area. When the CL signal is not detected (*i.e.,* it is below the detection limit, which is 0.3 ng/spot [76]) the area is classified as low in collagen. Conversely, if the CL signal is easily detectable, the area is classified as having a high collagen content. The identification of the two different area typologies on the basis of the CL signal allowed to guide the selection of areas for the elemental analysis, identifying possible differences in diagenetic pathways among samples (Figure 2.9).

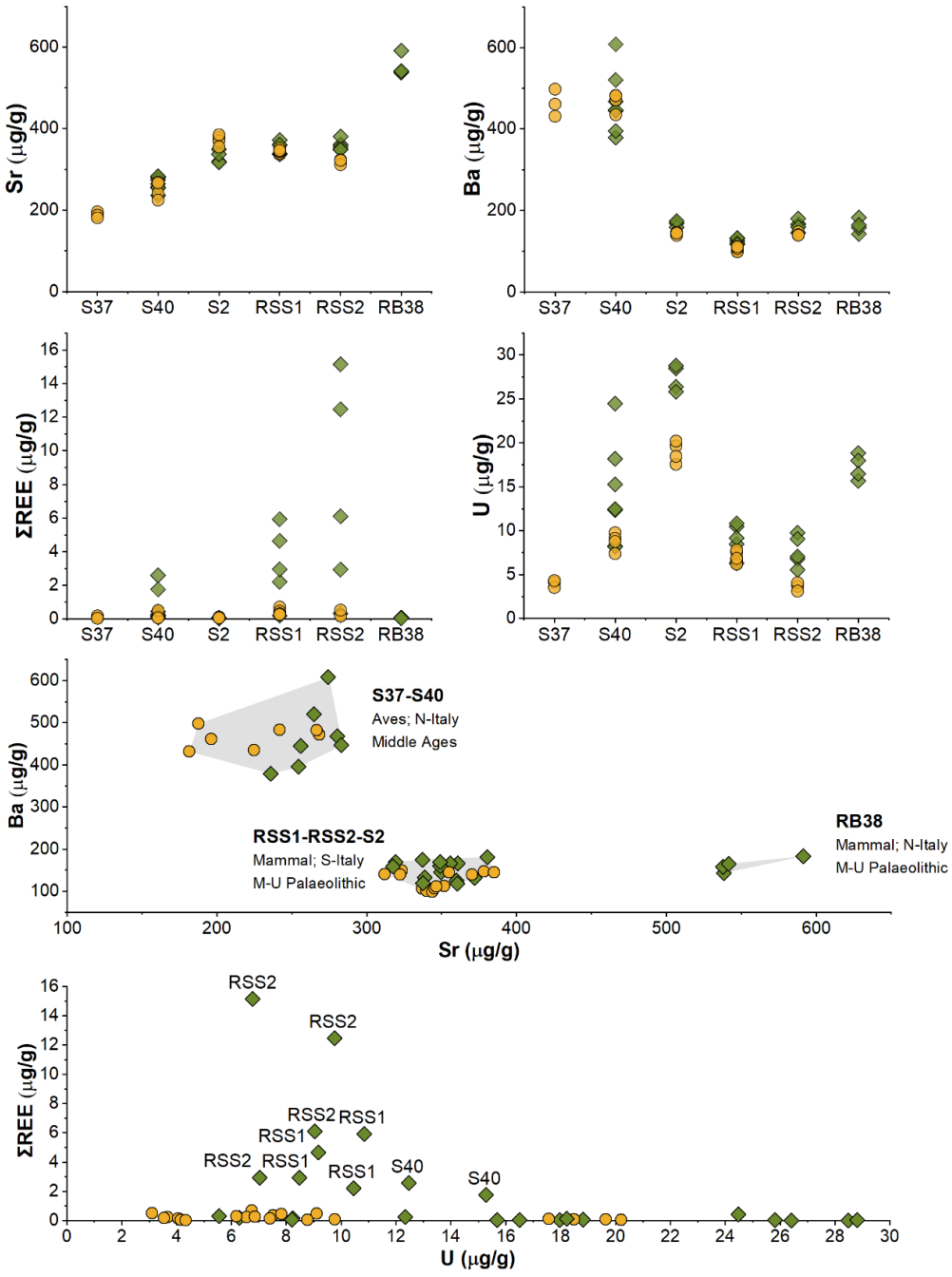

Figure 2.9. LA-ICP-MS spot analyses (ΣREE, U, Sr, Ba) on "high" (orange circles) and "low" (green squares) collagen areas of bone samples. These areas were visually selected based on CL images. A biplot of Ba vs. Sr content is reported to highlight inter-sample differences possibly arose in-vivo due to inputs such as diet, physiology, or local geology. A biplot of U vs. ΣREE content is also reported to highlight the

t-test results, showing the differences correlated to high and low collagen content areas in the bone specimens. Error bars (2 SE) are smaller than symbol size. Two-standard errors are calculated based on repeated measures (n = 9) of NIST SRM 1400 bone ash (Sr: 4 µg/g; Ba: 19 µg/g; U: 0.1 µg/g; ΣREE: 0.35 µg/g).

Table 2.3. Summary statics of LA-ICP-MS spot analyses on bone samples (*i.e.*, S37, S40, S2, RSS1, RSS2 and RB38).

Element	**Sr (µg/g)**		**Ba (µg/g)**		**ΣREE (µg/g)**		**U (µg/g)**	
Sampling area	Low coll.	High coll.	Low coll.	High coll.	Low coll.	High coll.	Low coll.	High coll.
Mean	358	304	241	245	2.34	0.22	14.4	8.8
St. Dev.	96	66	149	168	3.95	0.19	7.4	5.6
Median	349	330	167	145	0.25	0.16	12.3	7.1
Max	591	385	608	498	15.16	0.69	28.8	20.2
Min	236	182	118	99	0.02	0.03	5.6	3.1
***t*-test (low vs. high)**	$p = 0.038$ *		$p = 0.932$		$p = 0.021$ *		$p = 0.007$ **	

Results obtained for these samples are summarized in Table 2.3. A two-tailed *t*-test suggests that, on average, Sr, ΣREE and U contents are significantly higher in areas with low collagen content (Figure 2.9). The *t*-test performed for Sr data is likely biased by sample RB38, which shows an enrichment in Sr content (ca. 550 µg/g; see Discussion; *p* after RB38 removal is 0.342). Being apparently compromised in terms of organic preservation, for RB38 a comparison with a well-preserved collagen area is lacking. After removing RB38 from the dataset, no significant differences can be observed in Sr content between low and high collagen content areas (two-tailed *t*-test; p = 0.342; Figure 2.9). In terms of Ba content, low- and high collagen content areas are statistically indistinguishable (two-tailed *t*-test; p = 0.932).

Additionally, to further investigate the correlation between elemental and collagen distributions in these bones, sample S2 was subjected to LA-ICP-MS imaging (Figure 2.10). It is worth to notice that the normalization method employed for calculating absolute mass fraction in LA spots, *i.e.*, using ^{44}Ca as internal reference, might have smoothed potential differences in elemental mass fractions for those samples that have undergone recrystallization events. Ca content was indeed assumed as constant and equal to that of modern bone bioapatite ($\omega \sim 26.5$ %).

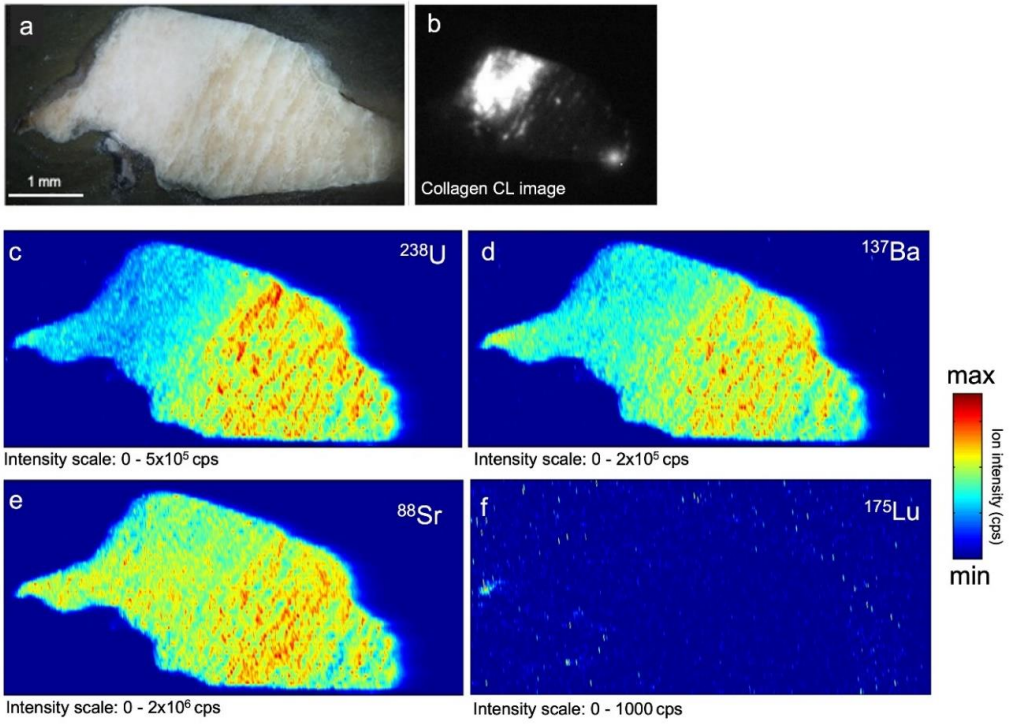

Figure 2.10. Elemental images of sample S2 obtained by LA-ICP-MS. (a) Photomicrographs of the sample, (b) CL image of the collagen distribution, (c) ^{238}U, (d) ^{137}Ba, (e) ^{88}Sr , (f) ^{175}Lu (as REE content proxy). Note that the elemental images are not reported normalized to an internal standard but as raw cps (counts per second). Maps were obtained using a MATLAB 2010a script [79].

Tooth sample

The integrated method was also applied to one tooth from a Southern Italy site of Roman Age (Velia_T440 [88], Figure 2.11a), to evaluate the correlation between collagen and element distribution in different types of skeletal remains. According to the tooth

composition, collagen was clearly localized in the dentin as shown by an intense CL signal, while, as expected, no signal was detected in the highly mineralized and collagen-free enamel (Figure 2.11b).

LA-ICP-MS spot analysis was performed on the dentin tissue (Figure 2.11c) according to the intensities of the CL signal, aiming at monitoring the diagenetic markers already observed for the bones. Specifically, data collected from spots D and E, in an area characterized by the absence of CL signal and thus with a likely poor collagen content, present as expected the highest Sr, Ba and ΣREE contents. On the contrary, lower Sr, Ba and ΣREE contents were detected in all other spots, characterized by a relatively high CL signal.

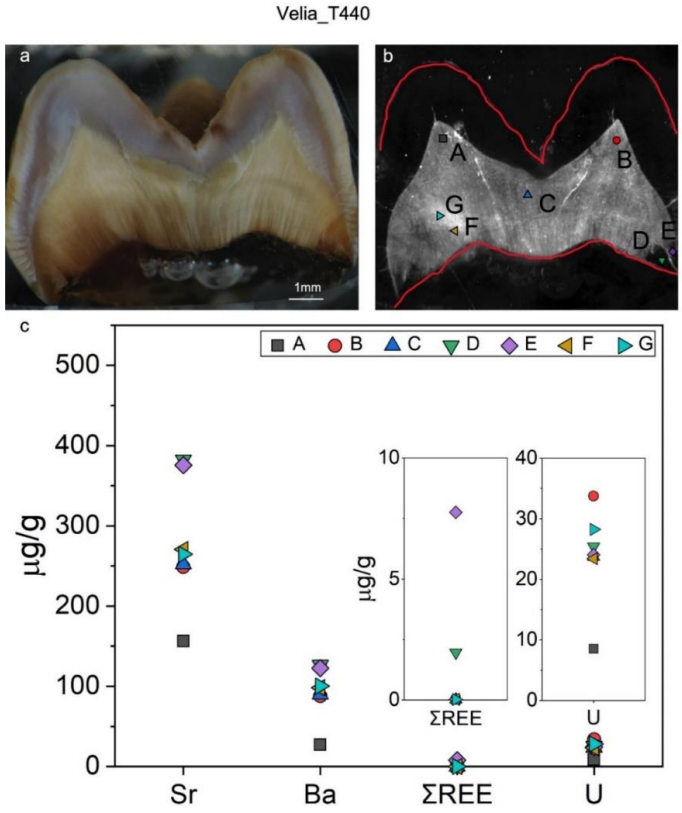

Figure 2.11. Image of tooth Velia_T440 (1.25x magnification). a) Optical microscope, b) CL image with points of LA-ICP-MS spot analysis. Bright lines are due to fissures, c) LA-ICP-MS spot analyses (ΣREE, U, Sr, Ba). Error bars (2 SE) are smaller than the symbol size. Two-standard errors are calculated based on repeated measures (n = 9) of NIST SRM 1400 bone ash (Sr: 4 µg/g; Ba: 19 µg/g; U: 0.1 µg/g; ΣREE: 0.35 µg/g).

2.4.2.2. Discussion

The results of this study clearly indicate different intra- and inter-sample states of preservation, leading to variable collagen and elemental composition even within the same sample. This may be ascribed to the heterogeneity of the degradation phenomena occurring after burial.

Owing to the specificity and the selectivity of the CL immunochemical imaging analysis, it was possible to unequivocally localize collagen [76] within skeletal samples of variable composition and preservation. It is worth noticing that the anti-collagen type I antibodies have high interspecies cross-reactivity [76], ensuring the identification of collagen in all the samples belonging to different species. Furthermore, the application of the integrated protocol revealed a strong correlation between organic content and the content of diagenetic marker elements (*i.e.*, REEs and U) in bone and dentin.

Uranium and REE have been already identified as diagenetic markers for bone fossilization, reflecting the surrounding post burial environment [63]. Both, U and REE are usually absent or only occur in very low mass fraction (< 1 μg/g) in fresh bone, but after burial they may be incorporated from groundwater and soil, increasing their mass fractions in specific areas of the buried bone [51], [56], [62]. Strontium and barium, on the other hand, are biomarkers for dietary reconstruction, in-vivo present within bones between tens and hundreds of μg/g (even less for Ba). However, their endogenous signature can be overprinted by post-depositional exogenous processes [42], [50]. This work revealed for the first time that diagenetic elemental markers for bioapatite could be applied for collagen preservation studies, due to their observed correlation with CL collagen signals. In our data, FK BI RS 1 showed high Sr and Ba values in the outer rim, coupled to U and REE enrichment, due to incorporation of elements from the surrounding environment within the bioapatite structure, possibly linked to a simple diffusion uptake model, as previously explained also by Ullman and colleagues [50], [52]. However, other bone samples showed remarkably variable Sr and Ba contents and lack of correlation with the degree of collagen preservation, highlighting a possible different diagenetic pathway. Indeed, differences in burial setting and/or postmortem element uptake processes could influence the differential digenetic alteration of Sr and Ba versus REE and U. As

expected, in LA-ICP-MS data a relatively high variability (see the coefficients of variation in Table 2.3, calculated as the std. deviation divided by the mean) was observed, as samples come from different taphonomic and temporal contexts. Moreover, as expected, diagenetic markers (*i.e.*, REEs and U) show higher variability than Sr and Ba. The LA-ICP-MS mapping results on S2 emphasized what observed by spot analyses. Interestingly, U was preferentially distributed in those areas lacking collagen preservation, mimicking the macroscopically visible vein-like diagenetic infilling further corroborating the negative correlation between collagen and trace element diagenetic markers. Similarly, Ba seems more concentrated in the diagenetically altered portions. REEs content (here lutetium distribution) in S2 is too low to be meaningfully interpreted. Strontium seems more homogeneously distributed in the sample, with some higher contents within the secondary veins. Moreover, in CL results the variability of collagen content was evident among samples from sites of similar ages (RB38, RSS1, RSS2) and also within the same specimen (RSS1, RSS2), suggesting that the environmental conditions and the post-burial histories of the bone samples may lead to very different conservation status. For instance, the absence of signal in RB38 agrees with the whitish coloration displayed, possibly indicating an exposure to high temperatures [89] that caused the degradation of organic matter. The different taphonomic contexts need also to be considered. Indeed, the local environmental setting (*i.e.*, pH, temperature, humidity, soil composition) and the taxonomy (*i.e.*, bone structure) can lead to different diagenetic pathways and histories [42], [50], [56], [60]. At the same time, the variability of the numerous *in-vivo* factors (*i.e.*, diet, mobility, physiology), hamper the decoupling of the unaltered bone elemental signals and the diagenetic overprints. In general, our data indicate a negative correlation between the preservation of collagen (and, more generally, organic fraction) and the elemental uptake during diagenesis. As similar result was obtained in previous research [52], in which a possible correlation between REE and collagen was stated. However, this hypothesis has not been based on the direct and spatially resolved correlation between elemental and immunochemical data, for a specific bone area. On the contrary, the analytical approach presented here initially involved a sensitive spatial localization of collagen in different areas of the same sample, based on which the investigation of chemical diagenetic markers was conducted, thus obtaining effective information on the correlation of data with a high spatial resolution. As

highlighted, specific diagenetic histories need to be evaluated from case to case. For example, the low REE content of sample RB38, associated with an almost null CL signal across the whole specimen, indicates that the local diagenetic end-member is characterized by a depleted REE signature. Yet, the elevated U and Sr contents still suggest that these samples underwent strong post-depositional modifications.

Because of the growing interest for teeth as biological archives of information, the combined organic and inorganic preservation of a tooth sample (Velia_T440) was investigated in order to better clarify dentin resistance to diagenetic alterations. Like bones, dentin contains high amounts of proteinaceous materials (ca. ω = 20 %) and is prone to post-burial alterations, while enamel is a hard tissue composed by a small organic fraction (ω < 5 %), whose major components are amelogenins [90]. The CL signal appears quite homogeneous, except for small areas macroscopically characterized by a darkish coloration. As expected, no CL response is visible within the tooth enamel. Results confirm the negative correlation between CL collagen signal and the relative enrichment of tracers for diagenetic alteration such as REEs. However, a site-specific diagenetic end-member might influence the preservation of *in-vivo* elemental signals, as in the case of Velia_T440.

It is worth to notice that U showed an unexpected trend in Velia_T440 compared to bones. Indeed, the highest U content is displayed in spot B, which is localized in a high-collagen area with low ΣREE, Sr, and Ba contents. For this tooth, ΣREE seems to better predict collagen degradation rather than U. Specifically, a remarkably high U content (up to ca. 35 μg/g) was observed in the dentin, despite the relatively recent age of the sample. This may suggest that local groundwaters were rich in U, maybe due to geologically-related (*i.e.*, volcanic) sources in the Campanian area [91]. Despite the seemingly poor elemental preservation of Velia_T440, collagen is still present and quite homogeneously distributed. Such evidence may indicate that, in this case, the diagenetic pathway was characterized by surface adsorption and/or complexations of ions with organic molecules (such as humic acids), with little collagen hydrolysis and limited reprecipitation of secondary mineral phases [92].

The results have shown that the innovative integration between CL microscope immunochemical detection and LA-ICP-MS analysis allows a significant improvement

of the information achieved regarding the degree of diagenetic alteration in bones and teeth, thus clarifying and demonstrating for the first time the mutual relation between variations in element mass fraction and collagen preservation.

To sum up, the diagenetic proxies considered in this study support the idea that post-burial collagen degradation is linked with the alteration of the bone *in-vivo* element composition. In particular, the diagenetic markers REE and U seem to show a stronger negative correlation with the presence of collagen than Sr and Ba, which can not always be associated with diagenetic variations. However, case-specific post-burial pathways might lead to different resulting elemental contents and collagen preservations. Our work shows that the combination of *in-situ* CL immunochemical imaging, for the first time applied on archaeological samples, and elemental analyses may help to unravel bone diagenesis history and understand the link between the primary organic content and the alteration of the mineral phase.

2.4.3. Conclusions

The combination of CL imaging and LA-ICP-MS indicated that REE and U contents of bone or dentin may be used as diagnostic chemical markers for collagen preservation. Thus, based on the results of this study, LA-ICP-MS elemental data can be used to better constrain least altered bone or dentin areas with higher collagen contents, according to the mass fraction of these diagenetic markers.

Exploiting the potentialities of CL imaging, future research studies will be focused on the combination of CL immunochemical analysis with NIR hyperspectral imaging to compare and integrate the information obtained to properly select well preserved area in bones and dentin to be submitted to C- and N-isotope analysis or DNA investigations.

2.5. Immunochemical analysis on teeth: amelogenin investigation

Human remains, both bones and teeth, provide information for past reconstruction. Fossil proteins have been mainly analyzed by AAs racemization, sequencing approaches, MS-based analyses, spectroscopy techniques and recently by immunochemical methods [93]. Bones remains have been more investigated, while studies of ancient proteins in tooth tissues are limited [94]–[99]. In last years, paleoproteomic renewed the interest in teeth proteins, due to the higher resistance of tooth tissues than bone matrix.

Despite their low amount, enamel proteins could be less affected by diagenesis than dentin ones, thanks to the mineral protection. In more detail, amelogenin, the main enamel protein, is self-assembled in nanospheres, which create a hydrophobic core and leave charged residues in -NH_2 and -COOH termini covering the surface of the spheres. The interaction between protein charges and HA assures their bond [100]. Thus, the amelogenin nanospheres are essential for the development of the mineral structure, and HA protect the protein preserving it overtime. The interest for this protein was mainly due to the possible sex determination [40], [94], [101]. In these previous works, amelogenin investigation has been achieved after protein extraction, digestion and LC-MS/MS analysis.

However, there is a lack of information about the spatial variation of the target proteins in teeth, that could be crucial to understand diagenetic processes. Moreover, the analysis of human teeth focused the attention on dentin proteins, mainly collagen, since collagen in dentin is metabolically stable during life [95].

In odontology, different immunohistochemical methods were used trying to clarify amelogenin distribution and function during the tooth formation. Nevertheless, they disagreed about amelogenin localization: some identified it only in ameloblasts [102], [103], while others also revealed its presence in association with odontoblasts in dentin before mineralization and as reaction to injuries [30], [104], [105] . Indeed, odontoblasts can repair teeth producing tertiary dentin and amelogenin has shown a curative effect on injured teeth [30], [104]. All the studies agree about the higher concentration of this protein in dentin-enamel junction (DEJ).

In the light of the previous considerations, this work aims at developing a new analytical method for amelogenin X identification on teeth cross-sections and powders. For this purpose, firstly an immunochemical CL imaging protocol was developed on teeth cross-sections. Secondly, an extraction from enamel powder and a CL immunochemical protocol on nitrocellulose membranes were elaborated. The first approach has the advantage to allow a sensitive identification and localization of the target protein on the sample surface. Despite the absence of the spatial information, the second approach: i) permits to extract the protein fraction encapsulated in HA crystals; ii) reduces the amount of sample needed; iii) allows the future development of a portable, fast and multiplex system for sex determination.

The results have shown that the sensitive protocols permit a significant improvement of the information achieved regarding the amelogenin X distribution in teeth and within enamel, thus clarifying the spatial localization and the enamel structure.

The present work was possible thanks to the collaboration with the Bones Lab (Ravenna Campus), Prof. Thomas Tütken (University of Johannes Gutenberg University of Mainz) and the Max Planck Institute for Chemistry (Alfredo Martínez García laboratory).

2.5.1. Materials and methods

2.5.1.1. Samples preparation

For the development of the protocol and the building of a calibration curve, pure amelogenin X isophorm (recombinant, expressed in *E. coli*, SAE0117, Sigma-Aldrich) was dissolved in distilled water (0.1 mg/mL) and then six dilutions 1:3 (v/v) were prepared and spotted on nitrocellulose membranes (1 µL each spot).

The teeth samples for the cross-sections, provided by the Bones lab, came from different contexts (period, location, type). One modern sample was included in the study as reference for the comparison with the ancient samples (Table 2.4). The samples were cut in half at the Bones Lab, and then documented at the M2ADL using a stereomicroscope Leica® MZ6 coupled to a digital camera Canon® power shot 550 with a resolution of 5.0 MP with Tungsten WB correction. The images were processed with Zoom Browser EX software. Then, the specimens were embedded in Implex® polyester resin and polished

using abrasive paper Micromesh™ grit 120-12000 [106]. All the cross-sections were documented after polishing with the stereomicroscope and an optical microscope OLYMPUS® model DP70.

Table 2.4. Description of teeth samples used for cross-sections.

Sample Name	Provenance	Details	Period	Origin	Type	Health status
Mod_36_1	NA	Upper right	Modern	Human	Deciduous	No caries
RP1	Roccapelago	NA	XVI-XVII cenutury	Human, mummy	Permanent	No caries
RM[1]_1	Roccapelago	Molar 1, upper right	XVI-XVII cenutury	Human, mummy	Permanent	No caries

For the development of the extraction protocol from enamel powder, a *Loxodonta africana* (AG-Lox) enamel powder, provided by Prof. Tütken and already grinded at Max Planck Institute for Chemistry, was used as reference sample.

2.5.1.2. Assay procedure on cross-sections

The immunochemical method used was an indirect, non-competitive CL immunoassay. This means that a two-antibodies system is required: the primary Ab bounded directly to the Ag, while the secondary Ab bounded to the primary one. Non-competitive immunoassay involves an excess of labelled antibody.

Samples were first incubated vertically in falcon tubes at room temperature for 1 h with a phosphate buffered saline (PBS)/milk5 blocking solution (PBS containing 5 % (w/v) non-fat dried milk (Sigma-Aldrich)). The samples were stirred every 15 minutes using a vortex. PBS for preparation of blocking solution and antibody solutions contained 10 mmol/L phosphate buffer and 137 mmol/L NaCl, with pH adjusted to 7.4. After 1 washing

for 5 min with PBS under stirring, they were incubated overnight at 4°C with the rabbit anti-amelX polyclonal antibody (primary antibody, 1 mg/mL stock concentration, PA5-31286, Invitrogen, Cambridge, UK) diluted 1:1000 (v/v) in PBS/milk1 (PBS containing 1 % (w/v) non-fat dried milk). Afterwards, the samples were washed (4x) with PBS under stirring and incubated for 4h at 4°C with the polyclonal horseradish peroxidase (HRP)-labeled anti-rabbit IgG antibody produced in goat (secondary antibody, 0.68 mg/mL stock concentration, 12-348, Sigma-Aldrich Co., St. Louis, MO) diluted 1:500 (v/v) in PBS/milk1. Negative control tests for assessing the specificity were instead performed both without primary antibody and using the polyclonal anti-chicken ovalbumin rabbit antibody (1.0 mg/mL stock concentration, ab181688, AbCam, Cambridge, UK) diluted 1:1000 (v/v) in PBS/milk1 as primary antibody [14]. For a comparison with collagen distribution, the anti-type I collagen polyclonal antibody (primary antibody, 0.90 mg/mL stock concentration, ab34710, AbCam, Cambridge, UK) 1:1000 (v/v) in PBS/milk1 was used. After incubation with the immunoreagents, samples were washed again (4x) with PBS, then 50 - 100 μL of the SuperSignal ELISA Femto CL substrate for HRP (ThermoFisher Scientific, Inc., Rockford, IL) was added to completely cover the cross-section. Finally, a sequence of CL images (image integration time 240000 ms and 120000 ms) was acquired using Olympus BX51M optical microscope (Olympus Corporation, Tokio, Japan) connected to a cooled ultrasensitive monochromatic Retiga Lumo™ CCD camera (Teledyne, Photometrics, Tucson, AZ). The microscope was enclosed in a homemade dark box to exclude any interference from ambient light. Live images of the samples were also acquired to assess the localization of the CL signals. The protocol is schematically described in Figure 2.12.

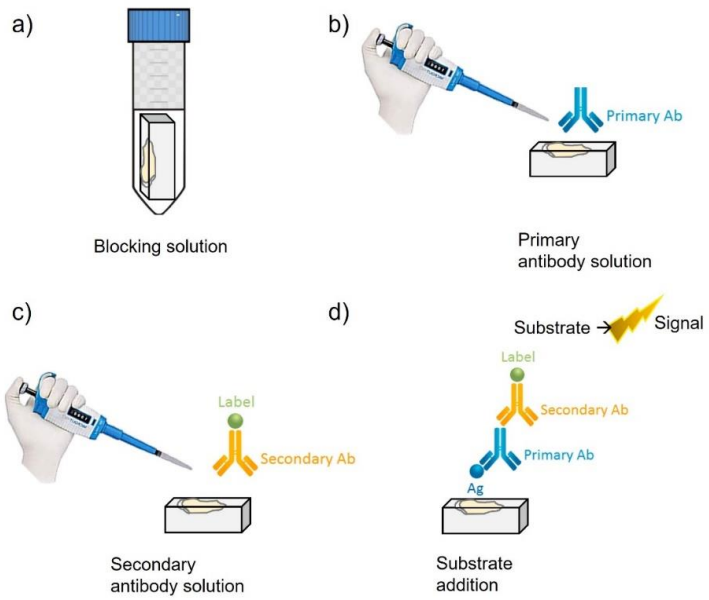

Figure 2.12. Schematic representation of the protocol: a) sample submerged in the blocking solution for 1 h; b) addition of the primary Ab solution (overnight); c) addition of the secondary Ab solution (4 h); d) substrate addition for signal detection.

2.5.1.3. Assay procedure on powders

For the extraction from enamel powder, 1 mg of *Loxodonta africana* enamel powder was weighed in an Eppendorf tube. Then, hydrochloric acid (HCl, 1.6 M, 20 µL/mg) was added and after different times (5, 10, 20, 30 minutes) it was slowly removed. The powder was washed 2 times with PBS, then resuspended in PBS and ultrasonicated for 10 minutes. From the supernatant, 1 µL was taken and spotted on nitrocellulose membrane.

The immunochemical protocol applied was the same previously developed for the standard protein. Membranes were rinsed in PBS, transferred in a petri dish and then covered with a PBS/milk5 blocking solution (PBS containing 5 % (w/v) non-fat dried milk (Sigma-Aldrich)) at room temperature for 1 h. As for the cross-sections, PBS contained 10 mmol/L phosphate buffer and 137 mmol/L NaCl, with pH adjusted to 7.4. After 1 washing for 5 min with PBS, they were incubated for 1 h at room temperature with the rabbit anti-amelX polyclonal antibody (primary antibody, 1 mg/mL stock

concentration, PA5-31286, Invitrogen, Cambridge, UK) diluted 1:1000 (v/v) in PBS/milk1 (PBS containing 1 % (w/v) non-fat dried milk). Afterwards, the samples were washed (3x) with PBS and incubated for 1 h at room temperature with the polyclonal horseradish peroxidase (HRP)-labeled anti-rabbit IgG antibody produced in goat (secondary antibody, 0.68 mg/mL stock concentration, 12-348, Sigma-Aldrich Co., St. Louis, MO) diluted 1:500 (v/v) in PBS/milk1. Negative control tests for assessing the specificity were instead performed without primary antibody. After incubation with the immunoreagents, samples were washed again (3x) with PBS, then 50 - 100 µL of the SuperSignal ELISA Femto CL substrate for HRP (ThermoFisher Scientific, Inc., Rockford, IL) was added to completely cover the membranes. Finally, a sequence of CL images (image integration time 30000 ms and 60000 ms) was acquired using Olympus BX51M optical microscope (Olympus Corporation, Tokio, Japan) connected to a cooled ultrasensitive monochromatic Retiga Lumo™ CCD camera (Teledyne, Photometrics, Tucson, AZ).

2.5.2. Results and discussion

2.5.2.1. Optimization of experimental conditions

The performance of the assay and the sensitivity of the immunoreaction can be improved optimizing several parameters, such as antibody concentration, incubation time, blocking solution concentration and washings steps. This is fundamental to reduce the aspecific binding of the immunoreagents.

The preliminary optimization was conducted on target protein on nitrocellulose membrane to evaluate the performance of the method and the specificity of the antibody. For the optimal performance of the immunoassays, an excess of both the primary and the secondary antibodies is required to bind all the target protein molecules in the sample and to reveal all the target-bound primary antibody, respectively. Nevertheless, a high excess of the immunoreagents should be avoided because it would increase the amount of aspecific binding to the cross-section, thus giving stronger background CL signals. Figure 2.13 shows the results obtained with the optimal conditions (blocking solution 5 % (w/v) of milk for 1 h, Ab' 1:1000 v/v for 1 h, Ab'' 1:500 v/v for 1 h). Figure 2.13a shows the CL images of nitrocellulose membranes with amel-X spots. The signal was clearly visible

confirming the possibility to perform selective identification of the protein on real samples. According to these results, a calibration curve was obtained for the target protein (Figure 2.13b) and the detection limits of the assays, estimated as the amount of protein giving a CL signal corresponding to the background signal plus 3 times its standard deviation, were estimated. In Table 2.5 are reported the values obtained. The limits of detection (LOD) was 1.3-2 µg/mL.

Table 2.5. Table with concentrations of the protein solutions and signal detected.

Concentration (µg/mL)	**Signal**
0.00	113225.6667
1.37	333 692
4.11	2 265 265
12.33	5 764 523
37.00	19 759 202

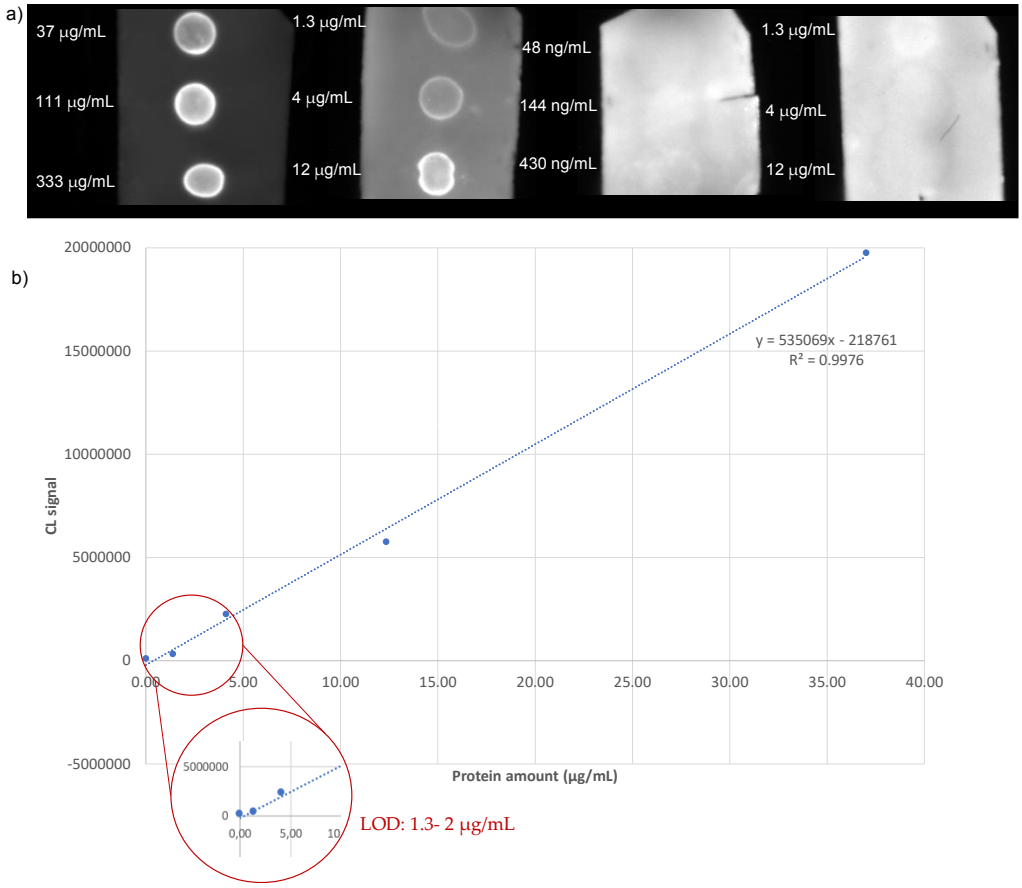

Figure 2.13. CL immunolocalization obtained with the optimized protocol of amel-X with different concentrations. a) CL images of nitrocellulose membranes; b) calibration curve obtained showed a LOD of 1.3-2 µg/mL.

A critical step was the application of the developed protocol on the porous tooth surface trying to reduce the aspecific adsorption of the immunoreagents. Different concentrations of the blocking solution were tested in different immunolocalization tests, in particular 5 % (w/v) and 8 % (w/v) of non-fat dried milk in PBS. The one that provided the optimal analytical performance was 5 % (w/v) as seen on nitrocellulose membranes too. Different blocking solution methods were also evaluated. During the first tests, samples were soaked in the blocking solution and left under stirring for 1 h. Then, the protocol was modified and the cross-sections were put in a vertical position in Falcon tubes, completely covered by the solution. Instead of 1 h under stirring, the tubes were stirred every 15 minutes avoiding aspecific signals in the CL images.

In addition to this, the solution was stirred and ultrasonicated before the use, in order to be sure that the milk was completely dissolved in PBS.

During the acquisition of the first CL images, it was noticed that the interface between outer enamel and resin produced a high CL signal. This was probably due to the smooth enamel surface, which did not allow a complete adhesion of the resin. To avoid this aspecific signal, the outer surface of the tooth was gently roughed with abrasive paper before the embedding to obtain a rougher surface. The same was done with the cavity due to the pulp chamber.

As concern the antibodies concentrations, the proper dilutions were the same used for the nitrocellulose membranes: 1:1000 (v/v) for the primary antibody and 1:500 (v/v) for the secondary antibody.

2.5.2.2. Cross-sections

The samples embedded in resin were three. The first one was a deciduous tooth from modern ages and thus used as a reference, while the other two came from the same archaeological site. The context of these two samples promoted the natural mummification of the remains. This process should guarantee the preservation of the samples, since it is known to preserve biomolecules due to cold temperatures or low oxygen levels [107].

For each sample were performed 4 different experiments: one negative without primary antibody, one negative with anti-OVA antibody, one for amel-X, one for collagen to better understand the spatial variation of the target protein. The signal was localized accordingly to the CL signal represented by the white light in the CL images.

In the deciduous modern tooth (Mod_36_1) the amelogenin signal was expected in the DEJ, but also in the dentin area, because ameloblasts occur in deciduous teeth dentin and have a key role in their development and crystallization [104]. It was also possible to notice a higher intensity of the signal near the pulp chamber (see Figure 2.14a), where odontoblasts are located. Indeed, the capability of odontoblasts to secrete amelogenin was demonstrated [30], [108].

On the contrary, collagen signal was homogenously distributed in the dentin, as expected. The two negative tests confirmed the actual presence of the two proteins, according to the absence of signal in DEJ and dentin.

The magnifications (Figure 2.15) confirmed what mentioned above.

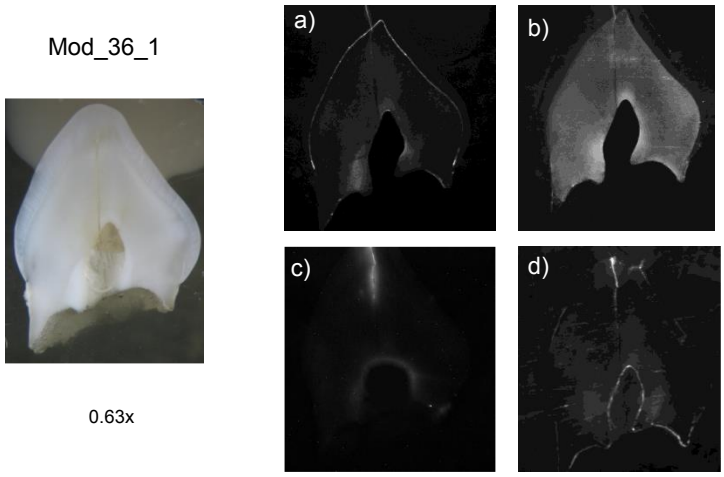

Figure 2.14. Live image and CL images of amel-X (a), collagen (b), negative (c), OVA (d) tests of sample Mod_36_1.

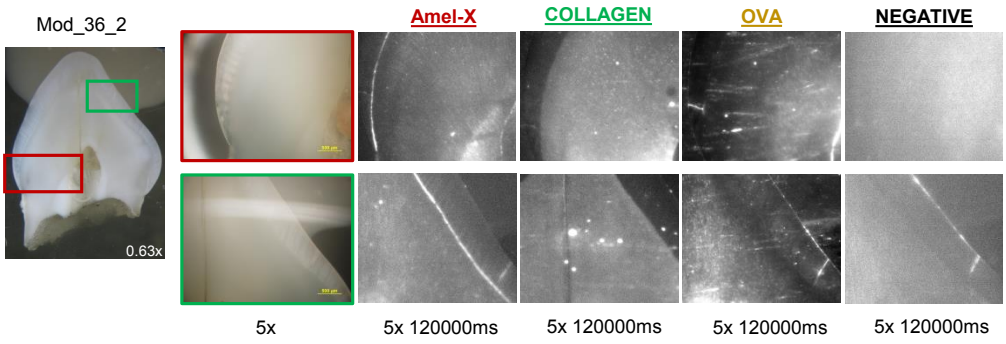

Figure 2.15. 5x magnification details of Mod_36_1; comparison of amel-X, collagen, OVA and negative tests of the DEJ area. Aspecific signal is present in some images due to irregularities of the surface. Especially cracks appeared or disappeared after polishing the sample.

The other two samples (RP1 and RM[1]_1) were permanent teeth from the site of Roccapelago (Modena). In sample RP1 (Figure 2.16) the CL signal confirmed the presence of amelogenin in DEJ area, according to the previous studies that investigated

the proteins presence in the DEJ and adjacent protein containing enamel matrix layer of healthy human molar teeth [108].

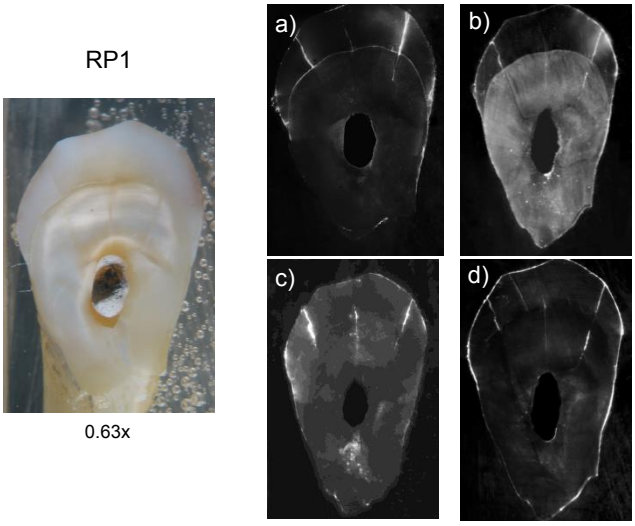

Figure 2.16. Live image and CL images of amel-X (a), collagen (b), negative (c), and OVA (d) of sample RP1.

Instead of what reported in literature [104], the zebra pattern was not detected. According to literature, the amelogenin in enamel shows alternating positive zones near the DEJ and in the outer enamel surface (OES), and a negative area between them [104]. However, the quantification of the protein was not reported.

It is known that proteins in mature enamel constitutes 1 % up to 3 % of the weight and vary in each sample according to enamel weight [90], [104]. The enamel weight is between 0.17 g (second incisor) and 0.59 g (first molar) [109], hence the relative amount of amelogenin should be in the range of mg. In the case of sample RP1, the range should be in the range of 2-5 mg, considering that it was a molar. However, even if the amelogenin amount was higher than the LOD of the protocol, the protein was localized only in the DEJ. This result is in agreement with what reported in literature about the predominantly presence of the organic components close to the DEJ [90]. However, the strong signal present in the DEJ could be justified not only by the actual presence of the protein, but also by the morphology of the DEJ, that shows the dentinal tubules and enamel prisms interruption [110], [111]. The absence of the enamel prisms facilitates the

detection of amelogenin in this area. Moreover, the DEJ is less subjected to environmental alteration and it is the most well-preserved in the fossil record [112].

The authenticity of the results obtained was confirmed by the comparison with the two negative tests and with collagen distribution. In fact, collagen was homogenously detected in the dentin. Some magnifications of the DEJ are reported in Figure 2.17.

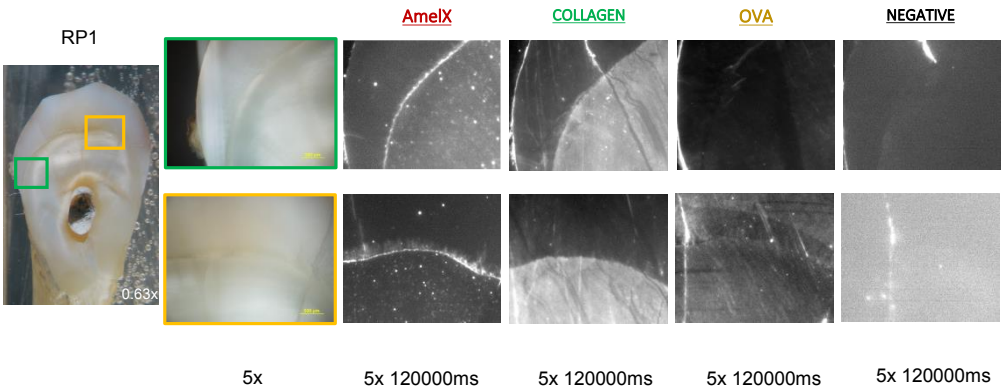

Figure 2.17. 5x magnification details of RP1; comparison of amel-X, collagen, OVA and negative tests of the DEJ area. Aspecific signal is present in some images due to irregularities of the surface. Especially cracks appeared or disappeared after polishing the sample.

On the contrary, sample RM[1]_1 showed a homogenous CL signal of both amelogenin and collagen in dentin (Figure 2.18). The homogenous distribution of the amelogenin in the dentin was also visible in the magnifications (Figure 2.19), while it was not detected in the OES.

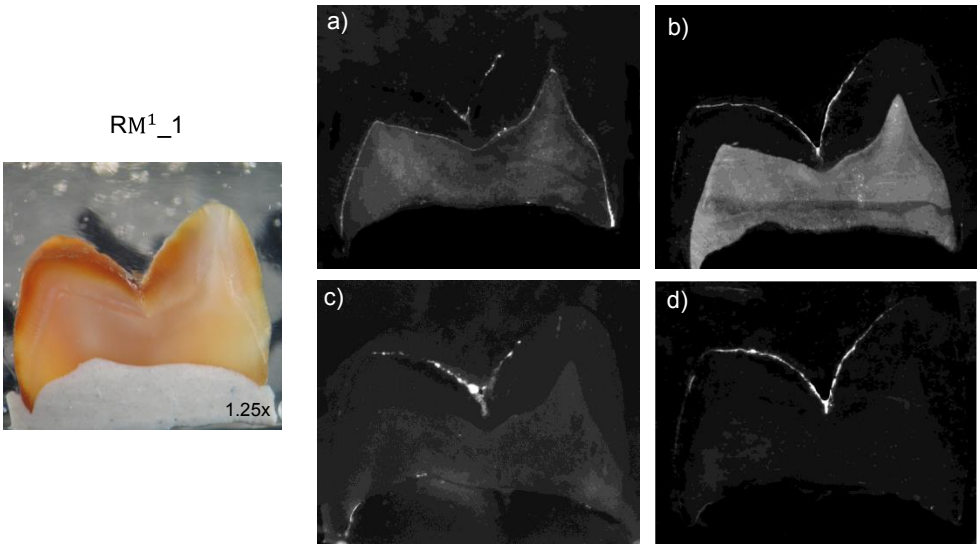

Figure 2.18. Live image and CL images of amel-X (a), collagen (b), negative (c), and OVA (d) of the sample RM[1]_1.

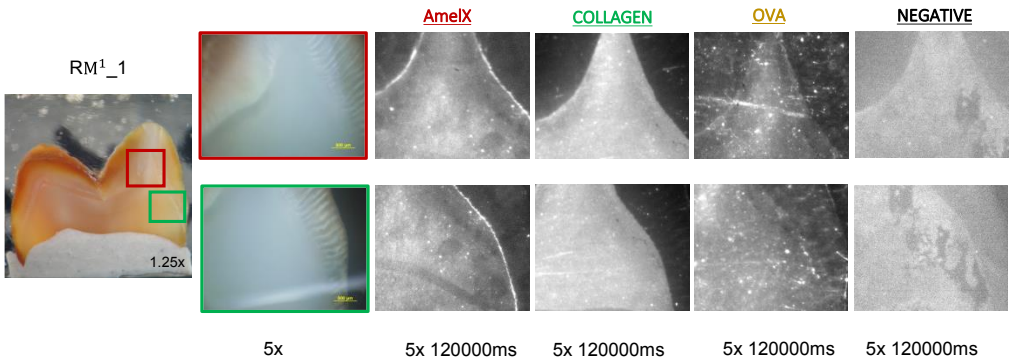

Figure 2.19. 5x magnification details of RM[1]_1; comparison of amel-X, collagen, OVA and negative tests of the DEJ area. Aspecific signal is present in some images due to irregularities of the surface. Especially cracks appeared or disappeared after polishing the sample.

Previous studies investigated the possible presence of amelogenin in deciduous teeth dentin [104], [108] and the possible secretion of this protein by odontoblasts, the cells which allow dentin formation and maintenance [30]. These studies demonstrated that also in mature odontoblasts amelogenin could be present, but its content decreases with the growth [30]. Moreover, amelogenin expression in odontoblasts was detected in case of

vitamin D deficiency, in presence of osteoporosis-like phenotype [30] or in association with a weak health status or injuries [30], [104], [113].

The absence of the signal in the OES in both the last samples could be due to the morphological and mineralogical features of the enamel. In fact, HA crystals encapsulate the nanoscale particles of amelogenin. This interaction protects the protein, thus when the immunoreagents interact with the sample surface during the incubation, the crystals may create shield that does not allow the antibody to bind the target protein.

Previous immunofluorescence studies performed on thin sections (5-10 μm) demonstrated the presence of amelogenin in the OES [30], [104], [108]. However, the samples were subjected to a demineralization before the analysis, confirming the hypothesis of the encapsulation of the protein. For this reason, an investigation of modern enamel powder, considerable as reference, was conducted.

2.5.2.3. Powders

In order to demonstrate the possible encapsulation of amelogenin in HA crystals, an amelogenin extraction on enamel powder was developed. AG-Lox was used as a reference modern powder to develop the protocol.

The extraction was performed in 1.6 M HCl, testing different times (5, 10, 20, 30 minutes) to identify the one with the maximum of protein concentration. The analyses were done in triplicate, which means that the same protocol was repeated on three different samples. The values obtained were then interpolated with the calibration curve to quantify the different amounts of protein. The results showed an increasing of the signal with the maximum at 20 minutes of extraction (~4.5 μg/mL) and then a decreasing, probably due to the effect of the acid on protein structure after a longer time (Figure 2.20, Table 2.6). Low times were not able to release the protein from the HA crystals, while long times attacked the protein too. The presence of signal after the extraction demonstrated the necessity of a demineralization step to have the Ag available for Ab bond.

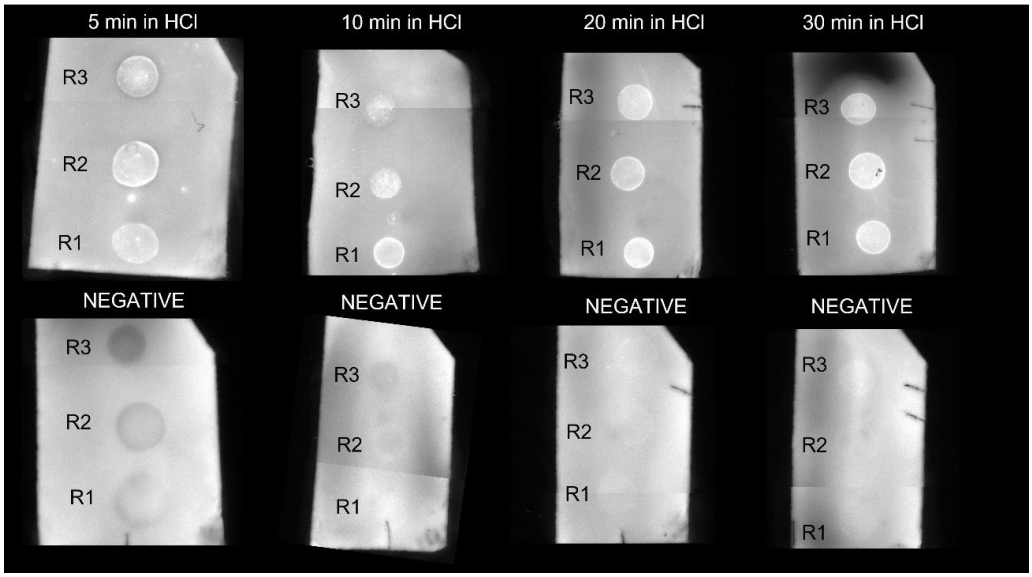

Figure 2.20. CL images of nitrocellulose membranes acquired at 30000 ms. The spots represent the amelogenin X signal after different times of extraction (from 5 to 30 minutes) from 1 mg of AG-Lox powder. The highest concentration was detected after 20 minutes of extraction. The negatives were performed in absence of the primary antibody.

Table 2.6. Table with concentrations of the amelogenin extracted from AG-Lox powder with different times (5, 10, 20, 30 minutes).

Time in HCl	Replicates	Concentration (µg/mL)
5 min	R1	1.5
	R2	1.2
	R3	1.6
10 minutes	R1	1.6
	R2	1.5
	R3	0.9
20 minutes	R1	4.4
	R2	4.9
	R3	4.1
30 minutes	R1	3.6

	R2	3.6
	R3	3.8

To exclude a possible loss of protein material, a test on the removed HCl was done. The acid was removed and left to evaporate overnight, the residues were resuspended in PBS and submitted to the protocol (spot on nitrocellulose membranes, blocking solution, primary and secondary Ab). The results were negative, demonstrating that no loss occurred during the extraction.

Firstly, the results showed a good reproducibility among different replicates. Secondly, it was possible to select 20 minutes as the optimal time for the procedure.

2.5.3. Conclusions and further perspectives

A chemiluminescence immunochemical protocol for proteins detection and localization in tooth cross-sections was developed in this work. Different teeth were analyzed, and the optimization of the experimental settings allowed the successful localization of collagen and amelogenin X in teeth. In detail, the protocol was effective for the detection of collagen, which was homogenously localized in the dentin. It was also selective for the amelogenin X, as demonstrated with the pure protein, and it was localized in the DEJ area.

However, amelogenin X was not detected in the OES and for this reason an extraction protocol was developed on enamel tooth powder. The developed method proved the effective encapsulation of the protein in HA crystals with a consequent reduction of protein availability to the Ab-Ag reaction on the cross-section surface.

The protocol developed on powder has to be implemented testing archaeological powders and testing anti-amelogenin Y antibody too. This could be a turning point for a fast sex determination, using only 1 mg of powder and thus saving the sample. Moreover, the protocol could be also optimized to reduce the amount of powder needed.

The development of a fast acidic treatment of tooth cross-sections could also be interesting to evaluate the possible localization of the protein exploring a wider range of

situations (*e.g.*, carious teeth, different burial settings, periods). This could be useful both for diagenetic investigations and for sampling for further analysis.

This work overcame the gap in literature, clarifying better amelogenin distribution and enamel structure and suggesting new frontiers in sex determination of archaeological remains.

2.6. References

[1] M. A. U. Azim, M. Hasan, I. H. Ansari, and F. Nasreen, "Chemiluminescence immunoassay: basic mechanism and applications," *Bangladesh J. Nucl. Med.*, vol. 18, no. 2, pp. 171–178, 2018, doi: 10.3329/bjnm.v18i2.35240.

[2] A. Roda and M. Guardigli, "Analytical chemiluminescence and bioluminescence: Latest achievements and new horizons," *Anal. Bioanal. Chem.*, vol. 402, no. 1, pp. 69–76, 2012, doi: 10.1007/s00216-011-5455-8.

[3] L. Hu and G. Xu, "Applications and trends in electrochemiluminescence," *Chem. Soc. Rev.*, vol. 39, no. 8, pp. 3275–3304, 2010, doi: 10.1039/b923679c.

[4] R. S. of C. Aldo Roda, Ed., *Chemiluminescence and Bioluminescence: Past, Present and Future*. Royal Society of Chemistry, 2011.

[5] Miroslav Ferencìk, *Handbook of Immunochemistry*. 1993.

[6] F. Barni, S. W. Lewis, A. Berti, G. M. Miskelly, and G. Lago, "Forensic application of the luminol reaction as a presumptive test for latent blood detection," *Talanta*, vol. 72, no. 3, pp. 896–913, 2007, doi: 10.1016/j.talanta.2006.12.045.

[7] M. E. Koivunen and R. L. Krogsrud, "Principles of immunochemical techniques used in clinical laboratories," *Lab. Med.*, vol. 37, no. 8, pp. 490–497, 2006, doi: 10.1309/MV9RM1FDLWAUWQ3F.

[8] R. Créton and L. E. Jaffe, "Chemiluminescence microscopy as a tool in biomedical research," *Biotechniques*, vol. 31, no. 5, pp. 1098–1105, 2001, doi: 10.2144/01315rv01.

[9] M. Mirasoli, M. Guardigli, and A. Roda, "Applied photochemistry," in *Applied Photochemistry*, G. Bergamini and S. Silvi, Eds. 2014, pp. 427–458.

[10] T. Brown and K. Brown, *Biomolecular Archaeology*. Wiley-Blackwell, 2011.

[11] G. Sciutto, "Development of advanced analytical approaches for the characterization of organic substances in artistic and archaeological samples," University of Bologna, 2011.

[12] A. Roda *et al.*, "Portable device based on chemiluminescence lensless imaging for personalized diagnostics through multiplex bioanalysis," *Anal. Chem.*, vol. 83, no. 8, pp. 3178–3185, 2011, doi: 10.1021/ac200360k.

[13] R. Mazzeo, *Analytical chemistry for cultural heritage*. 2017.

[14] L. S. Dolci *et al.*, "Ultrasensitive chemiluminescent immunochemical identification and localization of protein components in painting cross-sections by microscope low-light imaging," *Anal. Bioanal. Chem.*, vol. 392, no. 1–2, pp. 29–35, 2008, doi: 10.1007/s00216-008-2023-y.

[15] L. Cartechini *et al.*, "Immunodetection of proteins in ancient paint media," *Acc. Chem. Res.*, vol. 43, no. 6, pp. 867–876, 2010, doi: 10.1021/ar900279d.

[16] J. Arslanoglu, J. Schultz, J. Loike, and K. Peterson, "Immunology and art: Using antibody-based techniques to identify proteins and gums in artworks," *J. Biosci.*, vol. 35, no. 1, pp. 3–10, 2010, doi: 10.1007/s12038-010-0001-y.

[17] M. Zangheri *et al.*, "A portable device for on site detection of chicken ovalbumin in artworks by chemiluminescent immunochemical contact imaging," *Microchem. J.*, vol. 124, pp. 247–255, 2016, doi: 10.1016/j.microc.2015.08.026.

[18] G. Sciutto *et al.*, "Miniaturized biosensors to preserve and monitor cultural heritage: from medical to conservation diagnosis," *Angew. Chemie - Int. Ed.*, vol. 57, no. 25, pp. 7385–7389, 2018, doi: 10.1002/anie.201713298.

[19] G. Sciutto *et al.*, "Development of a multiplexed chemiluminescent immunochemical imaging technique for the simultaneous localization of different

proteins in painting micro cross-sections," *Anal. Bioanal. Chem.*, vol. 399, no. 9, pp. 2889–2897, 2011, doi: 10.1007/s00216-010-4258-7.

[20] A. Heginbotham, V. Millay, and M. Quick, "The use of immunofluorescence microscopy and enzyme-linked immunosorbent assay as complementary techniques for protein identification in artists' materials," *J. Am. Inst. Conserv.*, vol. 45, no. 2, pp. 89–105, 2006.

[21] B. Ramírez-Barat and S. de la Viña, "Characterization of proteins in paint media by immunofluorescence. A note on methodological aspects," *Stud. Conserv.*, vol. 46, no. 4, pp. 282–288, 2001, [Online]. Available: https://www.jstor.org/stable/1506777.

[22] L. Kockaert and P. Gausset, "Detection of ovalbumin in paint media by immunofluorescence," *Stud. Conserv.*, vol. 34, no. 4, pp. 183–188, 1989.

[23] E. Brandt, I. Wiechmann, and G. Grupe, "How reliable are immunological tools for the detection of ancient proteins in fossil bones?," *Int. J. Osteoarchaeol.*, vol. 12, no. 5, pp. 307–316, 2002, doi: 10.1002/oa.624.

[24] A. Loufouma-mbouaka, M. Binder, H. Noedl, and M. Gamble, "Evaluation of rapid diagnostic tests and Enzyme Linked Immunoassay in the detection of malaria in ancient human remains," *J. Archaeol. Sci.*, vol. 116, no. March, p. 105118, 2020, doi: 10.1016/j.jas.2020.105118.

[25] A. E. Moyer, W. Zheng, and M. H. Schweitzer, "Keratin durability has implications for the fossil record: Results from a 10 year feather degradation experiment," *PLoS One*, vol. 11, no. 7, pp. 1–18, 2016, doi: 10.1371/journal.pone.0157699.

[26] A. E. Moyer, W. Zheng, and M. H. Schweitzer, "Microscopic and immunohistochemical analyses of the claw of the nesting dinosaur, Citipati osmolskae," *Proc. R. Soc. B Biol. Sci.*, vol. 283, no. 1842, pp. 1–7, 2016, doi: 10.1098/rspb.2016.1997.

[27] J. A. Tripp, M. E. Squire, R. E. M. Hedges, and R. E. Stevens, "Use of micro-

computed tomography imaging and porosity measurements as indicators of collagen preservation in archaeological bone," *Palaeogeogr. Palaeoclimatol. Palaeoecol.*, vol. 511, no. May, pp. 462–471, 2018, doi: 10.1016/j.palaeo.2018.09.012.

[28] S. Cersoy, S. Zirah, A. Marie, and A. Zazzo, "Toward a versatile protocol for radiocarbon and proteomics analysis of ancient collagen," *J. Archaeol. Sci.*, vol. 101, no. April 2018, pp. 1–10, 2019, doi: 10.1016/j.jas.2018.10.009.

[29] T. P. Cleland, K. Voegele, and M. H. Schweitzer, "Empirical evaluation of bone extraction protocols," *PLoS One*, vol. 7, no. 2, pp. 1–9, 2012, doi: 10.1371/journal.pone.0031443.

[30] P. Papagerakis, M. MacDougall, D. Hotton, I. Bailleul-Forestier, M. Oboeuf, and A. Berdal, "Expression of amelogenin in odontoblasts," *Bone*, vol. 32, no. 3, pp. 228–240, 2003, doi: 10.1016/S8756-3282(02)00978-X.

[31] F. Brock, J. Ostapkowicz, C. B. Ramsey, A. Wiedenhoeft, and C. Cartwright, "Paired dating of pith and outer edge (terminus) samples from pre-hispanic caribbean wooden sculptures," *Radiocarbon*, vol. 54, no. 3–4, pp. 677–688, 2012, doi: 10.1017/s0033822200047342.

[32] R. S. Lacruz, S. Habelitz, J. T. Wright, and M. L. Paine, "Implications for oral health and disease ion transport fluoride and dental health," *Physiol Rev*, no. 97, pp. 939–993, 2021, doi: 10.1152/physrev.00030.2016.

[33] M. Jágr, P. Ergang, S. Pataridis, M. Kolrosová, M. Bartoš, and I. Mikšík, "Proteomic analysis of dentin–enamel junction and adjacent protein-containing enamel matrix layer of healthy human molar teeth," *Eur. J. Oral Sci.*, vol. 127, no. 2, pp. 112–121, 2019, doi: 10.1111/eos.12594.

[34] F. C. M. Driessen and R. M. H. Verbeck, *Biominerals*. Boca Raton Fla, 1990.

[35] C. Kendall *et al.*, "Diagenesis of archaeological bone and tooth," *Palaeogeogr. Palaeoclimatol. Palaeoecol.*, vol. 491, no. November 2017, pp. 21–37, 2018, doi: 10.1016/j.palaeo.2017.11.041.

[36] M. Buckley, S. Fraser, J. Herman, N. D. Melton, J. Mulville, and A. H. Pálsdóttir, "Species identi fication of archaeological marine mammals using collagen fi ngerprinting," *J. Archaeol. Sci.*, vol. 41, 2014, doi: 10.1016/j.jas.2013.08.021.

[37] P. Garnero, "The role of collagen organization on the properties of bone," *Calcif. Tissue Int.*, no. 97, pp. 229–240, 2015, doi: 10.1007/s00223-015-9996-2.

[38] G. Dal Sasso, M. Lebon, I. Angelini, L. Maritan, D. Usai, and G. Artioli, "Bone diagenesis variability among multiple burial phases at Al Khiday (Sudan) investigated by ATR-FTIR spectroscopy," *Palaeogeogr. Palaeoclimatol. Palaeoecol.*, vol. 463, pp. 168–179, 2016, doi: 10.1016/j.palaeo.2016.10.005.

[39] L. Wilson and A. M. Pollard, "Here today, gone tomorrow? Integrated experimentation and geochemical modeling in studies of archaeological diagenetic change," *Acc. Chem. Res.*, vol. 35, no. 8, pp. 644–651, 2002, doi: 10.1021/ar000203s.

[40] F. Lugli *et al.*, "Enamel peptides reveal the sex of the Late Antique 'Lovers of Modena,'" *Sci. Rep.*, vol. 9, no. 1, pp. 1–8, 2019, doi: 10.1038/s41598-019-49562-7.

[41] E. Cappellini *et al.*, "Early Pleistocene enamel proteome sequences from Dmanisi resolve Stephanorhinus phylogeny performed analyses and data interpretation," *Bienvenido Martínez-Navarro*, vol. 574, no. 7776, pp. 103–107, 2020, doi: 10.6084/m9.figshare.7212746.

[42] N. J. De Winter, C. Snoeck, R. Schulting, T. Fernández-crespo, and P. Claeys, "High-resolution trace element distributions and models of trace element diffusion in enamel of Late Neolithic / Early Chalcolithic human molars from the Rioja Alavesa region (north-central Spain) help to separate biogenic from diagenetic trends," *Palaeogeogr. Palaeoclimatol. Palaeoecol.*, vol. 532, no. June, p. 109260, 2019, doi: 10.1016/j.palaeo.2019.109260.

[43] M. Singh, J. S. Sehrawat, and V. Sharma, "Sensitivity and specificity of various techniques for the trace elemental analysis on teeth: a critical review," *Brazilian J.*

Forensic Sci. Med. Law Bioeth., vol. 7, no. 4, pp. 230–251, 2018, doi: 10.17063/bjfs7(4)y2018230.

[44] B. K. Nelson, M. J. Deniro, M. J. Schoeninger, D. J. De Paolo, and P. E. Hare, "Effects of diagenesis on strontium, carbon, nitrogen and oxygen concentration and isotopic composition of bone," *Geochim. Cosmochim. Acta*, vol. 50, no. 9, pp. 1941–1949, 1986, doi: 10.1016/0016-7037(86)90250-4.

[45] K. A. Hoppe, P. L. Koch, and T. T. Furutani, "Assessing the preservation of biogenic strontium in fossil bones and tooth enamel," *Int. J. Osteoarchaeol.*, vol. 13, no. 1–2, pp. 20–28, 2003, doi: 10.1002/oa.663.

[46] T. Prohaska, C. Latkoczy, G. Schultheis, M. Teschler-Nicola, and G. Stingeder, "Investigation of Sr isotope ratios in prehistoric human bones and teeth using laser ablation ICP-MS and ICP-MS after Rb/Sr separation," *J. Anal. At. Spectrom.*, vol. 17, no. 8, pp. 887–891, 2002, doi: 10.1039/b203314c.

[47] J. Anné *et al.*, "Advances in bone preservation: Identifying possible collagen preservation using sulfur speciation mapping," *Palaeogeogr. Palaeoclimatol. Palaeoecol.*, vol. 520, no. May 2018, pp. 181–187, 2019, doi: 10.1016/j.palaeo.2019.01.030.

[48] L. Beck, J. P. Cuif, L. Pichon, S. Vaubaillon, A. Dambricourt Malassé, and R. L. Abel, "Checking collagen preservation in archaeological bone by non-destructive studies (Micro-CT and IBA)," *Nucl. Instruments Methods Phys. Res. Sect. B Beam Interact. with Mater. Atoms*, vol. 273, pp. 203–207, 2012, doi: 10.1016/j.nimb.2011.07.076.

[49] J. Anné *et al.*, "Visualisation of developmental ossification using trace element mapping," *J. Anal. At. Spectrom.*, vol. 32, no. 5, pp. 967–974, 2017, doi: 10.1039/c7ja00042a.

[50] C. N. Trueman and N. Tuross, "Trace elements in recent and fossil bone apatite," *Phosphates Geochemical, Geobiol. Mater. Importance*, vol. 48, no. Nriagu 1983, pp. 489–522, 2002, doi: 10.2138/rmg.2002.48.13.

[51] B. Demarchi, *Amino Acids and Proteins in fossil Biominerals*. 2020.

[52] P. V. Ullmann *et al.*, "Molecular tests support the viability of rare earth elements as proxies for fossil biomolecule preservation," *Sci. Rep.*, vol. 10, no. 1, pp. 1–11, 2020, doi: 10.1038/s41598-020-72648-6.

[53] J. H. Burton, T. D. Price, and W. D. Middleton, "Correlation of Bone Ba/Ca and Sr/Ca due to Biological Purification of Calcium," *J. Archaeol. Sci.*, vol. 26, no. 6, pp. 609–616, 1999, [Online]. Available: http://linkinghub.elsevier.com/retrieve/pii/S0305440398903788.

[54] D. N. Grimstead, A. E. Clark, and A. Rezac, "Uranium and vanadium concentrations as a trace element method for identifying diagenetically altered bone in the inorganic phase," *J. Archaeol. Method Theory*, vol. 25, no. 3, pp. 689–704, 2018, doi: 10.1007/s10816-017-9353-z.

[55] M. Vašinová Galiová *et al.*, "Elemental mapping in fossil tooth root section of Ursus arctos by laser ablation inductively coupled plasma mass spectrometry (LA-ICP-MS)," *Talanta*, vol. 105, pp. 235–243, 2013, doi: 10.1016/j.talanta.2012.12.037.

[56] C. N. Trueman, K. Privat, and J. Field, "Why do crystallinity values fail to predict the extent of diagenetic alteration of bone mineral?," *Palaeogeogr. Palaeoclimatol. Palaeoecol.*, vol. 266, no. 3–4, pp. 160–167, 2008, doi: 10.1016/j.palaeo.2008.03.038.

[57] C. Argentino, F. Lugli, A. Cipriani, S. Conti, and D. Fontana, "A deep fluid source of radiogenic Sr and highly dynamic seepage conditions recorded in Miocene seep carbonates of the northern Apennines (Italy)," *Chem. Geol.*, vol. 522, no. May, pp. 135–147, 2019, doi: 10.1016/j.chemgeo.2019.05.029.

[58] D. Herwartz, T. Tütken, K. P. Jochum, and P. M. Sander, "Rare earth element systematics of fossil bone revealed by LA-ICPMS analysis," *Geochim. Cosmochim. Acta*, vol. 103, pp. 161–183, 2013, doi: 10.1016/j.gca.2012.10.038.

[59] L. Kocsis, C. N. Trueman, and M. R. Palmer, "Protracted diagenetic alteration of

REE contents in fossil bioapatites: Direct evidence from Lu-Hf isotope systematics," *Geochim. Cosmochim. Acta*, vol. 74, no. 21, pp. 6077–6092, 2010, doi: 10.1016/j.gca.2010.08.007.

[60] M. H. Schweitzer, R. Avci, T. Collier, and M. B. Goodwin, "Microscopic, chemical and molecular methods for examining fossil preservation," *Comptes Rendus - Palevol*, vol. 7, no. 2–3, pp. 159–184, 2008, doi: 10.1016/j.crpv.2008.02.005.

[61] A. Retzmann *et al.*, "A combined chemical imaging approach using (MC) LA-ICP-MS and NIR-HSI to evaluate the diagenetic status of bone material for Sr isotope analysis," *Anal. Bioanal. Chem.*, vol. 411, no. 3, pp. 565–580, 2019, doi: 10.1007/s00216-018-1489-5.

[62] C. N. Trueman, L. Kocsis, M. R. Palmer, and C. Dewdney, "Fractionation of rare earth elements within bone mineral: A natural cation exchange system," *Palaeogeogr. Palaeoclimatol. Palaeoecol.*, vol. 310, no. 1–2, pp. 124–132, 2011, doi: 10.1016/j.palaeo.2011.01.002.

[63] C. N. Trueman *et al.*, "Comparing rates of recrystallisation and the potential for preservation of biomolecules from the distribution of trace elements in fossil bones," *Comptes Rendus Palevol*, vol. 7, no. 2–3, pp. 145–158, 2008, doi: 10.1016/j.crpv.2008.02.006.

[64] J. Anné, R. A. Wogelius, N. P. Edwards, A. Van Veelen, K. Ignatyev, and P. L. Manning, "Chemistry of bone remodelling preserved in extant and fossil Sirenia," *Metallomics*, vol. 8, no. 5, pp. 508–513, 2016, doi: 10.1039/c5mt00311c.

[65] B. Pemmer *et al.*, "Spatial distribution of the trace elements zinc , strontium and lead in human bone tissue," *Bone*, vol. 57, pp. 184–193, 2013, doi: 10.1016/j.bone.2013.07.038.

[66] K. Weber *et al.*, "Diagenetic stability of non-traditional stable isotope systems (Ca, Sr, Mg, Zn) in teeth – An in-vitro alteration experiment of biogenic apatite in isotopically enriched tracer solution," *Chem. Geol.*, vol. 572, p. 120196, 2021, doi:

10.1016/j.chemgeo.2021.120196.

[67] M. Duval, M. Aubert, J. Hellstrom, and R. Grün, "High resolution LA-ICP-MS mapping of U and Th isotopes in an early Pleistocene equid tooth from Fuente Nueva-3 (Orce, Andalusia, Spain)," *Quat. Geochronol.*, vol. 6, no. 5, pp. 458–467, 2011, doi: 10.1016/j.quageo.2011.04.002.

[68] M. S. A. Horstwood, J. A. Evans, and J. Montgomery, "Determination of Sr isotopes in calcium phosphates using laser ablation inductively coupled plasma mass spectrometry and their application to archaeological tooth enamel," *Geochim. Cosmochim. Acta*, vol. 72, no. 23, pp. 5659–5674, 2008, doi: 10.1016/j.gca.2008.08.016.

[69] C. Stadlbauer, C. Reiter, B. Patzak, G. Stingeder, and T. Prohaska, "History of individuals of the 18th / 19th centuries stored in bones , teeth , and hair analyzed by LA – ICP – MS — a step in attempts to confirm the authenticity of Mozart ' s skull," *Anal. Bioanal. Chem.*, vol. 388, pp. 593–602, 2007, doi: 10.1007/s00216-007-1266-3.

[70] T. Tacail, L. Kova, J. Br, and V. Balter, "Science of the Total Environment Spatial distribution of trace element Ca-normalized ratios in primary and permanent human tooth enamel," *Sci. Total Environ.*, vol. 604, pp. 308–318, 2017, doi: 10.1016/j.scitotenv.2017.06.021.

[71] S. Weiner and O. Bar-Yosef, "States of preservation of bones from prehistoric sites in the Near East: A survey," *J. Archaeol. Sci.*, vol. 17, no. 2, pp. 187–196, 1990, doi: 10.1016/0305-4403(90)90058-D.

[72] Z. Patonai *et al.*, "Novel dating method to distinguish between forensic and archeological human skeletal remains by bone mineralization indexes," *Int. J. Legal Med.*, vol. 127, no. 2, pp. 529–533, 2013, doi: 10.1007/s00414-012-0785-4.

[73] E. F. Greene, S. Tauch, E. Webb, and D. Amarasiriwardena, "Application of diffuse reflectance infrared Fourier transform spectroscopy (DRIFTS) for the identification of potential diagenesis and crystallinity changes in teeth,"

Microchem. J., vol. 76, no. 1–2, pp. 141–149, 2004, doi: 10.1016/j.microc.2003.11.006.

[74] I. Kontopoulos *et al.*, "Screening archaeological bone for palaeogenetic and palaeoproteomic studies," *PLoS One*, vol. 15, no. 6, pp. 1–17, 2020, doi: 10.1371/journal.pone.0235146.

[75] C. N. G. Trueman, A. K. Behrensmeyer, N. Tuross, and S. Weiner, "Mineralogical and compositional changes in bones exposed on soil surfaces in Amboseli National Park, Kenya: Diagenetic mechanisms and the role of sediment pore fluids," *J. Archaeol. Sci.*, vol. 31, no. 6, pp. 721–739, 2004, doi: 10.1016/j.jas.2003.11.003.

[76] G. Sciutto *et al.*, "Single and multiplexed immunoassays for the chemiluminescent imaging detection of animal glues in historical paint cross-sections," *Anal. Bioanal. Chem.*, vol. 405, no. 2–3, pp. 933–940, 2013, doi: 10.1007/s00216-012-6463-z.

[77] G. Sciutto *et al.*, "Localization of proteins in paint cross-sections by scanning electrochemical microscopy as an alternative immunochemical detection technique," *Anal. Chim. Acta*, vol. 831, pp. 31–37, 2014, doi: 10.1016/j.aca.2014.04.058.

[78] A. Roda *et al.*, "Chemiluminescent Low-Light Imaging of Biospecific Reactions on Macro- and Microsamples Using a Videocamera-Based Luminograph," *Anal. Chem.*, vol. 68, no. 7, pp. 10733–1080, 1996.

[79] F. Sforna, M.C. and Lugli, "MapIT !: a simple and user-friendly MATLAB script to elaborate elemental distribution images from LA – ICP – MS data," *J. Anal. At. Spectrom.*, vol. 32, no. 5, pp. 1035–1043, 2017, doi: 10.1039/x0xx00000x.

[80] H. P. Longerich, S. E. Jackson, and D. Gunther, "Laser ablation inductively coupled plasma mass spectrometric transient signal data acquisition and analyte concentration calculation," *J. Anal. At. Spectrom.*, vol. 11, no. September, 1996.

[81] K. P. Jochum, U. Nohl, K. Herwig, E. Lammel, B. Stoll, and A. W. Hofmann, "GeoReM: A new geochemical database for reference materials and isotopic

standards," *Geostand. Geoanalytical Res.*, vol. 29, no. 3, pp. 333–338, 2005, doi: 10.1111/j.1751-908x.2005.tb00904.x.

[82] S. Voerkelius *et al.*, "Strontium isotopic signatures of natural mineral waters, the reference to a simple geological map and its potential for authentication of food," *Food Chem.*, vol. 118, no. 4, pp. 933–940, 2010, doi: 10.1016/j.foodchem.2009.04.125.

[83] T. Tütken, T. W. Vennemann, and H. U. Pfretzschner, "Early diagenesis of bone and tooth apatite in fluvial and marine settings: Constraints from combined oxygen isotope, nitrogen and REE analysis," *Palaeogeogr. Palaeoclimatol. Palaeoecol.*, vol. 266, no. 3–4, pp. 254–268, 2008, doi: 10.1016/j.palaeo.2008.03.037.

[84] T. Tütken, "Die Bedeutung der Knochenfrühdiagenese für die Erhaltungsfähigkeit in vivo erworbener Element — und Isotopenzusammensetzungen in fossilen Knochen.," *On-line Diss. Univ. Tübingen*, 2003.

[85] G. J. van Klinken and R. E. M. Hedges, "Experiments on Collagen-Humic Interactions: Speed of Humic Uptake, and Effects of Diverse Chemical Treatments," *J. Archaeol. Sci.*, vol. 22, no. 2, pp. 263–270, 1995, doi: 10.1006/jasc.1995.0028.

[86] A. Boaks, D. Siwek, and F. Mortazavi, "The temporal degradation of bone collagen: A histochemical approach," *Forensic Sci. Int.*, vol. 240, pp. 104–110, 2014, doi: 10.1016/j.forsciint.2014.04.008.

[87] F. De Chaumont *et al.*, "Icy: An open bioimage informatics platform for extended reproducible research," *Nat. Methods*, vol. 9, no. 7, pp. 690–696, 2012, doi: 10.1038/nmeth.2075.

[88] A. Nava, L. Bondioli, A. Coppa, C. Dean, P. F. Rossi, and C. Zanolli, "New regression formula to estimate the prenatal crown formation time of human deciduous central incisors derived from a Roman Imperial sample (Velia, Salerno, Italy, I-II cent. CE)," *PLoS One*, vol. 12, no. 7, pp. 1–21, 2017, doi: 10.1371/journal.pone.0180104.

[89] A. P. Mamede, D. Gonçalves, M. P. M. Marques, and L. A. E. Batista de Carvalho, "Burned bones tell their own stories: A review of methodological approaches to assess heat-induced diagenesis," *Appl. Spectrosc. Rev.*, vol. 53, no. 8, pp. 603–635, 2018, doi: 10.1080/05704928.2017.1400442.

[90] G. A. Castiblanco, D. Rutishauser, L. L. Ilag, S. Martignon, J. E. Castellanos, and W. Mejía, "Identification of proteins from human permanent erupted enamel," *Eur. J. Oral Sci.*, vol. 123, no. 6, pp. 390–395, 2015, doi: 10.1111/eos.12214.

[91] I. Guagliardi *et al.*, "Uranium, thorium and potassium insights on Campania region (Italy) soils: Sources patterns based on compositional data analysis and fractal model," *J. Geochemical Explor.*, vol. 212, no. October 2019, 2020, doi: 10.1016/j.gexplo.2020.106508.

[92] B. Reynard and V. Balter, "Trace elements and their isotopes in bones and teeth: Diet, environments, diagenesis, and dating of archeological and paleontological samples," *Palaeogeogr. Palaeoclimatol. Palaeoecol.*, vol. 416, pp. 4–16, 2014, doi: 10.1016/j.palaeo.2014.07.038.

[93] S. Dallongeville, N. Garnier, C. Rolando, and C. Tokarski, "Proteins in art, archaeology, and paleontology: from detection to identification," 2016, doi: 10.1021/acs.chemrev.5b00037.

[94] N. A. Stewart, R. F. Gerlach, R. L. Gowland, K. J. Gron, and J. Montgomery, "Sex determination of human remains from peptides in tooth enamel," *Proc. Natl. Acad. Sci. U. S. A.*, vol. 114, no. 52, pp. 13649–13654, 2017, doi: 10.1073/pnas.1714926115.

[95] N. Procopio, A. T. Chamberlain, and M. Buckley, "Exploring biological and geological age-related changes through variations in intra- and intertooth proteomes of ancient dentine," *J. Proteome Res.*, vol. 17, no. 3, pp. 1000–1013, 2018, doi: 10.1021/acs.jproteome.7b00648.

[96] J. Hendy, "Ancient protein analysis in archaeology," *Sci. Adv.*, vol. 7, no. 3, pp. 1–12, 2021, doi: 10.1126/sciadv.abb9314.

[97] M. T. Kirchner, H. G. M. Edwards, D. Lucy, and A. M. Pollard, "Ancient and modern specimens of human teeth: A fourier transform Raman spectroscopic study," *J. Raman Spectrosc.*, vol. 28, no. 2–3, pp. 171–178, 1997, doi: 10.1002/(sici)1097-4555(199702)28:2/3<171::aid-jrs63>3.0.co;2-v.

[98] Y. M. Coulson-Thomas *et al.*, "The identification of proteoglycans and glycosaminoglycans in archaeological human bones and teeth," *PLoS One*, vol. 10, no. 6, pp. 1–21, 2015, doi: 10.1371/journal.pone.0131105.

[99] N. A. Stewart *et al.*, "The identification of peptides by nanoLC-MS/MS from human surface tooth enamel following a simple acid etch extraction," *RSC Adv.*, vol. 6, no. 66, pp. 61673–61679, 2016, doi: 10.1039/c6ra05120k.

[100] P. A. Fang, J. F. Conway, H. C. Margolis, J. P. Simmer, and E. Beniash, "Hierarchical self-assembly of amelogenin and the regulation of biomineralization at the nanoscale," *Proc. Natl. Acad. Sci. U. S. A.*, vol. 108, no. 34, pp. 14097–14102, 2011, doi: 10.1073/pnas.1106228108.

[101] C. Froment *et al.*, "Analysis of 5000 year-old human teeth using optimized large-scale and targeted proteomics approaches for detection of sex-specific peptides," *J. Proteomics*, 2020, doi: 10.1016/j.jprot.2019.103548.

[102] A. Nanci *et al.*, "Comparative immunochemical analyses of the developmental expression and distribution of ameloblastin and amelogenin in rat incisors," *J. Histochem. Cytochem.*, vol. 46, no. 8, pp. 911–934, 1998, doi: 10.1177/002215549804600806.

[103] M. Nakamura, P. Bringas, A. Nanci, M. Zeichner-David, B. Ashdown, and H. C. Slavkin, "Translocation of enamel proteins from inner enamel epithelia to odontoblasts during mouse tooth development," *Anat. Rec.*, vol. 238, no. 3, pp. 383–396, 1994, doi: 10.1002/ar.1092380313.

[104] T. A. Mitsiadis, A. Filatova, G. Papaccio, M. Goldberg, I. About, and P. Papagerakis, "Distribution of the amelogenin protein in developing, injured and carious human teeth," *Front. Physiol.*, vol. 5, no. Nov, 2014, doi:

10.3389/fphys.2014.00477.

[105] A. L. J. J. Bronckers *et al.*, "Dentin sialoprotein: biosynthesis and developmental appearance in rat tooth germs in comparison with amelogenins, osteocalcin and colagen type-I," *Cell Tissue Res.*, vol. 272, no. 2, pp. 237–247, 1993, doi: 10.1007/BF00302729.

[106] R. Mazzeo, A. Roda, and S. Prati, "Analytical chemistry for cultural heritage: A key discipline in conservation research," *Anal. Bioanal. Chem.*, vol. 399, no. 9, pp. 2885–2887, 2011, doi: 10.1007/s00216-011-4672-5.

[107] T. M. Santiago-Rodriguez *et al.*, "Natural mummification of the human gut preserves bacteriophage DNA," *FEMS Microbiol. Lett.*, vol. 363, no. 1, pp. 1–8, 2015, doi: 10.1093/femsle/fnv219.

[108] L. Ye *et al.*, "Amelogenins in Human Developing," pp. 814–818, 2006.

[109] V. D. Cheyne and J. T. Oba, "Avarage weights of the permanent teeth, including the relative amounts of enamel to dentin and cementum," *J. Dent. Res.*, vol. 22, no. 3, pp. 181–184, 1943.

[110] S. J. Marshall, M. Balooch, S. Habelitz, G. Balooch, R. Gallagher, and G. W. Marshall, "The dentin - enamel junction - a natural, multilevel interface," *J. Eur. Ceram. Soc.*, vol. 23, no. 15, pp. 2897–2904, 2003, doi: 10.1016/S0955-2219(03)00301-7.

[111] T. Tütken and T. W. Vennemann, "Fossil bones and teeth: Preservation or alteration of biogenic compositions?," *Palaeogeogr. Palaeoclimatol. Palaeoecol.*, vol. 310, no. 1–2, pp. 1–8, 2011, doi: 10.1016/j.palaeo.2011.06.020.

[112] T. A. Monson, D. Fecker, and M. Scherrer, "Neutral evolution of human enamel–dentine junction morphology," *Proc. Natl. Acad. Sci. U. S. A.*, vol. 117, no. 46, p. 29241, 2020, doi: 10.1073/pnas.2021545117.

[113] M. Goldberg, D. Septier, O. Rapoport, M. Young, and L. Ameye, "Biglycan is a repressor of amelogenin expression and enamel formation: An emerging

hypothesis," *J. Dent. Res.*, vol. 81, no. 8, pp. 520–524, 2002, doi: 10.1177/154405910208100804.

CHAPTER 3

NEW APPLICATION OF PORTABLE MICRONIR SPECTROSCOPY ON ANCIENT BONES

Part of the chapter is reproduced from: "A new miniaturised short-wave infrared (SWIR) spectrometer for on-site cultural heritage investigations.

E. Catelli, G. Sciutto, S. Prati, M.V. Chavez Lozano, L. Gatti, F. Lugli, S. Silvestrini, S. Benazzi, E. Genorini, R. Mazzeo

Talanta, 2020, vol. 218

3.1. MicroNIR spectroscopy applied to cultural heritage

Near infrared (NIR) region goes from 780 to 2500 nm (from 12820 cm^{-1} to 4000 cm^{-1}) and it has been widely applied in food, pharmaceutical and forensic fields [1]–[4]. NIR spectrometers can be applied on liquid samples in transmission mode, or on solid samples in reflectance mode [5]. They have been used as both in bench and portable systems, developing miniaturize instruments. The main advantages of a miniaturized NIR spectrometer are to be fast, non-invasive, cost effective, to have a high-penetration radiation beam and to require no sample preparation [5]. Moreover, the miniaturization allows an on-site investigation of samples in different fields.

In last decades, it has been also applied on cultural heritage, thanks to the possibility to carry out analyses on-site without moving the work of art in a lab, allowing investigations also on immovable or precious cultural heritage. There are studies especially on stones [6], paintings [6], [7] and illuminated manuscript [8], [9], using optical fibre spot reflectance spectroscopy with different spectral range according to the type of sensor. Recently, researchers have shown a growing interest in archaeological field taking into account the possibility to use NIR spectrometers to investigate ancient bones [10]–[12].

NIR spectroscopy is based on the interaction between NIR radiation and sample, according to its chemical composition, leading to a spectrum with weak absorption bands. This region is useful because combination and overtone bands are not distorted by specular reflection, and they provide important chemical information. However, in this range only functional groups containing N-H, C-H, O-H, C-O and C-C bonds produce significant vibrational bands and they are broader and sometimes overlapped than the fundamental ones [3]–[5], [13], [14]. Moreover, if the surface is not planar, these peaks are enhanced by volume reflection.

Due to the weak and broad bands in NIR spectra, chemometric elaborations are essential to extrapolate and interpret relevant information. Indeed, other factors complicate NIR spectra, such as water, scattering effects or instrumental noise, making difficult to resolve usable baseline for peak-high or peak-area quantitative investigations as in mid-IR. For these reasons, adequate spectra processing is fundamental. Among the most used elaborations there are normalization methods to reduce instrument sensitivity effects,

derivatives to eliminate insignificant baseline changes and smooth to reduce instrumental noise [4], [5].

3.2. Chemometrics applied to NIR spectroscopy

Chemometrics is the chemical discipline in analytical chemistry, that interprets and solves multivariate problems. The International Chemometric Society defines this discipline as follow:

"Chemometrics is the chemical discipline that uses mathematical and statistical methods a) to design or select optimal measurements procedures and experiments, and b) to provide the maximum useful information for chemical problems, by analyzing chemical, physical or theoretical (computed) data."

Chemometrics represents the fusion and cooperation between mathematics and chemistry. Historically, NIR spectroscopy provided an important increase of chemometric application between 1980 and 1990, in particular in food and pharmaceutical field [15].

On complex matrix, such as different cultural heritage materials, univariate investigations, which consider one variable at a time, are not adequate. On the contrary, multivariate methods are able to consider the whole information obtained from the analysis [15], [16]. Chemometric elaborations are a useful strategy for chemists to screen their samples understanding which factors are fundamental in a process, such as using unsupervised exploratory analysis. Moreover, they offer the opportunity to optimize data for a clearer interpretation and to save time applying some data preprocessing. Finally, chemometric allows qualitative and quantitative analysis using simpler classification supervised analysis or more complex models, such as regression analysis [15], [17].

Data collected with different methods are usually organized in matrices, composed by rows, which correspond to samples, and columns, which correspond to each variable measured. Before any type of data interpretation, a correction of undesired effects must be done.

3.2.1. Data preprocessing

Different mathematical elaborations have been used according to the type of data and to the type of undesired effects. Focusing on NIR spectra, the main problems are vertical shifts and drifts, overlapping of different signals, random noise and undesired systematic variations (Figure 3.1) [4]. Some problems could be caused by the sample surface or to investigation conditions or to the instrument setting. However, in many cases some rows and columns elaborations of data matrices are needed to compress data, to emphasize small differences and to correct all distortions after data acquisition. This elaboration after the acquisition reduces the time of analysis, allowing investigation on more samples [17].

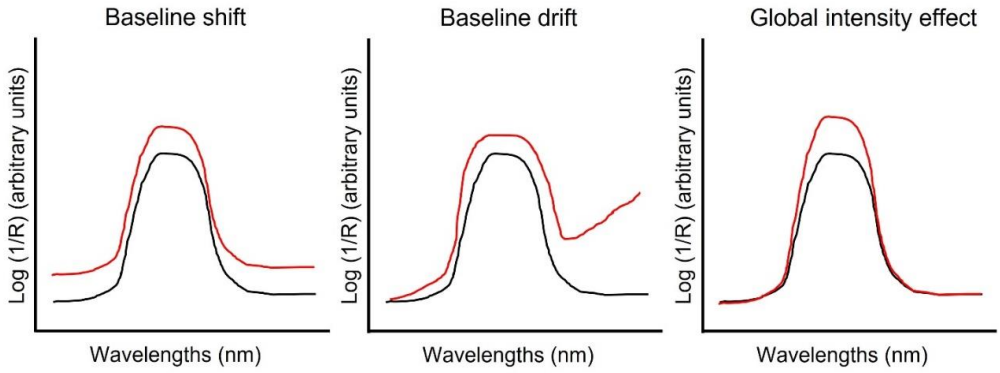

Figure 3.1. Undesired signal effects in NIR spectra: baseline shift, baseline drift and global intensity effect.

Row centering

Row preprocessing allows a correction of systematic differences among signals, acting on each one.

Each signal (y_i), defined by V variables (e.g., the absorption values in a NIR spectrum), is corrected individually by subtracting its mean value ($\bar{y}_i$) from each single value ($y_{i,v}$). The values of the row-centered signal ($y^*_{i,v}$) are obtained by [17]:

$$y^*_{i,v} = y_{i,v} - \bar{y}_i \qquad (3.1)$$

Row centering removes systematic location differences, especially baseline shifts, from a set of signals. This happens because, after transformation, the mean value of each signal is equal to 0 [17].

Standard normal variate transform (SNV)

Standard normal variate transform (SNV) is a mathematical technique used to transform signal, especially applied in spectroscopy, that is useful to correct baseline shifts and global intensity variations [17].

Each signal (y_i) is row-centered and then scaled by dividing the single values by the signal standard deviation (S_i). The values of the SNV transformed signal are obtained by the formula [17]:

$$y_{i,v}^{*} = \frac{y_{i,v} - \bar{y}_i}{S_i} \qquad (3.2.)$$

After the elaboration, each signal presents a mean value equal to 0 and a standard deviation equal to 1, with both location and dispersion systematic differences corrected.

SNV has the distinctive potential to shift informative regions all along the signal range; therefore, the original results interpretation may be misleading [17], [18].

Derivation after smoothing

The numerical differentiation of digitized signals allows different applications according to the derivation order, such as signal resolution improvement, increasing of the apparent resolution of overlapping peaks, emphasis of small structural differences between nearly identical signals, and correction of baseline shifts and drifts. In case of spectra, it means that inflection points in close peaks become turning points in derivatives [15], [17], [19].

In more detail, the first derivative of a signal $y = f(x)$ is the rate of change of y with x (*i.e.*, $y' = dy/dx$), which can be described as the slope of the tangent to the signal at each point. It returns null segments in correspondence to constant bands of the original signal and provides a correction for addictive effects [17].

The second derivative can be defined as a further derivation of the first one ($y'' = d^2y/dx^2$) and it describes a measure of the curvature of the original signal, thus the rate of change of its slope [17].

A disadvantageous effect of derivation could be an increase of the noise signal, which is typically characterized by high-frequency slope variations. To overcome this problem, smoothing algorithms have been applied, such as the Savitzky-Golay, which is a moving window averaging method permitting a simultaneous smooth and derivation of data [15], [17], [20], [21].

Column preprocessing (centering and autoscaling)

Column preprocessing is applied on data to act on each variable individually correcting systematic differences among variables. We can distinguish between column centering and column autoscaling.

Column centering corrects individually each variable that defines a set of signals. This is mathematically calculated subtracting its mean value ($\bar{y}_v$) from each value ($y_{i,v}$), as in the following formula [17]:

$$y^*_{i,v} = y_{i,v} - \bar{y}_v \qquad (3.3.)$$

After transformation, the mean value of each column is 0, to eliminate systematic location differences among variables.

Column autoscaling is often a default data pretreatment and it is particularly useful for data of different type. From a mathematical point of view, each variable mean value ($\bar{y}_v$) is subtracted from each of its values and then divided by its standard deviation (S_v). The autoscaled values are defined by [17]:

$$y^*_{i,v} = \frac{y_{i,v} - \bar{y}_v}{S_v} \qquad (3.4.)$$

This column treatment permits to eliminate systematic location and dispersion differences among heterogenous variables, assigning them the same importance and increasing differences among samples. In case of IR spectra, in which variables present the same nature and measurement unit, autoscaling could be useful in case of relatively low mean value and/or standard deviation, which enclose fundamental information. Otherwise, this operation could cause a reduction of signal-to-noise ratio, giving the same importance to noise and signals [17].

3.2.2. Data processing

Principal components analysis (PCA)

Principal Component Analysis (PCA) is the most used multivariate statistical methods in chemometric, thanks to the possibility to explore patterns in data. PCA is an unsupervised explanatory method that searches for directions of maximum variance, within a multivariate data space, based on the idea that high variance (*i.e.*, high variability) corresponds to large quantity of information. Thus, PCA represents a reduction of large and complex matrices in simpler ones, preserving their information. The searched directions take the name of principal components (PCs) and they are orthogonal, implying that they are not inter-correlated and they never take into account duplicate information, minimizing the squared reconstruction error. Therefore, first PC describes the maximum variance, while the second one is the direction with higher variance among directions orthogonal to the first one. In other words, PCs are new variables compounded by the linear combination of the old ones multiplied with coefficients called loadings. Loadings are mathematically described as the expression of the cosine of the angles between the PCs and the original variables, representing their role in PCs definition: if the absolute value of the cosine is high, the two directions are closer and its contribution for the PC definition is higher [15], [17], [22], [23]. The graphical result is a rotation of the original space in PCs space, mathematically described as:

$$S_{NV} = X_{NV} L_{VV} \qquad (3.5.)$$

where S is the score matrix, X is the original matrix and L is the loading orthogonal matrix.

The widely use of PCA is attributable to the possibility to obtain plots using two or three PCs representing the objects (score scatter plot), the original variables (loading plots) or both (biplots). Score scatter plots allow the observation of the objects distribution in the plane described by two or three selected PCs, providing information about multidimensional structures existing among the objects, such as similarity, groupings, and trend patterns. Loading plots are bi-dimensional representations of the loading values of the original variables on two selected PCs, providing information about the importance

of the variables and about their inter-correlation, with respect to the fraction of variance (i.e., information) explained by those PCs. Relationships existing between variables and objects can be described by joint examination of loading and score plots [15], [17], [22], [23].

Regression: Partial Least Squares (PLS)

Partial Least Square (PLS) is a regression technique, namely a statistical method to provide model for quantitative predictions on unknown samples. PLS literally signify projections onto latent structures, called latent variables (LVs), which are directions in the predictors space. This means that the first LV is defined by the maximum covariance with the selected response variable. Then it is subtracted from both the original predictors and the response [15], [17].

The optimal number of LVs is defined evaluating the prediction error with the best validation strategy. The two main parameters used are standard deviation of the error of calibration (SDEC), if calculated with the objects used for model building, or standard deviation of the error of prediction (SDEP), if calculated with different objects. Usually, the calibration error decreases with a higher number of LVs, because of the fitting increment. On the contrary, it increases in case of a too simple model with a low number of LVs. In order to solve this problem, an accurate choice of the number of LVs can be done for instance selecting the SDEP absolute minimum [15], [17].

The dataset used for model creation is called “training set”, while the dataset of unknown samples is called “test set”. The configuration of the training set is essential for a successful result. Indeed, if it is not clear or too small, the prediction will be difficult and the error increases. For the evaluation of the predictive accuracy of the model different validation methods can be applied. The first one is based on the use of the training and the test set, while a more efficient strategy uses three subsets (training, optimization and evaluation set)[15], [17].

In addition to traditional PLS, some variations have been used to develop nonlinear models or to predict more variables together [15], [17].

3.3. New portable microNIR prototype for selection of bone samples with enough collagen content

Due to diagenetic processes collagen preservation in ancient bones is heterogeneous, not only in different samples from the same site but also within the same specimen. The traditional techniques applied for bones investigation require an enough amount of collagen. For this reason, there is the necessity of adequate prescreening methods in order to select samples for further specific destructive analysis, without a useless loss of bone, money and time.

For this aim, the potential of a new miniaturized SWIR prototype has been proposed during this PhD thesis as a non-destructive, fast and portable method for preliminary prescreening of ancient bones, thanks to the collaboration with the Bones Lab (Ravenna Campus).

3.3.1. Materials and method

3.3.1.1. Standard samples

In order to evaluate the potential of the method for collagen prescreening, some standards with known percentage of collagen have been prepared in laboratory. The standards preparation involved the grinding of 200 mg of HA (Sigma-Aldrich) with different amount of pork collagen (Sigma-Aldrich): 0 %, 1 %, 3 %, 5 %, 8 %, 10 %, 15 %, 18 % and 20 %. The percentage were selected according to references, considering the maximum collagen content in fresh bone (20 %) and the minimum (0 %) [24]–[26]. For each percentage, standards were made in triplicate.

3.3.1.2. Real samples

After standard analysis, 7 real bone samples coming from different Italian archaeological sites (Table 3.1.) were analyzed. Samples were selected based on their ages (from ca. 45 ka to Early modern times) and provenance (from Southern to Northern Italy). Most of them (RB63, R313, UC86, UC88) were undetermined bone fragments of animal origin, while two bones (RP and SMM) belonged to Homo sapiens and sample OV was attributable to an ovicaprid. Bone samples were characterized by different state of conservation, according to the excavation site and age. On these bases it was possible to

argue that samples RP, SMM and OV could present a higher collagen content in comparison to samples RB and to those from Uluzzo archaeological site, which were more ancient than the previous.

Table 3.1. Bone samples investigated.

Sample	Provenance	Date	Species	Anatomy	Notes
RP	Roccapelago (Modena, Italy)	16th-18th cent.	Homo sapiens	Femur section	Partially mummified individual
SMM	Santa Maria Maggiore (Trento, Italy)	15th cent.	Homo sapiens	Talus	-
OV	Ostra Vetere (Ancona, Italy)	6th-7th cent.	Ovicaprid	Tibia	-
RB63	Riparo del Broion (Vicenza, Italy)	45 ka	Undetermined/fauna	Bone fragment	-
R313	Uluzzo (Nardò, Italy)	42 ka	Undetermined/fauna	Bone fragment	Badly preserved
UC86	Uluzzo (Nardò, Italy)	42 ka	Undetermined/fauna	Bone fragment	Badly preserved
UC88	Uluzzo (Nardò, Italy)	42 ka	Undetermined/fauna	Bone fragment	Badly preserved

3.3.1.3. Portable microNIR prototype and data elaboration

The NIR prototype was designed by Viavi Solutions (JDSU Corporation, Milpitas, CA) [1], [2]. The system measures the diffuse reflectance in the spectral region of 1208–2160.5 nm (8278– 4629 cm^{-1}). It is connected to a portable computer via USB port. It owes its potential to a linear-variable filter (LVF), used as dispersing element, allowing a constitutionally stability with temperature and time and a reduction of optical train. It is directly connected to a 128-pixel linear Indium Gallium Arsenide (InGaAs) uncooled detector, which results in a compact instrument. This ultra-compact device is coupled to a miniaturized redout electronics and two tungsten light bulbs, which were used as the radiation source (Figure 3.2.). The spot of analysis is approximately 3 mm in diameter.

All the collected spectra were recorded nominal spectral at a nominal resolution of 7.68 nm. Spectralon was used as the NIR-reflectance standard with 99% diffuse reflectance. The spectra acquisition was performed putting the instrument in contact with samples, with an integration time of 3 ms and 1000 scans resulting in a measurement time of 3 s per sample (Figure 3.3.).

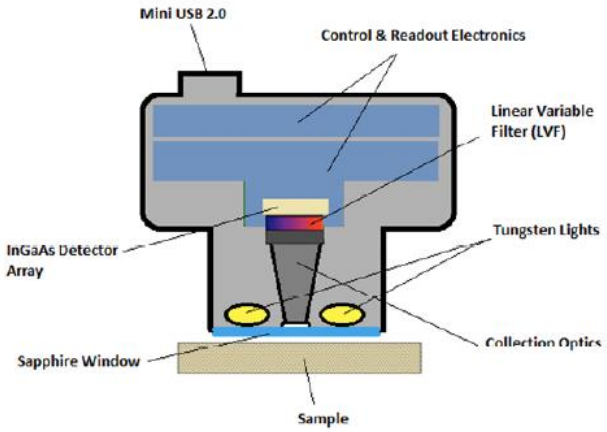

Figure 3.2. Description of the MicroNIR in diffuse reflection mode [1].

The MicroNIR Pro software (JDSU Corporation, Milpitas, CA) was used for data acquisition and multivariate data processing was performed by means of in-house Matlab routines (The Mathworks Inc., Natick, USA). Suitable row pre-treatments were selected and applied in attempt to minimize systematic unwanted variations, which could affect the signals. In more details, SNV transform was selected to correct both baseline shifts and global intensity variations, while first Savitzky-Golay first derivation was applied to enhance details within complex spectral features (*e.g.*, unresolved broad shape bands). Afterwards, the spectra range considered was from 1254.9 to 2122.1 nm. Column centering was performed prior to principal component analysis (PCA).

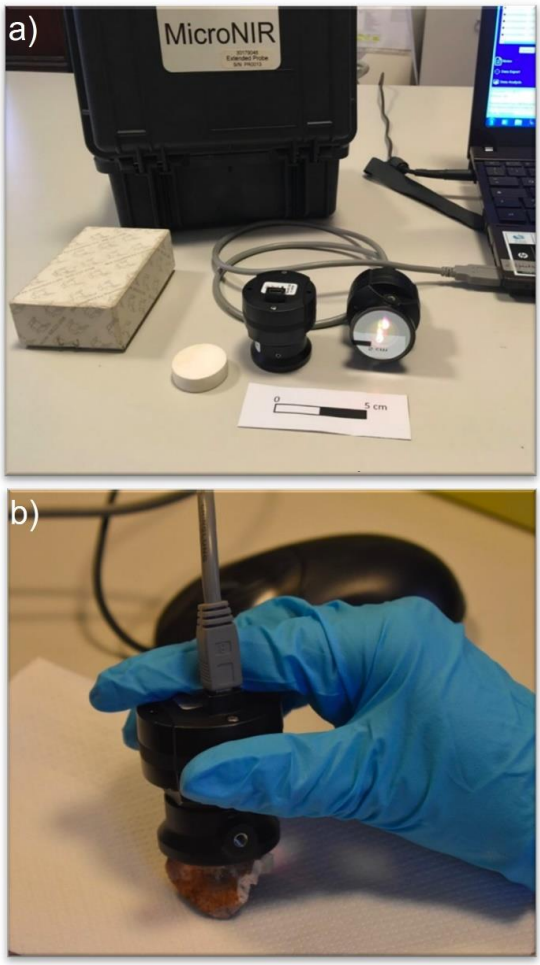

Figure 3.3. MicroNIR Viavi Solutions (a) and its application on bone sample (b).

3.3.2. Results and discussion

The characterization of bone proteins in ancient human and animal remains is essential for phylogenetic and diagenetic studies. However, as said in previous chapters, traditional methods for providing these information are dependent to the collagen amount and distribution. Thus, prescreening methods are essential for researchers in order to select samples. Raman and FTIR spectroscopy have been proposed as screening techniques for collagen detection on bones, both in laboratory and on-site [27]–[32]. However, these are destructive and/or time consuming, restricting the number of samples for the application.

NIR has been applied both for taxonomical discrimination of bones and for the evaluation of their preservation status [11], [12], [33]–[36]. Bone collagen content has been detected thanks to the presence of diagnostic proteinaceous peaks [11], [12], [35]. Until now, bones have been mainly analyzed in laboratories with benchtop instruments, while only a portable NIR spectrometer coupled with fibre-optic reflectance probe has been recently applied for *in situ* investigations [11].

Our new miniaturized NIR prototype, which is cost-effective and easier to use than the conventional ones, has shown great potential to become a fast and simple method for *in situ* bone prescreening.

3.3.2.1. Standard samples

To evaluate the potential of our instrument, we decided to test it on standard samples before real bones analysis. Despite their structurally difference from real bones, they were useful to recognize characteristic bands attributable to hydroxyapatite and collagen, evaluating their variability according to their percentage.

Raw and preprocessed spectra (Figure 3.4) clearly showed peaks attributed to the mineral fraction. Indeed, there were always visible bands around 1400 nm and 1910 nm, assigned to OH stretching of hydroxyapatite. Spectra of standards with high collagen content allowed the identification of collagen bands around 1690 nm and 1740 nm (1668 nm and 1722 nm in derivative), assigned to C-H stretching vibration, and at 2045 nm (2029 nm in first derivative), attributed to N-H combination band [11]. The other bands identified in pure collagen spectrum cannot be identified in standards due to the overlapping with hydroxyapatite bands.

The PC1 vs PC2 score plot allows a recognizable separation among samples (Figure 3.4.c). Looking to the score plot (each point is a spectrum acquired), standards from 0 % to 10 % a clear separation among samples was possible, while from 15 % to 20 % the separation was less evident. The loading plot revealed the fundamental role of the band at 2045 nm (2029 nm in first derivative), allowing a separation of samples according to their collagen percentage.

The results obtained from the analysis of spectra and PCA showed the ability of our prototype, combined with chemometric data treatment, to distinguish among samples with different content of collagen. Moreover, this first evaluation of standards was essential to be sure about mineral and organic peaks attribution and role in samples distribution.

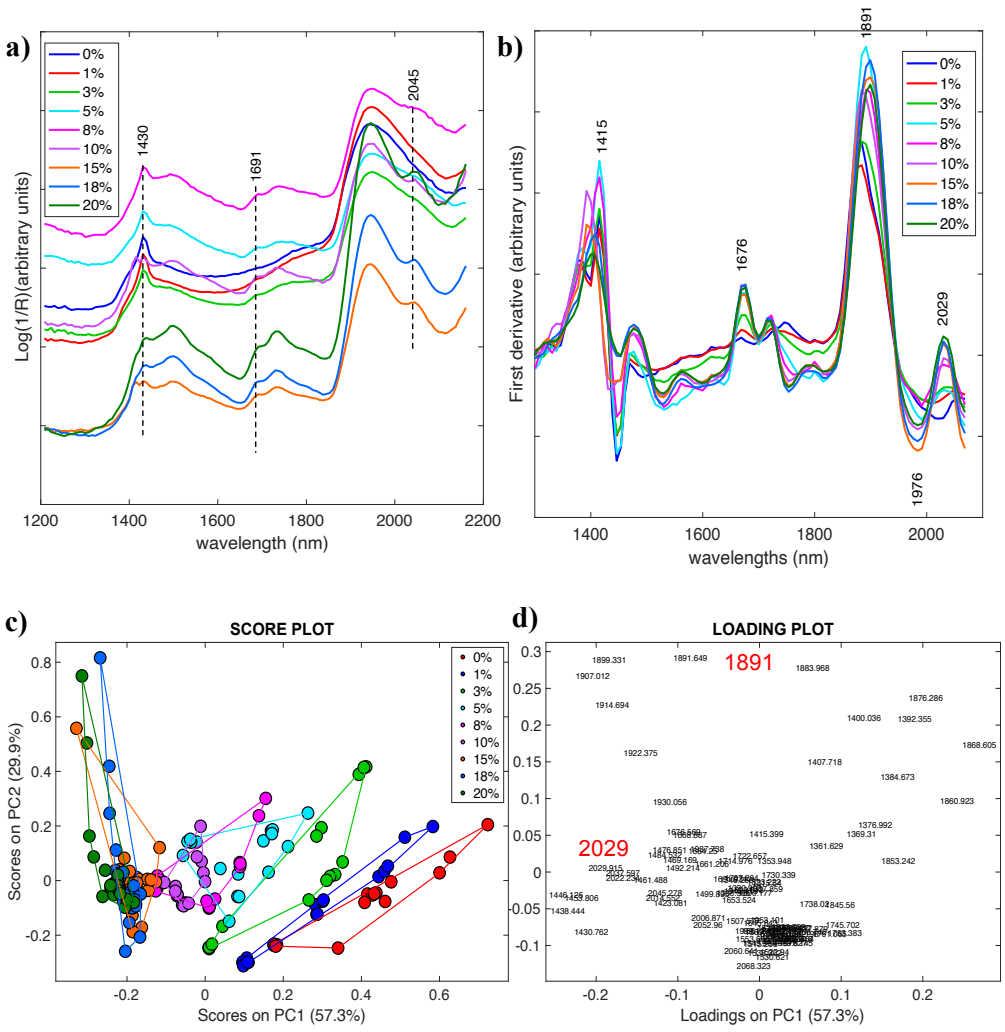

Figure 3.4. Standard samples: a) representative spectra of samples 0 %, 1 %, 3 %, 5 %, 8 %, 10 %, 15 %, 18 %, 20 %; b) first derivative spectra of the same samples; c) score plot of standard samples with convex polygons calculated for each class; d) loading plot.

3.3.2.2. Real bone samples

To confirm standard output and to evaluate prototype performance, we decided to test real samples from different sites and period and with different preservation. We speculated a higher collagen content (%) for specimen RP (partially mummified individual) and a lower content for the Palaeolithic samples (RB63, R313, UC86 and UC88; ca. 1%). Although older in terms of absolute age, macroscopically sample RB63 appears to be better preserved than the Uluzzo samples (R313, UC86 and UC88). This may be related to the different burial environments of the two places. RB63 comes from the northern site of the Riparo Broion (Vicenza, Italy), which has a lower mean annual temperature than Uluzzo (Nardò, Italy), while UC86 and UC88 are from Uluzzo, which is colder and close to the sea. Samples OV and SMM, from the Late Antiquity and Late Medieval periods respectively, should present a collagen content that is somewhere between the content found in Palaeolithic and modern specimens.

Our preliminary hypothesis, based on age, site and appearance, were in line with the results obtained through portable MicroNIR (Figure 3.5). Indeed, spectra allowed the identification of collagen characteristic band at 2053 nm, assigned to N-H combination band, in samples RP, SMM, OV and RB63. In addition to this, samples RP, SMM and OV showed a shoulder band at 1692 nm due to C-H stretching, but it was more visible after first derivative correction at 1677 nm. Conversely, in the other samples no traces of collagen were detected in the raw data or after spectra corrections. There were visible only peaks due to the hydroxyapatite, which is the mineral component of bones.

The PC1 vs PC3 score plot permits to see an appreciable separation of the samples (Figure 3.5. c). Observing the score plot RP, SMM, OV and RB63 showed a good reproducibility with a consequent low dispersion, while R313, UC86 and UC88 were characterized by a higher dispersion, leading to a difficult separation among them.

The loading plot confirmed the fundamental role of the band at 2053 nm (2022 nm in first derivative) previously seen with standards, permitting a separation of samples according to their collagen content. The wavelength around 1910-1935 nm (1891-1945 nm in derivative), that can be attributed to the O-H bands of the hydroxyapatite or to the water content in the samples, appeared to influence the dispersion of spectra belonging to the same sample.

After the evaluation of both spectra profiles and PCA distribution, we can tentatively describe samples according to their collagen content. In more detail, RP was the sample with the higher collagen content, followed by SMM and OV. This result was also in line with their period and site of provenance. RB63 also presented collagen content in a lower amount, while UC86 and UC88 showed the lowest collagen content. Due to the absence of collagen band, it could be in a very low amount or even completely absent.

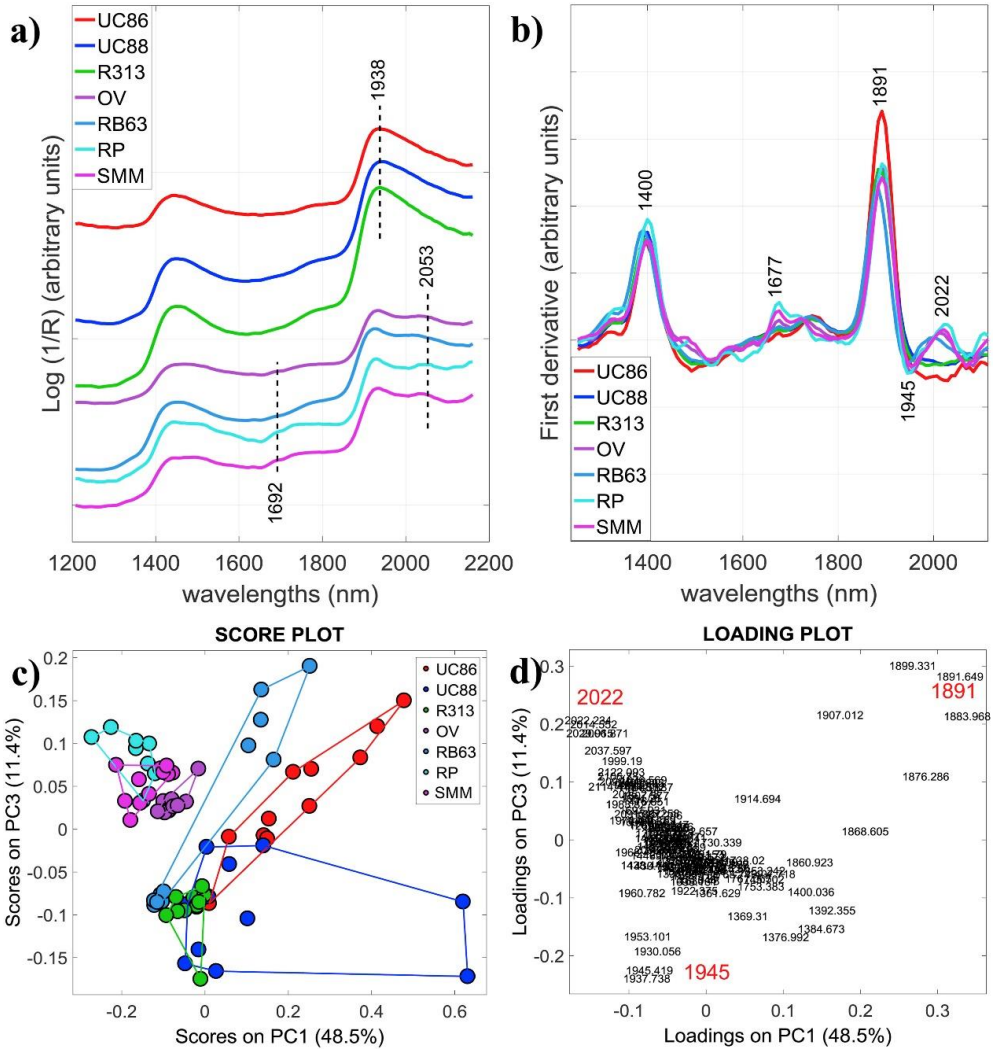

Figure 3.5. Real bone samples: a) representative spectra of samples UC86, UC88, R313, OV, RB63, RP, SMM; b) first derivative spectra of the same samples; c) score plot of bone samples with convex polygons calculated for each class; d) loading plot.

3.3.3. Conclusions and further perspectives

The main interest of archaeologists and paleontologists is the investigation of the past populations, preserving bone integrity as much as possible. The final objective is the exposure of remains in museums for the public. For these reasons, low cost and low-time consuming prescreening acquired higher importance for archaeologist in order to select samples according to their conservation and collagen presence. Techniques used for dating, taxonomy and diet evaluation require a lot of samples without the guarantee of collagen presence. In this context, prescreening methods become fundamental for the evaluation of collagen preservation level in different samples, avoiding sample loss.

In this study we proposed bone prescreening with a new microNIR spectrometer prototype, which is completely non-invasive, combined with appropriate data processing. The results showed a good prospect towards the knowledge of collagen content, thanks to the good separation of samples according to their collagen content. These results could be the starting point for the creation of a predictive model applying on the data a PLS, able to quantify the collagen content of bones preserving them. The model could be created using standard samples and/or real bones with known collagen content. This prescreening could save bone integrity and could allow to select bones for further destructive analyses.

3.4. References

[1] D. M. Friedrich, C. A. Hulse, M. von Gunten, E. P. Williamson, C. G. Pederson, and N. A. O'Brien, "Miniature near-infrared spectrometer for point-of-use chemical analysis," *Photonic Instrum. Eng.*, vol. 8992, p. 899203, 2014, doi: 10.1117/12.2040669.

[2] M. Alcalà *et al.*, "Qualitative and quantitative pharmaceutical analysis with a novel hand-held miniature near infrared spectrometer," *J. Near Infrared Spectrosc.*, vol. 21, no. 6, pp. 445–457, 2013, doi: 10.1255/jnirs.1084.

[3] N. A. O'Brien *et al.*, "Miniature near-infrared (NIR) spectrometer engine for handheld applications," *Next-Generation Spectrosc. Technol. V*, vol. 8374, p. 837404, 2012, doi: 10.1117/12.917983.

[4] C. A. Teixeira Dos Santos, M. Lopo, R. N. M. J. Páscoa, and J. A. Lopes, "A review on the applications of portable near-infrared spectrometers in the agro-food industry," *Appl. Spectrosc.*, vol. 67, no. 11, pp. 1215–1233, 2013, doi: 10.1366/13-07228.

[5] G. L. Bosco, "James L. Waters Symposium 2009 on near-infrared spectroscopy," *TrAC - Trends Anal. Chem.*, vol. 29, no. 3, pp. 197–208, 2010, doi: 10.1016/j.trac.2010.01.003.

[6] M. Bacci, M.Picollo, G.Trumpy , M. Tsukada, and D. Kunzelman, "Non-Invasive Identification of White Pigments on 20th-Century Oil Paintings by Using Fiber Optic Reflectance Spectroscopy", *J. Am. Inst. Conserv.*, vol. 46, no. 1, pp. 27-37, 2007.

[7] K. A. Dooley *et al.*, "Mapping of egg yolk and animal skin glue paint binders in Early Renaissance paintings using near infrared reflectance imaging spectroscopy," *Analyst*, vol. 138, no. 17, pp. 4838–4848, 2013, doi: 10.1039/c3an00926b.

[8] J. K. Delaney *et al.*, "Use of imaging spectroscopy, fiber optic reflectance spectroscopy, and X-ray fluorescence to map and identify pigments in illuminated manuscripts," *Stud. Conserv.*, vol. 59, no. 2, pp. 91–101, 2014, doi: 10.1179/2047058412Y.0000000078.

[9] M. Aceto *et al.*, "Characterisation of colourants on illuminated manuscripts by portable fibre optic UV-visible-NIR reflectance spectrophotometry," *Anal. Methods*, vol. 6, no. 5, pp. 1488–1500, 2014, doi: 10.1039/c3ay41904e.

[10] E. Brandt, I. Wiechmann, and G. Grupe, "How reliable are immunological tools for the detection of ancient proteins in fossil bones?," *Int. J. Osteoarchaeol.*, vol. 12, no. 5, pp. 307–316, 2002, doi: 10.1002/oa.624.

[11] M. Sponheimer, C. M. Ryder, H. Fewlass, E. K. Smith, and W. J. Pestle, "Saving old bones: a non-destructive method for bone collagen prescreening," *Sci. Rep.*, vol. 9, no. 13928, 2019, https://doi.org/10.1038/s41598-019-50443-2.

[12] E. T. Stathopoulou, V. Psycharis, G. D. Chryssikos, V. Gionis, and G. Theodorou, "Bone diagenesis: New data from infrared spectroscopy and X-ray diffraction," *Palaeogeogr. Palaeoclimatol. Palaeoecol.*, vol. 266, no. 3–4, pp. 168–174, 2008, doi: 10.1016/j.palaeo.2008.03.022.

[13] R. Mazzeo, *Analytical chemistry for cultural heritage*. 2017.

[14] B. G. Osborne, "Near-infrared spectroscopy in food analysis," *Encycl. Anal. Chem.*, pp. 1–14, 2000, doi: 10.1002/9780470027318.a1018.

[15] R. G. Brereton, *Applied Chemometrics for Scientists*. John Wiley & Sons, Ltd, 2007.

[16] G. Sciutto, P. Oliveri, S. Prati, E. Catelli, I. Bonacini, and R. Mazzeo, "A multivariate methodological workflow for the analysis of FTIR chemical mapping applied on historic paint stratigraphies," *Int. J. Anal. Chem.*, vol. 2017, 2017, doi: 10.1155/2017/4938145.

[17] P. Oliveri, M. C. Casolino, and M. Forina, "Chemometric Brains for Artificial Tongues," *Adv. Food Nutr. Res.*, vol. 61, no. C, pp. 57–117, 2010, doi: 10.1016/B978-0-12-374468-5.00002-7.

[18] T. Fearn, "The effect of spectral pre-treatments on interpretation," *NIR news*, vol. 20, no. 6, pp. 15–16, 2009, doi: 10.1255/nirn.1146.

[19] V. M. Taavitsainen, "Denoising and signal-to-noise ratio enhancement: Derivatives," in *Comprehensive Chemometrics*, vol. 2, 2009, pp. 57–66.

[20] A. Savitzky and M. J. E. Golay, "Smoothing and differentiation of data by simplified least squares procedures," *Anal. Chem.*, vol. 36, no. 8, pp. 1627–1639, 1964, doi: 10.1021/ac60214a047.

[21] V. Sharma and R. Kumar, "Trends of chemometrics in bloodstain investigations," *TrAC - Trends Anal. Chem.*, vol. 107, pp. 181–195, 2018, doi: 10.1016/j.trac.2018.08.006.

[22] R. Bro and A. K. Smilde, "Principal component analysis," *Anal. Methods*, vol. 6,

no. 9, pp. 2812–2831, 2014, doi: 10.1039/c3ay41907j.

[23] P. Oliveri, C. Malegori, R. Simonetti, and M. Casale, “The impact of signal pre-processing on the final interpretation of analytical outcomes – A tutorial,” *Anal. Chim. Acta*, vol. 1058, pp. 9–17, 2019, doi: 10.1016/j.aca.2018.10.055.

[24] S. W. Keenan and A. S. Engel, “Early diagenesis and recrystallization of bone,” *Geochim. Cosmochim. Acta*, vol. 196, pp. 209–223, 2017, doi: 10.1016/j.gca.2016.09.033.

[25] S. W. Keenan, A. S. Engel, A. Roy, and G. Lisa Bovenkamp-Langlois, “Evaluating the consequences of diagenesis and fossilization on bioapatite lattice structure and composition,” *Chem. Geol.*, vol. 413, pp. 18–27, 2015, doi: 10.1016/j.chemgeo.2015.08.005.

[26] C. M. Nielsen-Marsh and R. E. M. Hedges, “Patterns of diagenesis in bone I: The effects of site environments,” *J. Archaeol. Sci.*, vol. 27, no. 12, pp. 1139–1150, 2000, doi: 10.1006/jasc.1999.0537.

[27] A. Toncala *et al.*, “On the premises of mixing models to define local bioavailable $^{87}Sr/^{86}Sr$ ranges in archaeological contexts,” *Sci. Total Environ.*, vol. 745, p. 140902, 2020, doi: 10.1016/j.scitotenv.2020.140902.

[28] C. Chadefaux *et al.*, “Curve-fitting micro-ATR-FTIR studies of the amide I and II bands of type I collagen in archaeological bone materials", *E-Preservation Science, Morana RTD d.o.o.*, vol. 6, pp. 129-137, 2009.

[29] I. Kontopoulos *et al.*, “Screening archaeological bone for palaeogenetic and palaeoproteomic studies,” *PLoS One*, vol. 15, no. 6, pp. 1–17, 2020, doi: 10.1371/journal.pone.0235146.

[30] G. Pothier Bouchard *et al.*, “Portable FTIR for on-site screening of archaeological bone intended for ZooMS collagen fingerprint analysis,” *J. Archaeol. Sci. Reports*, vol. 26, no. May, p. 101862, 2019, doi: 10.1016/j.jasrep.2019.05.027.

[31] C. A. M. France, D. B. Thomas, C. R. Doney, and O. Madden, “FT-Raman

spectroscopy as a method for screening collagen diagenesis in bone," *J. Archaeol. Sci.*, vol. 42, no. 1, pp. 346–355, 2014, doi: 10.1016/j.jas.2013.11.020.

[32] S. E. Halcrow, J. Rooney, N. Beavan, K. C. Gordon, N. Tayles, and A. Gray, "Assessing Raman spectroscopy as a prescreening tool for the selection of archaeological bone for stable isotopic analysis," *PLoS One*, vol. 9, no. 7, 2014, doi: 10.1371/journal.pone.0098462.

[33] D. Baykal, O. Irrechukwu, P. C. Lin, K. Fritton, R. G. Spencer, and N. Pleshko, "Nondestructive assessment of engineered cartilage constructs using near-infrared spectroscopy," *Appl. Spectrosc.*, vol. 64, no. 10, pp. 1160–1166, 2010, doi: 10.1366/000370210792973604.

[34] M. Tomassetti, F. Marini, R. Bucci, A. Coppa, and L. Campanella, "Comparison of NIR spectroscopy coupled to chemometrics and derivative thermogravimetry for relative dating of human fossil bones," *J. Therm. Anal. Calorim.*, vol. 130, no. 1, pp. 559–565, 2017, doi: 10.1007/s10973-017-6428-8.

[35] D. B. Thomas, C. M. Mcgoverin, and M. Manley, "Near infrared analysis of fossil bone from the Western Cape of South Africa," vol. 159, no. March, pp. 151–159, 2011, doi: 10.1255/jnirs.926.

[36] D. Vincke *et al.*, "Analysis of collagen preservation in bones recovered in archaeological contexts using NIR Hyperspectral Imaging," *Talanta*, vol. 125, pp. 181–188, 2014, doi: 10.1016/j.talanta.2014.02.044.

CHAPTER 4

NEAR-INFRARED HYPERSPECTRAL IMAGING (NIR-HSI) AND NORMALIZED DIFFERENCE IMAGE (NDI) DATA PROCESSING: AN ADVANCED METHOD TO MAP COLLAGEN IN ARCHAEOLOGICAL BONES.

Part of the chapter is reproduced from: “Near-infrared hyperspectral imaging (NIR-HSI) and normalized difference image (NDI) data processing: an advanced method to map collagen in archaeological bones.”

F. Lugli, G. Sciutto, P. Oliveri, C. Malegori, S. Prati, L. Gatti, S. Silvestrini, M. Romandini, E. Catelli, M. Casale, S. Talamo, P. Iacumin, S. Benazzi, R. Mazzeo

Talanta, 2021

4.1. Hyperspectral Imaging (HSI)

Hyperspectral imaging (HSI) is an analytical technique able to combine spectroscopy and imaging, obtaining both spectral and spatial information [1], [2]. It has been applied in different contexts (*e.g.*, food system, agronomy, blood analysis) and it can be implemented with different sensors or cameras. Thanks to the non-invasive approach, it has been applied also on cultural heritage, mainly on paintings and manuscripts, for qualitative and quantitative investigations. It has been mainly employed in reflectance mode covering the visible (Vis), Near Infrared (NIR) and Short-Wave Infrared (SWIR) regions [2], [3]. In comparison to Multispectral Imaging (MSI), HSI allows a high spectral resolution, a moderate spatial resolution, a large area coverage and a continuous spectral reflectance curve [4], [5]. In hyperspectral image each band, corresponding to a particular wavelength, has a dimension in which each pixel represents a digital number reflecting the radiance value collected by the sensor. In detail, the HSI cube (Figure 4.1.) **D** is described by three dimensions $X \times Y \times \lambda$ in which each pixel, described by $X \times Y$, contains a spectrum (λ information) [4]–[6].

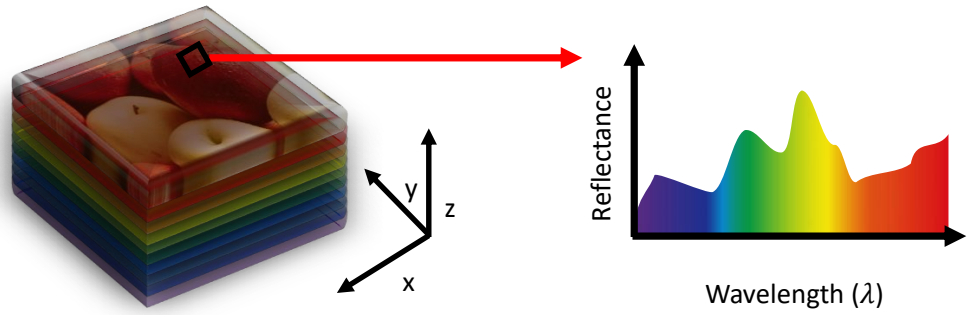

Figure 4.1. Hyperspectral data cube.

However, the huge amount of information in the hyper cube includes also redundant data, noise and different types of artifacts. For this reason, an adequate preprocessing of the data is essential to extrapolate the desired information [5], [7]. Chemometrics allows the selection and treatment of the data according to the final aim.

As for NIR spectra, for HSI preprocessing methods allow the reduction or removal of some spatial and spectral artifacts due to different phenomena (*e.g.*, light scattering, background, rough surface). In particular, the baseline drift (*i.e.*, additive scattering) can be corrected by the SNV and multiplicative scatter correction (MSC) (*i.e.*, multiplicative scattering). The first and second derivate are applied not only to reduce the scattering, but also to highlight the information present in lowest peaks [5], [7].

Moreover, different de-noising methods can be applied to remove the noise. This is different pixel by pixel and thus different de-noising level should be used. The simplest method is smoothing, but other complex algorithms have been developed [4].

The data exploration is based on unsupervised method, such as especially PCA, which allows to understand the trends among different pixels without a class previously known. Segmentation is the set of clustering methods which divide pixels in groups according to their similarities [5].

The final step is the construction of descriptive or predictive models. The first one consists in classification methods, which distinguish pixels with the same class (*i.e.*, same spectral information). The spectral unmixing is one of the most used classification methods and its goal is the resolution of chemical information contained in each pixel, based on the spectral profile. The result obtained is a classification map in which pixels with the same spectral information have the same color [4], [5]. The second one, predictive model, consists in the determination of bulk or pixel concentration of a component and it is possible to apply multivariate regression methods [8]. The principal methods used are multiple linear regression, principal component regression and partial least squares.

4.2. Collagen mapping in archaeological bones

Previous chapters have highlighted the necessity to gather sufficient information about collagen amount and distribution in ancient bones, in order to have successful results from specific and complex analyses. For these reasons, more sustainable non-invasive analytical methods are now needed, as well as systematic documentation, across laboratories, on ancient humans and related species remains and on the success rate of data recovery. Thus, the possibility to gather a suitable amount of well-preserved collagen

from bone specimens is crucial to obtain robust results and, potentially, to enable the analysis of those samples with low-bulk collagen but presenting specific areas with higher content. Recently, several efforts have been focused on the development of reliable non-destructive prescreening methods for the detection of collagen in bone specimens and the evaluation of their state of conservation. Spectroscopic techniques - as *e.g.* Fourier-transform infrared (FTIR) [9], Raman [10], [11] and near-infrared (NIR) [12]–[14] played a focal role, but the possibility of an extensive mapping of samples has not been explored yet. Indeed, up to now, spectroscopic techniques allowed researchers to perform only point analyses on the bone specimens, without the possibility to clearly understand the spatial distribution of collagen – a crucial issue in heterogeneous samples. A previous study reported on the use of a NIR camera, with a reduced spectral range (900–1700 nm), on small cross-sectioned samples, using spectral bands associated with hydroxyapatite (O–H vibration modes) [15] to evaluate the diagenetic status of skeletal remains in support of Sr isotopic analyses.

During this thesis project an innovative and non-invasive near-infrared hyperspectral imaging (NIR-HSI) method was developed for the simultaneous detection and localization of collagen in ancient bones, exploiting the short-wave infrared (SWIR) range (1000–2500 nm). In more detail, a fast and straightforward protocol to generate false colour chemical maps of the collagen distribution was proposed, based on the calculation of normalized difference images (NDI). The NDI method has been recently proposed in the frame of forensic and environmental applications [1], [16]. It was implemented employing the NDI values extracted from each pixel of the HSI and comparing the computed median values among real and reference samples. These values are reported in the ordinate axis of the box and whisker plot to support the comparison and the evaluation of data obtained; thus, the joint examination of reference bones and test samples led to estimate the collagen content in each sample and within its different areas, supporting the identification of proper sampling points.

The NDI approach is efficient when the target analytes have distinctive absorptions in the spectrum and are present at a detectable concentration in the sample analyzed. The effect of signal interferences such as baseline effects is minimized by the mathematical

transform itself. This approach can radically reduce the destruction rate of precious samples, thus increasing the number of bones that can be submitted to guided micro-destructive sampling. In addition, the rapid prescreening of large bones may contribute to optimize the time and the budget dedicated to time- and cost-consuming analyses, such as radiocarbon, stable isotopes and proteomics, reducing the total number of specimens analyzed and, thus, potentially leading to a drastic drop in average research costs in these fields.

The method was, at first, assessed on six faunal samples with previously determined collagen content used as reference samples and then tested on three bone samples, characterized by different chronological period and site of excavation. To validate the method, the test bones were sampled in areas with different collagen content and quantitative analysis was performed through an acid demineralization method and compared with the outcomes of NIR imaging.

The present project was conducted in collaboration with the Department of Pharmacy of the University of Genova and the Bones laboratory (University of Bologna, Ravenna campus).

4.2.1. Materials and methods

4.2.1.1. Samples

The method was applied on six reference samples with known collagen content (sample ID: FB-A, FB-B, FB-C, FB-D, FB-E, FB-F; see Table 4.1.). Afterwards, the method was also tested on real test samples characterized by different chronological period and site of excavation. In detail, a human femur (MV-F) and a coxal bone (MV-C) coming from an Iron Age Italian site (Monterenzio Vecchio, Bologna, ca. 4th-3rd century BC) [17], and a fauna sample from a Middle-Upper Paleolithic Italian site, namely RB (Riparo del Broion, Vicenza, Veneto, Italy, ca. 45′ 000 years BP) [18].

Table 4.1. Samples information. Collagen yields were calculated as the percentage of the extracted collagen weight over the total weight of the original bone sample after HCl demineralization. Samples with numbers (1, 2 and 3) are subsamples of the same bone.

Sample name	Bone type	Collagen yield (%wt)	Whole-bone median NDI value	Provenance	Date	Reference
FB-A	Fauna	2.9	0.22	Savorgnano (Udine)	End of 7th century AD	-
FB-B	Fauna	2.9	0.23	Savorgnano (Udine)	End of 7th century AD	-
FB-C	Fauna	8	0.26	Savorgnano (Udine)	End of 7th century AD	-
FB-D	Fauna	8.5	0.26	Savorgnano (Udine)	End of 7th century AD	-
FB-E	Fauna	15	0.27	Savorgnano (Udine)	End of 7th century AD	-
FB-F	Fauna	20	0.29	Savorgnano (Udine)	End of 7th	-

					century AD	
RB	Fauna	8.7	0.20	Riparo del Broion (Vicenza)	45,000 years BP	[18]
MV-F1	Human	25	0.32	Monterenzio Vecchio (Bologna)	4^{th}-3^{rd} cent. BC	[17]
MV-F2	Human	12.5	-	Monterenzio Vecchio (Bologna)	4^{th}-3^{rd} cent. BC	[17]
MV-C1	Human	5.3	0.27	Monterenzio Vecchio (Bologna)	4^{th}-3^{rd} cent. BC	[17]
MV-C2	Human	13.5	-	Monterenzio Vecchio (Bologna)	4^{th}-3^{rd} cent. BC	[17]
MV-C3	Human	26.4	-	Monterenzio Vecchio (Bologna)	4^{th}-3^{rd} cent. BC	[17]

4.2.1.2. Hyperspectral imaging

HSI-NIR data were acquired by a push-broom system composed by a SWIR3 hyperspectral camera working in the 1000–2500 nm spectral range, at 5.6 nm spectral resolution (Specim Ltd, Finland). The instrumental setting is characterized by three halogen lamps (35 W, 430 lm, 2900 K, each) as illumination sources and a horizontal line scanner (40 × 20 cm moving stage) on which samples are laid down. The system is controlled by the Lumo Scanner v. 2.6 software (Specim Ltd, Finland). Prior to each measurement, dark (closed shutter) and white (99% reflectance Spectralon® rod) images were automatically recorded and used to compute the spectral reflectance value (R) for each pixel and wavelength. For the acquisition, the scan parameters were set as follow:

frame rate equal to 50.00 Hz and exposure time equal to 9.00 ms; manual focus was tuned before the scan. The collected image data were organized in a three-dimensional data matrix, often called hypercube or, alternatively, spectral cube. The first two dimensions of the 3D array are vertical and horizontal spatial coordinates (pixels), while the third dimension represents the wavelengths (spectral dimension).

4.2.1.3. NIR-HSI data analysis

Collagen distribution was obtained according to the formula [1], [16]:

$$NDI = \frac{R_{\lambda h} - R_{\lambda c}}{R_{\lambda h}} \qquad (4.1)$$

where $R_{\lambda h}$ is the reflectance value at 1959 nm, attributed to O-H banding second overtone and O-H stretching combination band of hydroxyapatite, while $R_{\lambda c}$ is the reflectance value at 2195 nm, attributed to N-H bending second overtone and C=O stretching combination of collagen. Plotting the NDI values for each pixel in a scale where red represents the maximum values and blue the minimum values, a false colour chemical map is obtained, which represents the distribution of collagen. Owing to their high signal-to-noise ratio, spectra were used for the data analysis as raw data without any pre-treatment [19].

Regions of interest (ROIs) at predominant red, green and blue colours were automatically selected by defining, respectively, three numerical selection ranges of the colour values of the pixels in the resulting NDI maps. For each of the three ROI, the average NIR spectrum was computed by averaging the subset of spectra corresponding to the selected pixels.

NDI values of each different sample were also visualized in a box-and-whisker plot, in which the central mark of each box indicates the median, and the bottom and top edges of the box indicate the 25th and 75th percentiles, respectively. The comparison of the NDI median values calculated for reference samples with the ones obtained for the test samples enabled the estimation of collagen content in the test samples.

4.2.1.4. Collagen extraction and quantification

Bone collagen was extracted from reference and test samples and quantified at the Stable Isotope Laboratory of the University of Parma (Italy), following the protocol described by Ref. [20]. In brief, ca. 200 mg of bone was demineralized with 0.5 M HCl until no effervescence was observed. The resulting collagen 'pseudomorphs' were then treated with NaOH and lyophilized. Finally, collagen yields were calculated as the percentage of the extracted collagen weight over the total weight of the original bone sample.

4.2.2. Results and discussion

Collagen distributions were obtained calculating the normalized difference images (NDI) [1], [16] as reported in the Materials and Methods paragraph, using the reflectance value at 2195 nm of collagen (N-H bending second overtone and C=O stretching combination band) and the band at 1959 nm of hydroxyapatite (O-H bending second overtone and O-H stretching combination band) [13]. For the reference samples (labelled as FB) with known collagen content, merged chemical maps were obtained combining each sample in a single portfolio image, in which the chromatic scale was defined considering the NDI values calculated for each pixel in all the samples (Figure 4.2.). The colours observed in the maps are related to the different relative content of collagen (pure red: highest content, green: intermediate content, pure blue: lowest content). Samples FB-A and FB-B, which correspond to the lowest collagen content (2.9 % wt of collagen), exhibited a bluish-light green colour (Figure 4.2.). Samples with a mid-level collagen content FB-C, FB-D and FB-E (ranging between 8 % and 15 % wt) showed a greenish hue with some yellow and light blue areas (Figure 4.2.). FB-F (20 % wt of collagen) was characterized by several red and yellow pixels (highest content, >20 % wt), distributed mainly on the bottom part of the sample (Figure 4.2.b). However, it can be noted that, in the upper left part of the sample, the distribution of collagen presented several blue spots, indicating a noticeably lower concentration, with respect to the bottom part. Each map can be range-scaled individually to enhance the colour contrast and, consequently, the visualization of differences in collagen distribution within a single sample. For FB-D, for instance, the map analyzed was range-scaled individually, from the lowest (pure blue) to the highest NDI value (pure red), to visually enhance the intra-sample variability in collagen content

(Figure 4.2.c and e). The strategy followed for data processing enabled the automatic extraction of the average spectra from the three areas identified. As expected, the diagnostic bands associated to the presence of collagen at 2060 nm (N–H stretching combination band), 2195 nm and at 2293 nm (C–H stretching and bending combination band) [11] increased according to the collagen content (lower in the blue areas, higher in the red ones). This means that, depending on the sampling point, the quantity of collagen extracted by destructive analytical procedures (as the demineralization) may be remarkably different [21].

Thus, NIR-HSI maps revealed a very heterogeneous collagen distribution, both at a macro- and at a micro-scale (pixel size = 500 μm). Such heterogeneity was observed in all the samples, pointing out an urgent issue in bioarchaeology researches regarding the need for non-destructive prescreening methods to support the identification of the richest collagen areas for designing further examinations.

Analyses of the reference set of samples showed that the NIR-HSI results were coherent with the collagen extraction yield. In particular, the NDI median values tended to increase according to the average collagen content (Figure 4.3.). This enabled a quick comparison among different specimens to identify the most suitable area to be submitted to further investigations by means of destructive analytical methods.

For sample FB-F, with the highest collagen content (20 % wt), the highest NDI median was obtained (0.29), with box boundaries (25th and 75th percentiles) at 0.25 and 0.33. The median NDI value of sample FB-E (15 % wt) was 0.27, with box boundaries at 0.24 and 0.29. FB-D (8.5 % wt) and FB-C (8 % wt) showed a similar median value, at around 0.26, with box boundaries at 0.23–0.29 for FB-D and at 0.24–0.29 for FB-C, exhibiting a partial box overlapping even with sample FB-E. Samples FB-A and FB-B, with the lowest amount of collagen (2.9 % wt for both), showed a median NDI value at 0.22 and 0.23, respectively (with boundaries at 0.21 and 0.24 for FB-A, and at 0.21 and 0.25 FB-B). The distribution of the NDI values for each sample reported in the box and whisker plot (Figure 4.3.) showed that the median NDI values were positively correlated with the collagen content and that they increased according to the yield of the extracted collagen. These outcomes indicate the potential of NIR-HSI as a rapid tool to compare different

bone remains to select the most interesting pieces and the most appropriate areas for the collection of micro-samples to be submitted to destructive analyses.

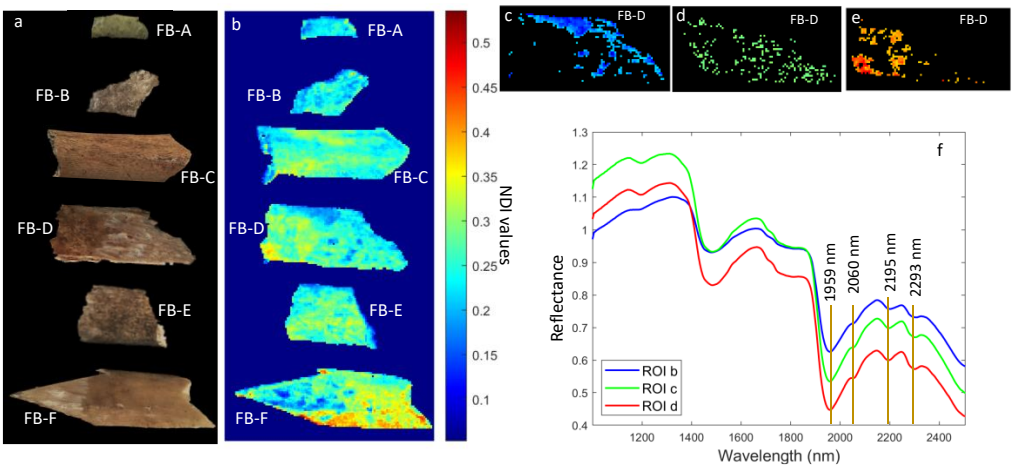

Figure 4.2. NIR-HSI results on reference samples. a) Photographs of samples; b) NDI merged images of the same samples (from the above): FB-A, FB-B, FB-C, FB-D, FB-E, FB-F; c,d,e) ROIs of areas with different collagen content (blue: low, green: medium, red: high) in sample FB-D individually-scaled map; f) extracted averaged spectra from each ROI identified with peaks attributed to HA (1959 nm: O-H banding second overtone and O-H stretching combination band) and collagen (2060 nm: N-H stretching combination band; 2195 nm: N-H bending second overtone and C=O stretching combination; 2293 nm: C-H stretching and bending combination band).

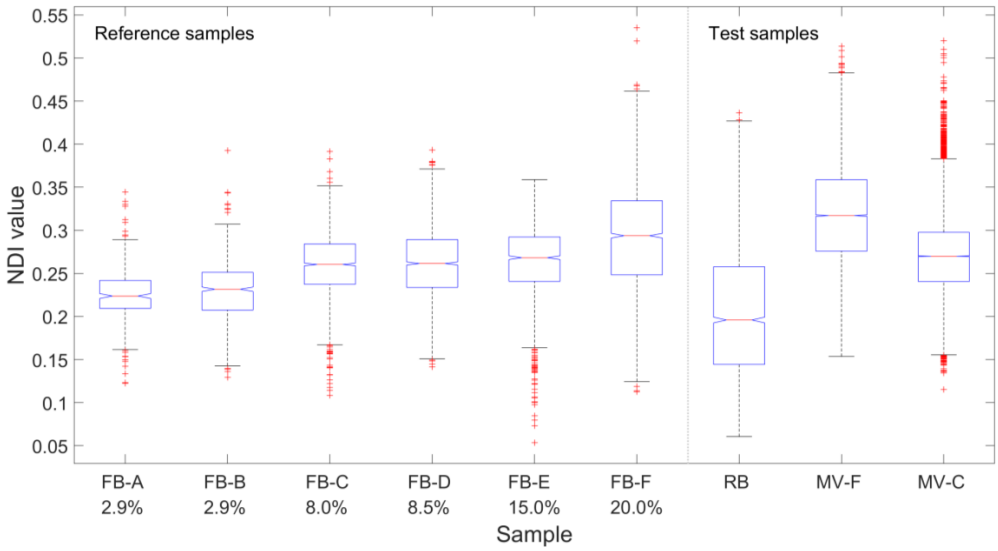

Figure 4.3. Box-and-whisker plot with NDI values. Box-and-whisker plot reporting the NDI values of reference (left) and test samples (right). Collagen yield obtained by acid demineralization is also reported for reference samples. On each box, the central red mark indicates the median, and the bottom and top blue edges of the box indicate the 25th and 75th percentiles, respectively. The black whiskers extend to the most extreme data points not considered as outliers, and outliers are plotted individually using the '+' red symbol. Number of pixels for each sample: FB-A: 312; FB-B: 693; FB-C: 2116; FB-D: 2226; FB-E: 1379; FB-F: 2412; RB: 3380; MV-F: 26933; MV-C: 54392.

To further demonstrate the feasibility of the NIR-HSI in the selection of sampling areas, three test samples with unknown collagen content (RB, MV-F, MV-C) with unknown collagen content were, at first, not-invasively mapped and, then, sampled in different points according to the collagen content distributions obtained. The NDI merged map showed an evident heterogeneity, in terms of both collagen content and distribution (Figure 4.4.). RB, dated back to the Middle-Upper Palaeolithic (ca. 45 ka), resulted in be the samples with the lowest content, reflecting a post-depositional loss of organic matrix. The distribution of collagen content in this latter specimen was highly heterogeneous, as suggested by the presence of a large dark blue area with some green-yellowish spots, mainly present in a half of the sample. Conversely, the number of red and yellow pixels in the MV-F sample (4^{th}-3^{rd} cent BC) was remarkably elevate and widely distributed, indicating a higher collagen content localized in specific areas. MV-C (4^{th}-3^{rd} cent BC) showed a predominant green-yellowish tonality, in which some light blue and red areas

were clearly identified. The highlighted intra-sample variability may be related to several factors as, *e.g.*: 1) diagenetic alterations [22]; 2) physiological differences in collagen density due to age [23]; 3) bio-mechanical properties of bone [24], [25].

Test samples were analyzed to compare collagen distributions obtained with NIR-HSI with quantitative determinations of specific areas. Accordingly, in the box and whisker plot, the MV-F bone presented the highest NDI median value (0.32, with box boundaries equal to 0.28 and 0.36), while the median NDI values of MV-C was of 0.27, with box boundaries at 0.24 and 0.30. RB showed a high variability of the NDI values with a median of 0.20 (the lowest median value in all the samples analyzed) and box boundaries at 0.14 and 0.26, suggesting a very heterogeneous collagen distribution.

The relative distributions of collagen deduced by examination of the NDI were confirmed by the quantitative determination in selected areas of samples MV-F, MV-C and RB, using HCl demineralization. Sample taken from the areas characterized by a high NDI value in MV-F (Figure 4.4. a and b) showed a higher collagen content (25 % wt) than what was observed in the sample taken from the areas with low NDI value of the same sample (12.5 % wt of collagen), confirming the heterogeneity of collagen distribution in the femur. The same behaviour was observed in MV-C, where the collagen content was highly superior in the areas presenting a high NDI value (26.4 % wt of collagen) with respect to ones with low NDI value (5.3 % wt of collagen). A fragment taken from the area richest in collagen (high NDI value area) of sample RB showed a value of collagen of about 8.7 % (wt). Interestingly, the maximum NDI value of RB, equal to 0.25 (Figure 4.3.), is of the same order of magnitude of the median value of samples FB-C and FB-D which contain a similar percentage of collagen.

These outcomes agree with the collagen yield of human bones from other Italian Metal-Age sites [26], reaching up ~30 % wt. The coxal bone (sample MV-C) seemed characterized by an averagely lower collagen content with respect to MV-F, with collagen mostly localized in the exposed trabecular portion and part of the ilium. Due to the different remodeling rate between cortical and trabecular bone, an inter-tissue variability was expected [27]. Hence, higher collagen yield in the trabecular bone might be explained as relatively lower mineral content, if compared to the highly-mineralized cortical tissue

[27], [28]. The Middle-Upper Paleolithic bone from Riparo Broion (RB) showed, as expected, a relatively low collagen yield, as observed by NIR imaging and collagen quantification (by performing acid demineralization). This may have been determined by the old age of the sample RB and by a strong post-depositional loss of organic matter, probably due to the combination of microbial attack and collagen hydrolysis [29].

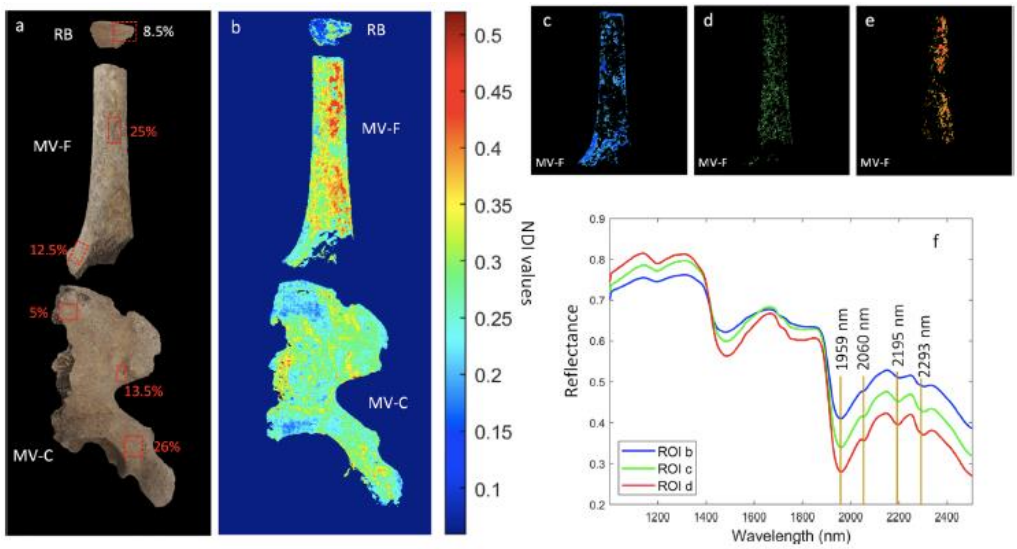

Figure 4.4. NIR-HSI results on test samples. a) Photographs of samples with indication of points for collagen extraction (red rectangles) and collagen percentage obtained; b) NDI merged images of the same samples (from the above): RB, MV-F, MV-C; c,d,e) ROIs of areas with different collagen content (blue: low, green: medium, red: high) in sample MV-F individually-scaled map; f) extracted averaged spectra from each ROI identified with peaks attributed to HA (1959 nm: O-H banding second overtone and O-H stretching combination band) and collagen (2060 nm: N-H stretching combination band; 2195 nm: N-H bending second overtone and C=O stretching combination; 2293 nm: C-H stretching and bending combination band).

4.2.3. Conclusions and further perspectives

The new NIR-HSI method developed provided an efficient mapping of collagen distribution, enabling an intra- and inter-sample comparison, fully exploiting the potentialities of the NDI data processing translated into chemical maps or into box and whisker plots, leading to a qualitative and semi-quantitative evaluation of the relative collagen content distribution.

Being fast and completely non-invasive, the NIR-HSI approach may help bone prescreening, to identify interesting areas within the same specimen on which to drive subsequent targeted analyses, reducing size and number of samples, ultimately contributing to save money, time and to preserve bone integrity. Findings of the present study demonstrate that the high collagen content in old bones may be often restricted to a few areas, clearly indicating the importance of an adequate screening method to avoid incorrect evaluations and to maximize the ratio between information gain and sample destruction.

Based on the resulted showed here, further researches are now in progress to develop linear and non-linear multivariate regression models to extract quantitative data from the NDI-HSI chemical images.

4.3. References

[1] C. Malegori *et al.*, "Identification of invisible biological traces in forensic evidences by hyperspectral NIR imaging combined with chemometrics," *Talanta*, vol. 215, no. March, 2020, doi: 10.1016/j.talanta.2020.120911.

[2] M. Picollo, C. Cucci, A. Casini, and L. Stefani, "Hyper-spectral imaging technique in the cultural heritage field: New possible scenarios," *Sensors (Switzerland)*, vol. 20, no. 10, 2020, doi: 10.3390/s20102843.

[3] H. Liang, "Advances in multispectral and hyperspectral imaging for archaeology and art conservation," *Appl. Phys. A Mater. Sci. Process.*, vol. 106, no. 2, pp. 309–323, 2012, doi: 10.1007/s00339-011-6689-1.

[4] V. Sowmya, K. P. Soman, and M. Hassaballah, "Hyperspectral image: Fundamentals and advances," *Stud. Comput. Intell.*, vol. 804, no. January, pp. 401–424, 2019, doi: 10.1007/978-3-030-03000-1_16.

[5] M. Amigo, "Hyperspectral and multispectral imaging : setting the scene," 2020.

[6] F. Franch-Lage, J. M. Amigo, E. Skibsted, S. Maspoch, and J. Coello, "Fast assessment of the surface distribution of API and excipients in tablets using NIR-hyperspectral imaging," *Int. J. Pharm.*, vol. 411, no. 1–2, pp. 27–35, 2011, doi:

10.1016/j.ijpharm.2011.03.012.

[7] M. Amigo and C. Santos, “Preprocessing of hyperspectral and multispectral images,” 2020, pp. 37–53.

[8] I. Torres and J. M. Amigo, “An overview of regression methods in hyperspectral and multispectral imaging,” in *Data Handling in Science and Technology*, vol. 32, 2020, pp. 205–230.

[9] G. Pothier Bouchard *et al.*, “Portable FTIR for on-site screening of archaeological bone intended for ZooMS collagen fingerprint analysis,” *J. Archaeol. Sci. Reports*, vol. 26, no. May, p. 101862, 2019, doi: 10.1016/j.jasrep.2019.05.027.

[10] C. A. M. France, D. B. Thomas, C. R. Doney, and O. Madden, “FT-Raman spectroscopy as a method for screening collagen diagenesis in bone,” *J. Archaeol. Sci.*, vol. 42, no. 1, pp. 346–355, 2014, doi: 10.1016/j.jas.2013.11.020.

[11] O. Madden, D. M. W. Chan, M. Dundon, and C. A. M. France, “Quantifying collagen quality in archaeological bone: Improving data accuracy with benchtop and handheld Raman spectrometers,” *J. Archaeol. Sci. Reports*, vol. 18, no. November 2017, pp. 596–605, 2018, doi: 10.1016/j.jasrep.2017.11.034.

[12] D. Vincke *et al.*, “Analysis of collagen preservation in bones recovered in archaeological contexts using NIR Hyperspectral Imaging,” *Talanta*, vol. 125, pp. 181–188, 2014, doi: 10.1016/j.talanta.2014.02.044.

[13] M. Sponheimer, C. M. Ryder, H. Fewlass, E. K. Smith, and W. J. Pestle, “Saving Old Bones: a non-destructive method for bone collagen prescreening,” *Sci. Rep.*, vol. 9, no. 13928, 2019, https://doi.org/10.1038/s41598-019-50443-2.

[14] E. Catelli *et al.*, “A new miniaturised short-wave infrared (SWIR) spectrometer for on-site cultural heritage investigations,” *Talanta*, vol. 218, no. April, 121112, 2020, doi: 10.1016/j.talanta.2020.121112.

[15] A. Retzmann *et al.*, “A combined chemical imaging approach using (MC) LA-ICP-MS and NIR-HSI to evaluate the diagenetic status of bone material for Sr isotope

analysis," *Anal. Bioanal. Chem.*, vol. 411, no. 3, pp. 565–580, 2019, doi: 10.1007/s00216-018-1489-5.

[16] S. Piarulli *et al.*, "Rapid and direct detection of small microplastics in aquatic samples by a new near infrared hyperspectral imaging (NIR-HSI) method," *Chemosphere*, vol. 260, p. 127655, 2020, doi: 10.1016/j.chemosphere.2020.127655.

[17] R. Sorrentino *et al.*, "Unravelling biocultural population structure in 4th/3rd century BC Monterenzio Vecchio (Bologna, Italy) through a comparative analysis of strontium isotopes, non-metric dental evidence, and funerary practices," *PLoS One*, vol. 13, no. 3, pp. 1–25, 2018, doi: 10.1371/journal.pone.0193796.

[18] M. Romandini *et al.*, "A late Neanderthal tooth from northeastern Italy," *J. Hum. Evol.*, vol. 147, pp. 1–13, 2020, doi: 10.1016/j.jhevol.2020.102867.

[19] P. Oliveri, C. Malegori, R. Simonetti, and M. Casale, "The impact of signal pre-processing on the final interpretation of analytical outcomes – A tutorial," *Anal. Chim. Acta*, vol. 1058, pp. 9–17, 2019, doi: 10.1016/j.aca.2018.10.055.

[20] S. H. Ambrose, "Preparation and characterization of bone and tooth collagen for isotopic analysis," *J. Archaeol. Sci.*, vol. 14, no. 4, pp. 431–451, 1990.

[21] T. H. and T. D. E. Jacob, D. Querci, M.Caparros, C. Barroso Ruiz, "Nitrogen content variation in archaeological bone and its implications for stable isotope analysis and radiocarbon dating," 2018.

[22] C. Kendall *et al.*, "Diagenesis of archaeological bone and tooth," *Palaeogeogr. Palaeoclimatol. Palaeoecol.*, vol. 491, no. November 2017, pp. 21–37, 2018, doi: 10.1016/j.palaeo.2017.11.041.

[23] X. Wang, X. Shen, X. Li, and C. Mauli Agrawal, "Age-related changes in the collagen network and toughness of bone," *Bone*, vol. 31, no. 1, pp. 1–7, 2002, doi: 10.1016/S8756-3282(01)00697-4.

[24] A. L. Boskey, T. M. Wright, and R. D. Blank, "Collagen and bone strength," *J.*

Bone Miner. Res., vol. 14, no. 3, pp. 330–335, 1999, doi: 10.1359/jbmr.1999.14.3.330.

[25] J. P. Spalazzi, A. L. Boskey, N. Pleshko, and H. H. Lu, "Quantitative mapping of matrix content and distribution across the ligament-to-bone insertion," *PLoS One*, vol. 8, no. 9, pp. 1–16, 2013, doi: 10.1371/journal.pone.0074349.

[26] M. A. Tafuri, O. E. Craig, and A. Canci, "Stable isotope evidence for the consumption of millet and other plants in bronze age Italy," *Am. J. Phys. Anthropol.*, vol. 139, no. 2, pp. 146–153, 2009, doi: 10.1002/ajpa.20955.

[27] A. L. Boskey and R. Coleman, "Critical reviews in oral biology & medicine: Aging and bone," *J. Dent. Res.*, vol. 89, no. 12, pp. 1333–1348, 2010, doi: 10.1177/0022034510377791.

[28] P. Pietschmann *et al.*, "Bone structure and metabolism in a rodent model of male senile osteoporosis," *Exp. Gerontol.*, vol. 42, no. 11, pp. 1099–1108, 2007, doi: 10.1016/j.exger.2007.08.008.

[29] R. E. M. Hedges, "Bone diagenesis : an overview of processes," vol. 3, pp. 319–328, 2002.

CHAPTER 5

ORGANIC IN FOSSIL TEETH: AMINO ACIDS PRESERVATION IN DEEP-TIMES

5.1. Essential and non-essential amino acids

Amino acids (AAs) are the protein subunits, and they are defined as components with both amino and carboxyl groups [1], [2]. Among the huge number of AAs in nature, only 20 are the principal ones which constitutes protein blocks. These 20 AAs are: arginine, lysine, histidine, aspartic acid, glutamic acid, serine, threonine, asparagine, glutamine, cysteine, glycine, proline, alanine, valine, isoleucine, leucine, methionine, phenylalanine, tyrosine, tryptophan. All of them are α-AA, thus they have a primary amino and carboxyl group bounded to the α-carbon atom. All of them, except for glycine, are chiral, hence they have L- and D-isoforms. Moreover, except for glycine, they have optical activity and they are stable in aqueous solutions at pH 7, except for cysteine and glutamine [2].

These 20 AAs have been classified in essential and non-essential amino acids from a nutritional point of view. Essential amino acids (EAA) have been defined as the ones that cannot be synthetized by the body or that are insufficiently synthetized for the maintenance of the organism. These AAs are provided by the diet, thus their availability could vary according to different dietary intakes. Non-essential amino acids (NEAA) are the ones that can be completely synthetized by the body, hence they do not need to be integrated [2]–[4]. All the EAAs and NEAAs for different animals are reported in Table 5.1.

Table 5.1. List of EAA and NEAA in mammals, fishes and poultries, as reported in [2].

Mammals and fish		**Poultry**	
EAA	**NEAA**	**EAA**	**NEAA**
Arginine	Alanine	Arginine	Alanine
Histidine	Asparagine	Glycine	Asparagine
Isoleucine	Aspartic acid	Histidine	Aspartic acid
Leucine	Cysteine	Isoleucine	Cysteine
Lysine	Glutamic acid	Leucine	Glutamic acid
Methionine	Glutamine	Lysine	Glutamine
Phenylalanine	Glycine	Methionine	Serine

Threonine	Proline	Phenylalanine	Tyrosine
Tryptophan	Serine	Proline	
Valine	Tyrosine	Threonine	
		Tryptophan	
		Valine	

5.2. Characterization of total amino acids (THAA) in ancient teeth

Teeth are composed by three different mineralized tissues: cementum, dentin and enamel. All of these present a mineral fraction, mainly composed by bioapatite (*i.e.* a carbonate-containing biogenic calcium phosphate), and an organic fraction, that is mainly collagen in dentin and cementum, while ameloblastins and amelogenins, expressed by both X and Y chromosomes, in enamel [5], [6].

Owing to their composition, teeth are more resistant to physico-chemical alterations than bones and for this reason they are abundant in archaeological sites. They could provide essential information on taxonomy, diet, environment and period. To obtain these information different methods have been used, such as isotopes and elements investigation, proteomic analyses, morphological analyses [7]–[11]. Despite the high interest for collagen in dentin, the organic fraction of enamel received little attention by the palaeoscience community until recently [12].

Enamel is the hardest tissue and previous studies suggested the idea that amino acids could be trapped by HA crystals. According to this, it is possible to distinguish between an inter-crystalline fraction and an intra-crystalline fraction. The first one can exposed to external contaminations by exogenous organic matter (*e.g.* microorganisms), while the second one could be considered as a “closed system”, able to preserve the original biomolecules [1], [12]–[14].

For deep-time fossil teeth, it is still unclear how and where protein-cleavage products are bounded and for how much time they can persist within the enamel tissue as peptides or amino acids (AAs). Indeed, proteins preservation depends on different factors such as temperature, humidity, sediment and matrix characteristics [15]. AAs preservation

overtime has been widely studied in archaeological remains, such as mollusk shells, due to their importance for taxonomic origin reconstruction and their possible use for dating [1], [14], [16]. However, AAs in enamel have been less studied and the few researches about them were focused on amino acid racemization for dating (AAR). AAR is based on the determination of L- and D-amino acids for geochronological purposes, which is typically achieved by HPLC analysis with fluorescence detection [1], [12]–[15], [17], [18].

Based on the previous considerations, the first aim of this work was the development of a protocol for the detection of total hydrolysable amino acids (THAA) to understand how back in time they are preserved. Moreover, a database of modern samples from different species was needed to have references and to clarify possible variations in AAs composition according to the taxon.

To these purposes, modern and fossil samples were analyzed through a High-Pressure Liquid Chromatography (HPLC) [19] with a Diode Array Detector (DAD) and an Agilent AdvanceBio AAA LC column at the Max Planck Institute for Chemistry. Firstly, the injection procedure was optimized with inhouse standard solutions, and a protocol for enamel powders cleaning was developed in order to remove contaminations and mineral fractions. Then, the entire procedure was applied to enamel samples: modern teeth from 16 different species and fossil teeth from 3 different species, sites and periods (0-48 Ma).

This work could contribute to clarify how long biomolecules could survive and which factors could affect this phenomenon overturning our knowledge on deep-time preservation of organics in tooth enamel and opening new perspectives in the use of omics sciences in palaeontology and palaeoanthropology.

The present research was possible owing to the win of the Marco Polo scholarship for three months. The work was conducted in collaboration with the Max Planck Institute for Chemistry, within the Alfredo Martínez-García group.

5.2.1. Materials and methods

5.2.1.1. Standard and real samples

To develop the protocol, standard inhouse solutions of mixed amino acids (AA) were prepared in known concentrations (Table 5.2). The AAs included in the solutions were: aspartic acid (Asp), glutamic acid (Glu), serine (Ser), histidine (His), glycine (Gly), threonine (Thr), arginine (Arg), alanine (Ala), tyrosine (Tyr), cysteine (Cys), valine (Val), methionine (Met), phenylalanine (Phe), isoleucine (Ile), leucine (Leu), lysine (Lys), hydroxyproline (Hyp), proline (Pro).

Table 5.2. Inhouse standard dilutions of AAs with different concentrations.

ID	Concentration nM/mL
D0	2500
D1	1250
D2	625
D3	312.5
D4	100
D5	50
D6	25
D7	10
D8	5
D9	2.5
D10	1

The standards were used for the optimization of the protocol: to identify the AAs retention times, to evaluate the effects of column filtration, to develop the injection method reducing the sample use and to obtain the LOD of the method, building a calibration curve for each AA.

Enamel powder from a *Loxodonta africana* (AG-Lox) was used as reference for protocol development. This sample (provided by Prof. T. Tütken) is currently employed as internal standard at the Max Planck Institute for several different physico-chemical analyses. Modern samples (20) from different species were analyzed to evaluate the variation of AA content overtime. Moreover, it was considered that eventual variation in AA composition may arise from differences in diet, due to the different type of AAs (in particular essential AAs) processed and incorporated in the enamel organic structure (Table 5.3). Then the method was applied on 41 fossil samples from different sites and species (rhino, elephant and horse) going back in time, from 0.04 Ma to 48 Ma (Table 5.4).

All the samples were grinded with a mortar and then 2 mg of powder were cleaned.

Table 5.3. Description of modern samples: taxon, species, provenance and type of tooth, when known.

Sample ID	Species	Provenance	Tooth
Z EQ SI 50 P1	*Equus caballus*	Siberia, Aldan river mouth	M3
Z RA SI 52	*Rangifer tarandus*	SW Greenland	nd
Z CN 3	*Canis lupus*	Banks Island, Kanada	nd
Z HAI 7	*Carcharias carcharodon*	South Africa	nd
Z RH 13	*Ceratotherium simum*	Uganda	M1, sin, low
Z EL 30	*Alces alces*	Sweden, Vaddo	nd
Z SI 33	*Trichechus inunguis*	Brasil, Amazon, R. Solimoes, Codajas	nd
Z HO Tu	*Homo sapiens*	Tubingen	M3
Z PU ZO	*Felis concolor*	Univ. Clinic Tubingen	nd
Z KR 1	*Crocodylus niloticus*	Ferme aux crocodiles Pierr Lattes, near Lyin	nd

Z HI 4	*Hippopotamus amphibus*	Africa	nd
Z PON 2-9395	*Pongo pygmaeus*	West Sumatra, Indonesia	nd
WB	*Sus scrofa*	Taunus	nd
C.A.E.	*Barbus longiceps*	Israel, Lake Kinneret	nd
2.5.T	*Sparus aurata*	Mediterranean, Israel	nd
GPC2-R	*Cavia porcellus*	Carnivore diet (Lucerne)	nd
GPC2-T	*Cavia porcellus*	Carnivore diet (Lucerne)	nd
GPH6-R	*Cavia porcellus*	Herbivore diet (Lucerne)	nd
GPH6-T	*Cavia porcellus*	Herbivore diet (Lucerne)	nd
AG-Lox 1	*Loxodonta africana*	Africa	nd

Table 5.4. Description of provenance and period of fossil samples.

Sample	Taxon ID	Species	Age (Ma)	Tooth	Fossil site	Country	Site ID	MN
FZ MA ND 9	MA	*Mammuthus primigenius*	0.045	M3	Niederweningen	CH	ND	14C
NMN 12	EQ	*Equus caballus*	0.125	Molar	Neumark Nord 2	GER	NN	nd
NMN 18	EL	Elephant	0.125	Molar	Neumark Nord 2	GER	NN	nd
NMN 20	RH	Rhino	0.125	Molar	Neumark Nord 2	GER	NN	nd
FZ CE RS 2 B	CE	*Megalocerus giganteus*	nd	Molar	Rhine River gravel	GER	RS	nd
FZ MAS RS 4	MA	*Palaeoloxodon antiquus*	nd	Molar	Rhine River gravel	GER	RS	nd

FZ MA RS 7	MA	*Mammuthus primigenius*	nd	M3	Rhine River gravel	GER	RS	nd
FZ MA NS PL bulk	MA	*Mammuthus primigenius*	0.0427	M3	Brown Bank, North Sea	NED	NS	nd
FZ MA JAV bulk	MA	*Stegodon trigonocephalus*	1.0	p1/p2	Sangiran, Java	IDN	JAV	nd
FZ MA WIL 4	MA	*Anancus avernensis*	3.0		Willershausen	GER	WILL	MN 16
FZ MA WÖ 9	MA	*Anancus avernensis*	3.6	M3 sup. sin.	Wölfersheim	GER	WÖ	MN 15
FZ MA EP 1	MA	-	10.0		Eppelsheim	GER	EP	MN 9
FZ RH EP 1	RH	*Rhinoceros* sp.	11.0		Eppelsheim	GER	EP	MN 9
FZ EQ EP 1	EQ	*Hippotherium primigenium*	12.0	Molar	Eppelsheim	GER	EP	MN 9
FZ BO HW 4	BO	*Miotragoceros*	10.3	M2	Höwenegg	GER	HW	MN 9
FZ RH HW 10	RH	*Rhinoceros* sp.	11.3	Molar	Höwenegg	GER	HW	MN 9
HW 164/55 (9)	EQ	*Hippotherium primigenium*	12.3	P4	Höwenegg	GER	HW	MN 9
FZ EQ CH 1 (12)	EQ	*Hipparion gracile*	10.0	M3 inf. dext.	Charmoille	CH	CH	MN 9
FZ MA CH 1	MA	*Mastodon* sp.	11.0	Molar	Charmoille	CH	CH	MN 9
FZ RH CH 4	RH	*Rhinoceros* sp.	12.0	M3 sup. dext.	Charmoille	CH	CH	MN 9
FZ MA MA 5	MA	-	12.0		Massenhausen	GER	MA	MN 8

FZ EQ ST 6	EQ	*Anchitherium aurelianense*	13.6	Molar	Steinheim a. Albbuch	GER	ST	MN 7
FZ RH ST 7	RH	*Alicornops simorrensis*	14.6	M3 inf. sin.	Steinheim a. Albbuch	GER	ST	MN 7
FZ EL ST 1	MA	*Gomphotherium steinheimense*	15.6	M3 sup.	Steinheim a. Albbuch	GER	ST	MN 7
FZ EQ SAN 1	EQ	*Anchitherium aurelianense*	14.6	P sup. sin.	Sansan	FR	SAN	MN 6
FZ RH SAN 1	RH	*Aceratherium sp.*	15.6	M3 sup.	Sansan	FR	SAN	MN 6
FZ EL SAN 1	EL	*Mastodon augustidens*	16.6	Molar	Sansan	FR	SAN	MN 6
FZ MA Kä 3	MA	*Gomphotherium augustidens*	16.2	Molar	Käpfnach	CH	Kä	MN 5
FZ RH SA 1a	RH	*Plesiacerotherium fahlbuschi*	16.2	M3 inf.	Sandelzhausen	GER	SA	MN 5
FZ MA SA 3	MA	*Gomphotherium angustidens*	17.2	Molar	Sandelzhausen	GER	SA	MN 5
FZ EQ SA 4	EQ	*Anchitherium aurelianense*	18.2	Molar	Sandelzhausen	GER	SA	MN 5
FZ MA BEN 2	MA	*Mastodon augustidens*	17.2	Molar	Benken am Kohlfirst	GER	BEN	MN 4
FZ RH BEN 3	RH	*Rhinoceros indet*	17.2	Molar	Benken am Kohlfirst	GER	BEN	MN 4
FZ MA AR 1	MA	*Mastodon augustidens*	18.4	Molar	Artenay Artroche	FR	AR	MN 3b
FZ RH AR 1	RH	*Brachypotherium*	18.4	M3 sup.	Artenay Artroche	FR	AR	MN 3b
ULM 04	RH	*Rhinoceros*	21.7	M	Ulm-Westtangente	GER	UL	MN 2a
FZ RH ENG 2	RH	*Rhinoceros* indet	22.9	Molar	Engehalde	CH	ENG	MN 1
FZ RH RI 2	RH	*Ronzotherium romani*	24.4	M1/M2 sup. sin.	Rickenbach	CH	RI	MP 29

FZ RH BU 2	RH	*Aceratherium incisivum*	27.8	Molar	Bumbach	CH	BU	MP 25
FZ EQ ME 1	EQ	*Propalaeotherium hassiacum*	48	Molar	Messel	GER	ME	MP 11
SMF ME 11096	EQ	*Eurohippus*	48	molar	Messel	GER	ME	MP 11

5.2.1.2. HPLC instrument and reagents

The analyses were performed at the Max Planck Institute for Chemistry (Alfredo Martínez-García laboratory) using an Agilent AdvanceBio AAA LC Column 4.6 x 100 mm, 2.7 m 655950-802 and a Diode Array Detector (DAD).

For the precolumn derivatization OPA (10 mg/mL each of o-phthalaldehyde and 3-mercaptopropionic acid in 0.4 M borate buffer) and FMOC (2.5 mg/mL in acetonitrile, 9-fluorenylmethylchloroformate) reagents were used, both purchased by Agilent Technologies.

For the preparation of the OPA, a syringe was rinsed 5 times with MilliQ water and 5 times with new MilliQ water, and 100 µL of the reagent were transferred in each vial. For the preparation of the FMOC the syringe was rinsed 5 times with acetonitrile and 5 times with new acetonitrile, and 100 µL of the reagent were transferred in each vial. The reagents were stored at 4°C for 7 days and then new vials were prepared.

The injection diluent was prepared transferring 100 mL of mobile phase C in a bottle and adding 400 µL of phosphoric acid (H_3PO_4).

Two mobile phases were used: mobile phase B and C. The mobile phase B was prepared in a brown bottle mixing acetonitrile, methanol and MilliQ water in the proportions 45:45:10. The bottle was then ultrasonicated 30 minutes to remove bubbles. For the mobile phase C disodium hydrogen phosphate (Na_2HPO_4, 1.4 g) was mixed with sodium tetraborate decahydrate ($Na_2B_4O_7 \cdot 10H_2O$, 3.8 g) and 1L of MilliQ water. When it was dissolved the pH was adjusted at 8.2 adding slowly 32 % HCl. At the end it was filtered and transferred in a brown bottle.

5.2.1.3. HPLC optimized protocol

Oxidative cleaning

Powders were weighed in sterile vials (2 mg) and 4.25 mL of sodium hypochlorite (NaOCl, Sigma Aldrich) 10-15 % were added. This method was chosen because it is recognized as an effective oxidizing agent, able to isolate the intra-crystalline biomolecules avoiding heating [16]. The vials were shaken at 110 rpm for 24 h. Then NaOCl was removed using a pipette connected to the vacuum pump and the powder was washed 5 times with MilliQ water (the last one in a clean room) and 1 time with methanol. After the samples were completely dried, 1 mg of clean powder was weighed into Microbore vials for AAs extraction.

Hydrolysis and phosphate removal

For THAA investigation, samples were subjected to hydrolysis adding 20 µL/mg of 7 M HCl. The vials were heated in the oven at 110°C for 24 h and then the acid was removed through evaporation for 40 minutes. Before the evaporation, 2 µL of Norvaline in known concentration (312.5 pM/µL) were added to evaluate the effect of evaporation and phosphate removal.

Powder was dissolved in 20 µL/mg of 1M HCl and sonicated for 10 minutes. To remove the high concentration of phosphate ions, a previously developed protocol was follow [13]. Potassium hydroxide (1 M KOH, Sigma Aldrich) was added (35 µL/mg) to the samples and they were centrifuged for 10 minutes, and the supernatant was collected and evaporated for 50 minutes.

Before the HPLC analysis, 35 µL of spike HCl (L-Homoargenine solution in 0.1N HCl in known concentration) were added. This was the safe volume for a 20 µL injection.

The addition of the two internal standards allowed to correct both the recovery (norvaline) and the derivatization (L-Homoargenine).

5.2.1.4. Data elaboration

The values of the peaks integrated areas in the chromatograms were normalized interpolating the areas of each AA with the related calibration curve obtained with inhouse standard solutions and divided for the samples weights. The concentrations (pM/mg) obtained were then normalized for the derivatization percentage (~ 90 %). To obtain this derivatization percentage, a calibration curve for the internal standard (L-Homoargenine) was obtained adding 35 µL of three different concentrations of pure L-homoargenine solutions (100 pM/µL, 32.25 pM/µL, 1 pM/µL) to AG-Lox samples. This method was used instead of pure solutions, due to the enhancing of the peaks areas in presence of treated powder. Then the percentage of derivatization was calculated dividing the concentration of the internal standard in each sample for the expected concentration. Principal component analysis was then performed using two different approaches. First, PCA was run on calibrated data after applying a row centering and a column centering or autoscaling. This approach is useful to consider the absolute changes in AAs according to the chronological age. Second, data were forced to sum to 100 % to obtain relative concentrations (*e.g.* [17]). This second approach is useful to evaluate the relative abundance of each AA in the different samples, avoiding the influence of the sample antiquity on single-AA concentrations. In addition, this approach also limits possible variability in terms of total AAs content across different specimens, for example those pertaining to different taxa. All the data elaboration and analysis were performed using in-house MATLAB scripts.

5.2.2. Results and discussion

5.2.2.1. Optimization of the method

The powder cleaning was performed in NaOCl following the procedure traditionally used in the laboratory for corals and foraminifera. However, the phosphate removal and the instrument were never used before in the lab.

For this reason, different steps for the optimization were needed. Firstly, standard solution was used to identify the retention times of the different AAs comparing the results with the peaks in the Application note AdvanceBioAAA cell culture [21]. Different injection programs were tested on inhouse standard dilutions in order to maximize the measure and

reduce the sample. In more detail, two injection methods were selected: 1 µL out of 20 µL, 15 µL, 10 µL and 5 µL, and 20 µL out of 35 µL. The best result was obtained with the last one. The impact of column filtration was evaluated too. The solution was injected with a syringe through a filter and then the product was analyzed. After all the evaluations, standard solutions were used to create a calibration curve for each AA.

Secondly, during the phosphate removal procedure, special attention was paid for the evaporation method and the pH, after both the first and the second evaporation steps. A long nitrogen flux evaporation was tested, but it required overly long times and the reproducibility was low. The selected evaporation method employed a rocket evaporator, which was fast and homogenous. After the first tests with the full optimized procedure, a reproducibility problem, due to the pH, was noticed. The crucial step was the addition of KOH.

At first the protocol was followed as in the reference paper [13], adding 28 µL/mg of 1 M KOH, but a low reproducibility was detected with AG-Lox standard. Different amounts of KOH were tested to improve the reproducibility of the method: 30 µL/mg, 35 µL/mg and 40 µL/mg. The best reproducibility (around 10 % error according to the AA) was obtained with 35 µL/mg. The full procedure is reported in Figure 5.1.

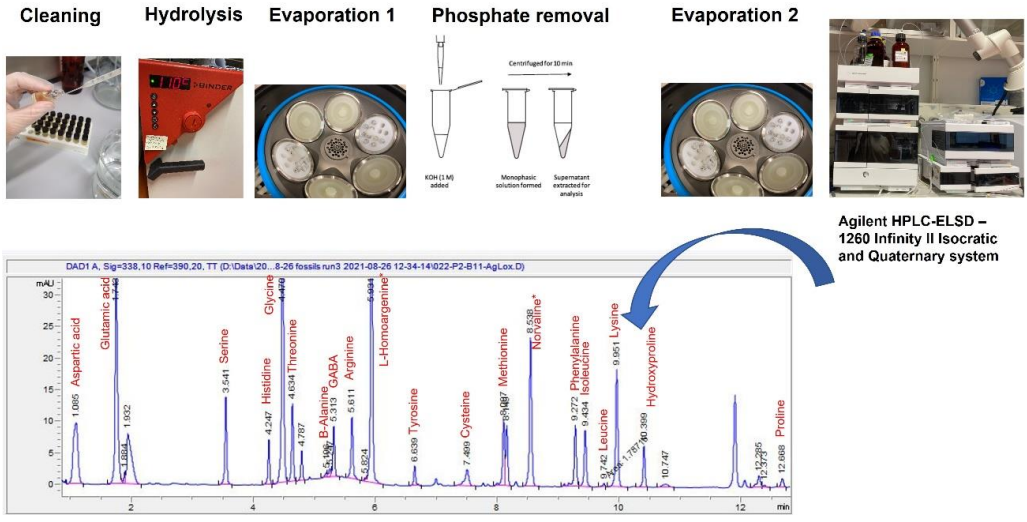

Figure 5.1. Schematic representation of the full developed protocol: powder cleaning, hydrolysis at 110°C, rocket evaporation, phosphate removal and measurement with the output (chromatogram).

5.2.2.2. Real samples

In previous studies, few information about the AAs composition of enamel are reported, both in terms of different taxa and chronological age [13]–[15], [22]. The renewed interest for fossil enamel requires a deeper knowledge of the modern species, in order to have enough references to understand variations across time.

The results obtained in this research on modern samples (Figure 5.2) have clarified the relative AAs composition of different animal species, revealing similar abundances of the AAs. In detail, glycine (20-45 %), aspartic acid (~ 7 %), glutamic acid (10-20 %), serine (6-10 %) and proline (1-24 %) were the most abundant AAs. PCA was performed on the data to evaluate the possible separation between different species according to their relative AAs content (Figure 5.3). In the score plot, it is interesting to notice that the human, shark and elephant are outliers in terms absolute content (Figure 5.3.a) and they are well distinguished from the others. Among the others, no trends were detected due to their environment or specie. In addition to this, from the relative abundances in the pie charts and PCA on relative AA data (Figure 5.4), no particular trends were deducible. In the PCA on relative AA data (Figure 5.4), fishes (carp, seabream) seemed to be closer each other, due to higher abundance of glycine and hydroxyproline. However, more replicates of the same and different samples should be analyzed to confirm the AAs relative and absolute content and to better clarify the relation between different species.

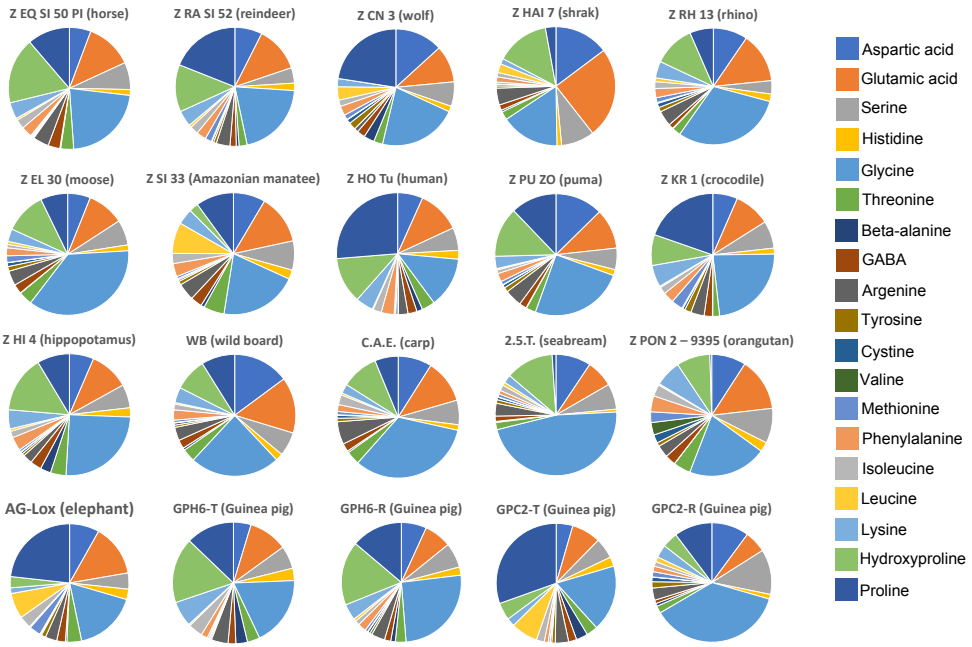

Figure 5.2. AA relative abundance in modern samples from different species. The data were forced to close to 100. Glycine was detected as the most abundant AA in all the species.

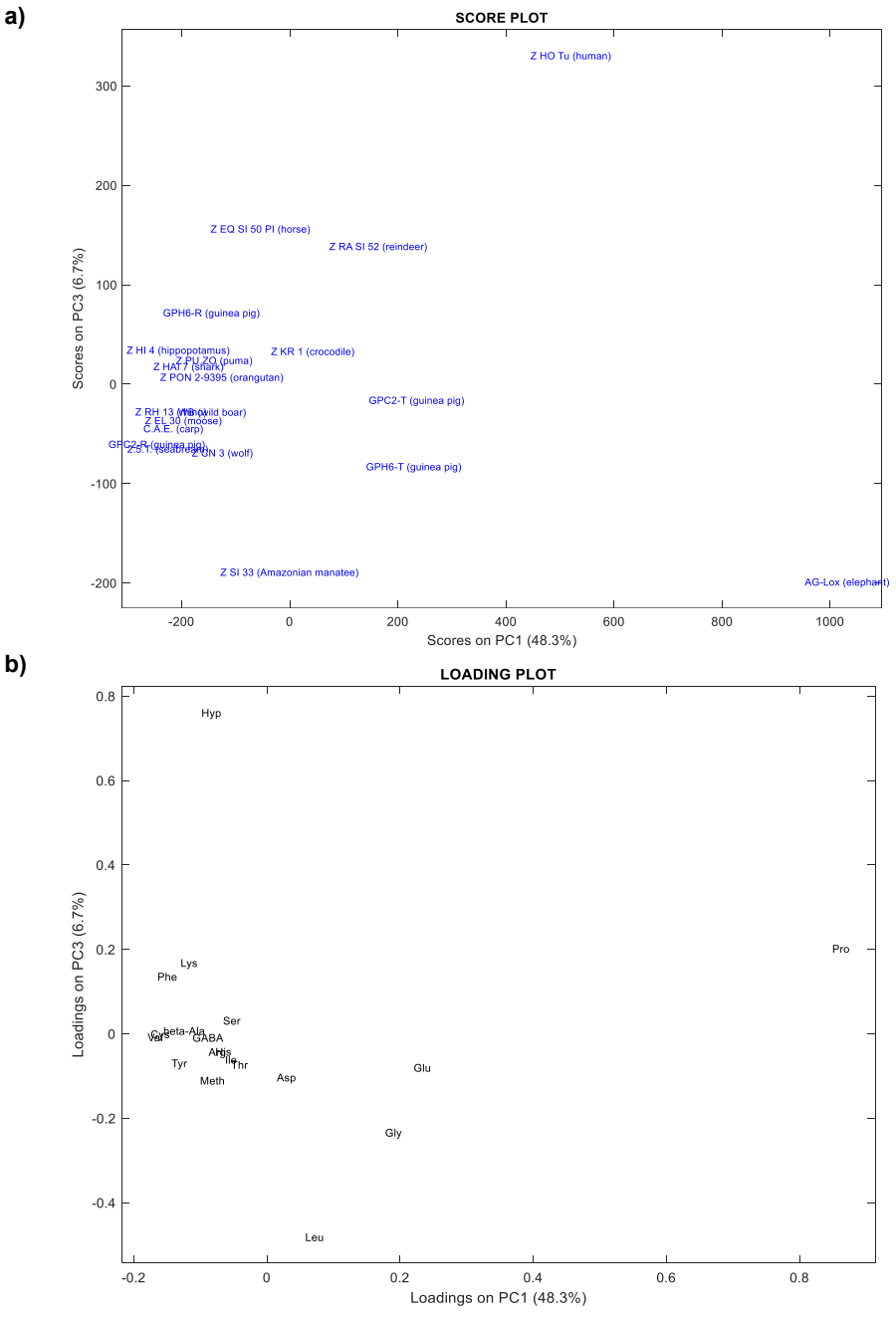

Figure 5.3. PCA on modern samples. The data were normalized through the calibration curves and then according to an internal standard (L-Homoargenine) and elaborated in Matlab (row centering, column centering). The score plot (a) showed the separation among samples. The loading plot (b) showed the AAs responsible for separations.

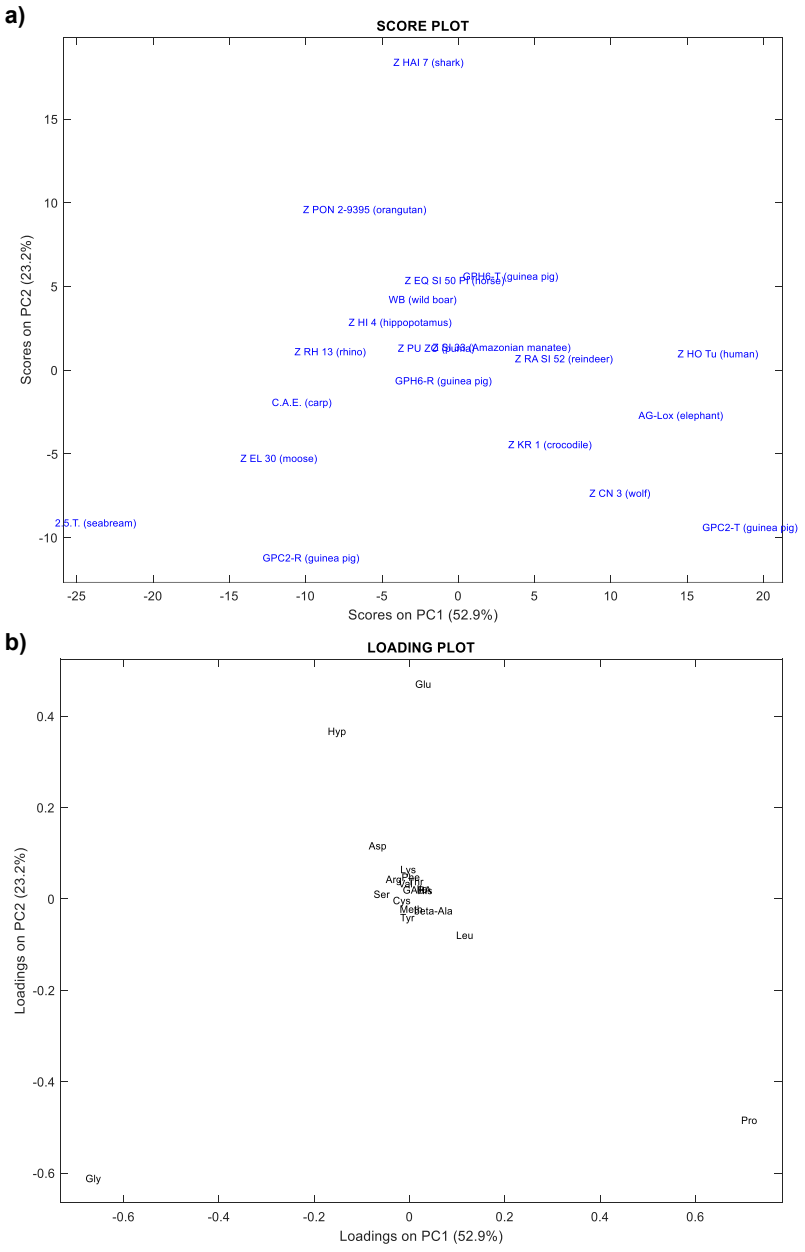

Figure 5.4. PCA on modern samples. The data were forced to sum to 100 % and then elaborated in Matlab (row centering, column centering). The score plot (a) showed the separation among samples. The loading plot (b) showed the AAs responsible for separations.

Two guinea pig samples with different diets were analyzed to evaluate the possible contribution of diet on AAs composition. In GPC2 (carnivore diet) all the AAs were

present in low percentages, except for glycine, aspartic acid, glutamic acid, serine and proline. In GPH6 (herbivore diet) a higher variability of AAs was detected, thus the percentage of glycine decreased and the others increased (Figure 5.2). However, these results are in doubt due to the low number of samples, thus more individuals with different diets need to be analyzed to corroborate this hypothesis.

For these two samples, it was also evaluated the possible difference in AAs distribution within the same sample, collecting powder from the radical (R) immature enamel and the tip (T) mineralized enamel. The guinea pigs with an herbivore diet showed the same pattern in R and T enamel, except for hydroxyproline and proline concentrations which are inverted. On the other hand, the individuals with a carnivore diet revealed a higher variability between R and T enamel, especially for lysine, isoleucine, methionine and glycine. T enamel had a lower content of glycine and a higher content of all the other AAs then R enamel. On the contrary, R enamel showed a higher concentration of glycine. These results are in line with the $\delta^{15}N_{enamel}$ values previously detected on the same samples, that revealed the higher nitrogen content in mineralized enamel then in immature enamel [23].

The analysis of modern samples provided a reference for the evaluation of changes of AAs overtime in fossil samples. The fossil samples allowed to consider different factors of impact: species, site or period. The data revealed that species seemed to impact the AA content in a limited way. It is evident from the pie plots, that the same species from different sites and period could showed a different AAs distribution or, on the contrary, different species from the same site could present a similar composition (Figure 5.5).

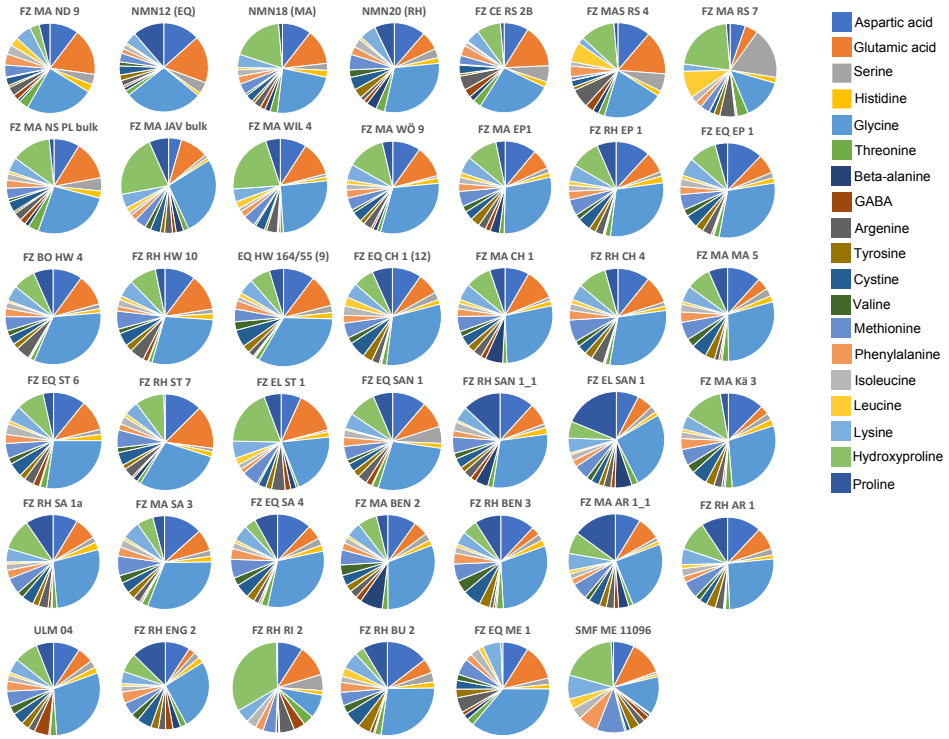

Figure 5.5. AA relative abundance in fossil samples.

The PCA has been performed both on relative and semi-quantitative data and the results showed interesting perspectives. The PCA on the absolute data from all the samples allowed to distinguish between modern and fossils samples. Based on the loading plot, glycine, glutamic acid, serine and proline are the AAs present in higher amounts in modern or well-preserved teeth (Figure 5.6). On the contrary, the PCA on relative data (*i.e.*, AAs forced to sum to 100 %) revealed the percentage of each AA within a specimen. Based on the loading plot, glutamic acid, arginine and serine showed the highest relative percentage in fossil samples (Figure 5.7). This was possibly due to the lower preservation of the others, with a consequent increasing of those AAs more resistant to chemical degradation [15]. The relative data of glycine, glutamic acid and aspartic acid were in line with the data obtained by the few works regarding tooth enamel [13], [24]. For this reason, we suggest that these AAs could be used as a proxy for enamel preservation.

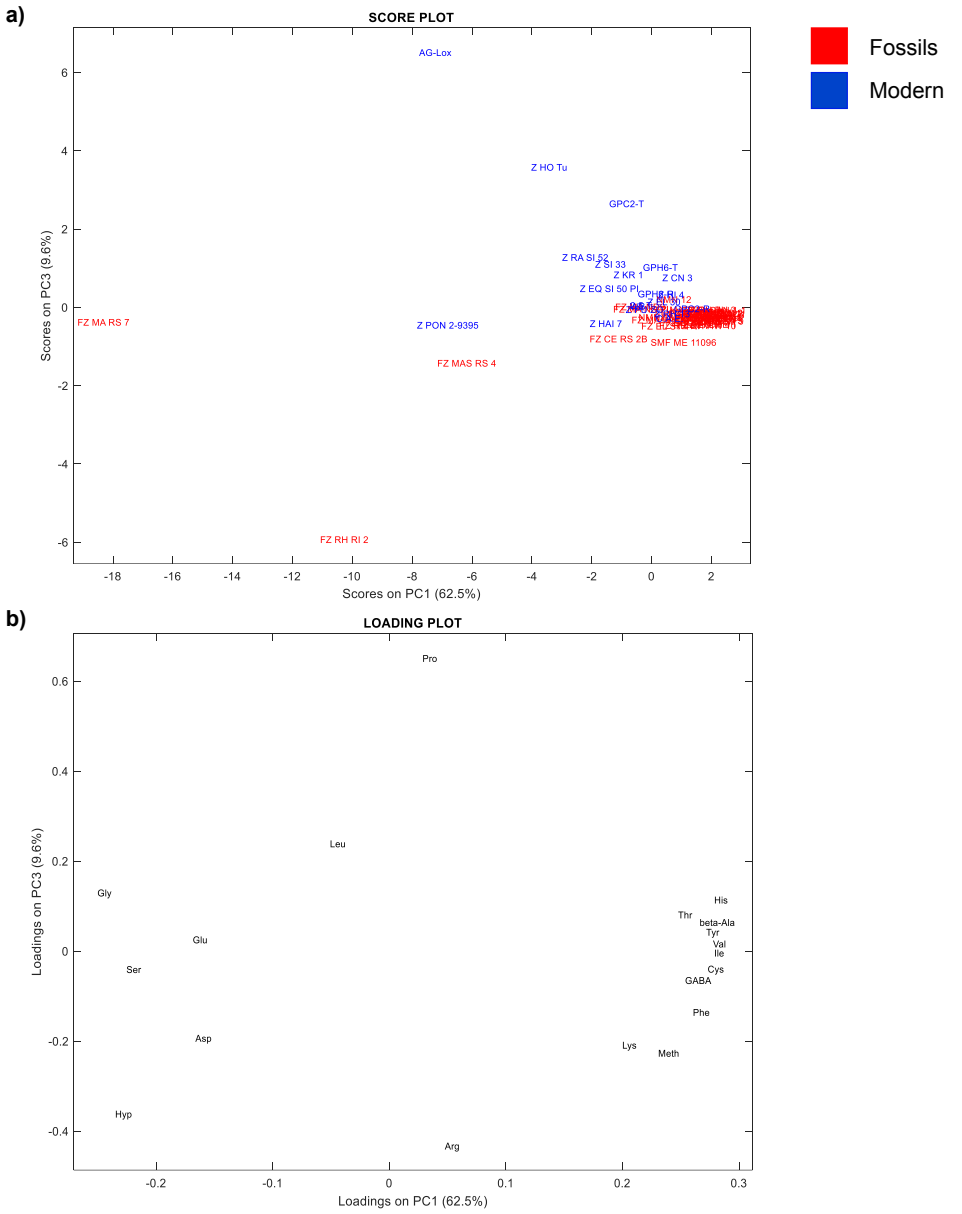

Figure 5.6. PCA on modern and fossil samples. The data were normalized through the calibration curves and then according to an internal standard (L-Homoargenine) and elaborated in Matlab (row centering, column autoscaling). The score plot (a) showed the separation among samples according to their antiquity. Blue samples are modern and red samples are fossils. The loading plot (b) showed the AAs responsible for preservation.

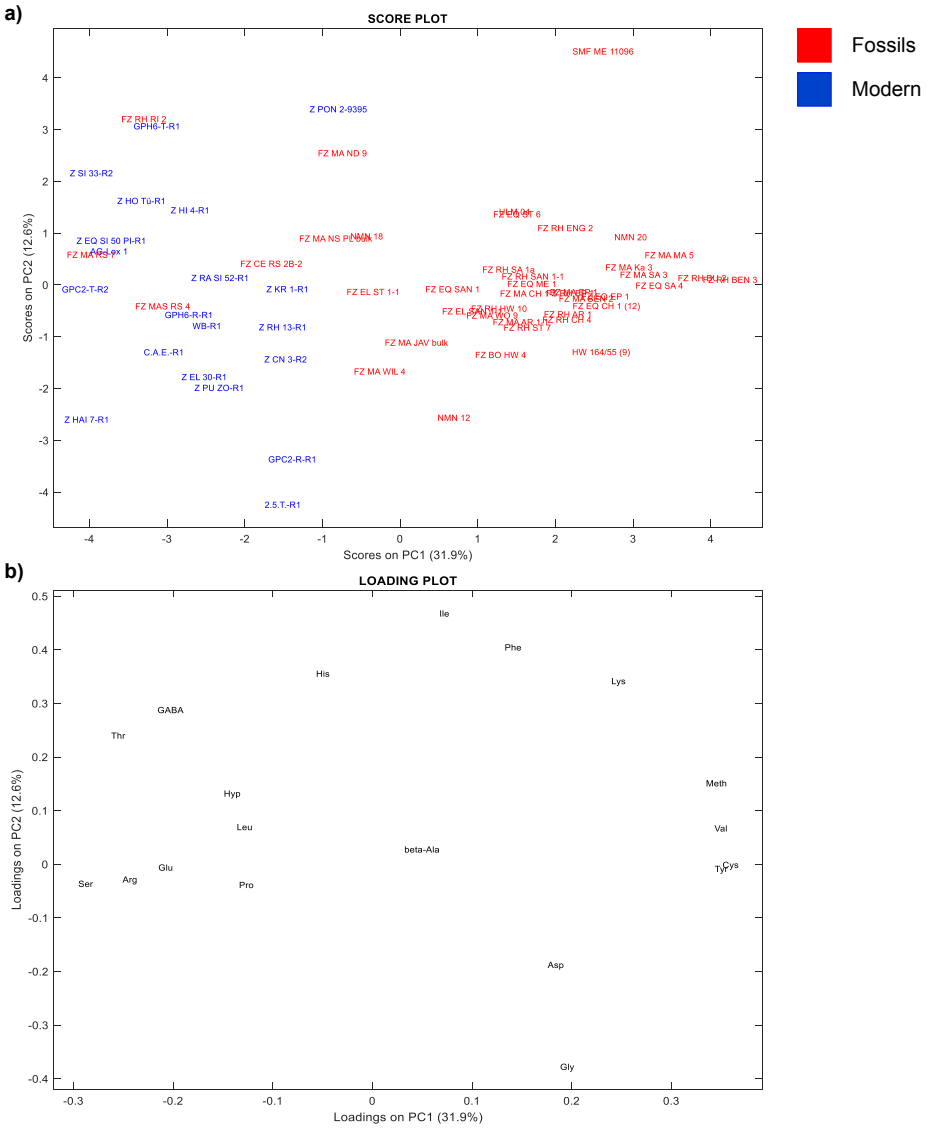

Figure 5.7. PCA on modern and fossil samples. The data were forced to sum to 100 % and then elaborated in Matlab (row centering, column autoscaling). The score plot (a) showed the separation among samples according to their antiquity. Blue samples are modern and red samples are fossils. The loading plot (b) showed the AAs responsible for preservation.

Looking closely at absolute mastodons (MA) data, it is possible to confirm that sample antiquity is the main influence factor for absolute AAs variation. This is evident both from the PCA (Figure 5.8) and from the scatter plot of some individual AAs, selected based on the loading plot (Figure 5.9). Comparing the scatter plots of the same AAs in

MA, rhino (RH) and horse (EQ), it is interesting to notice that this progressive temporal decreasing of AAs is only present in MA samples. This suggested that the preservation of AAs could be affected by the dental morphology and/or microstructure of a specific taxon. The site contributed on preservation only in some specific cases, where particular environmental factors played a significant role (*e.g.*, RI site).

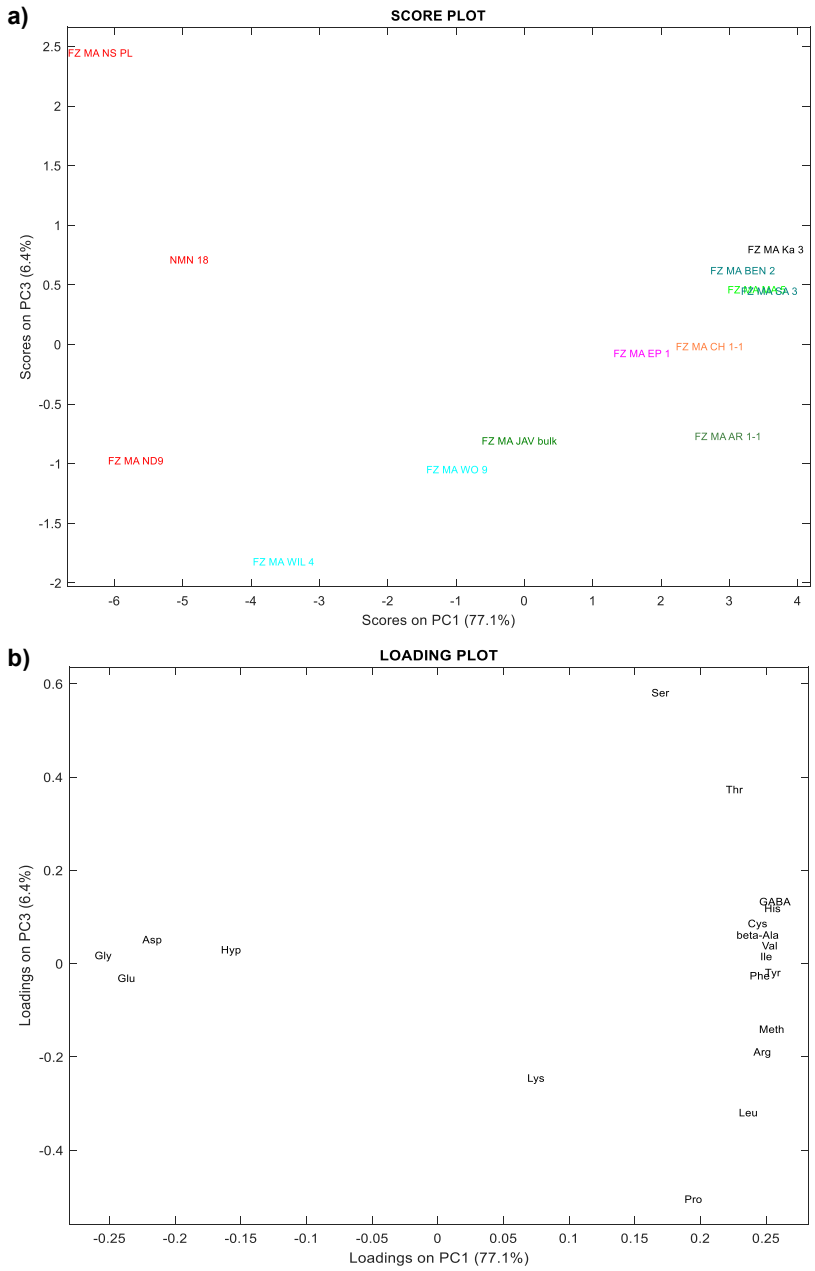

Figure 5.8. PCA on MA samples. The data were normalized through the calibration curves and then according to an internal standard (L-Homoargenine) and elaborated in Matlab (row centering, column autoscaling). The score plot (a) showed the separation among samples mainly according to their chronological age. The loading plot (b) showed the AAs responsible for preservation.

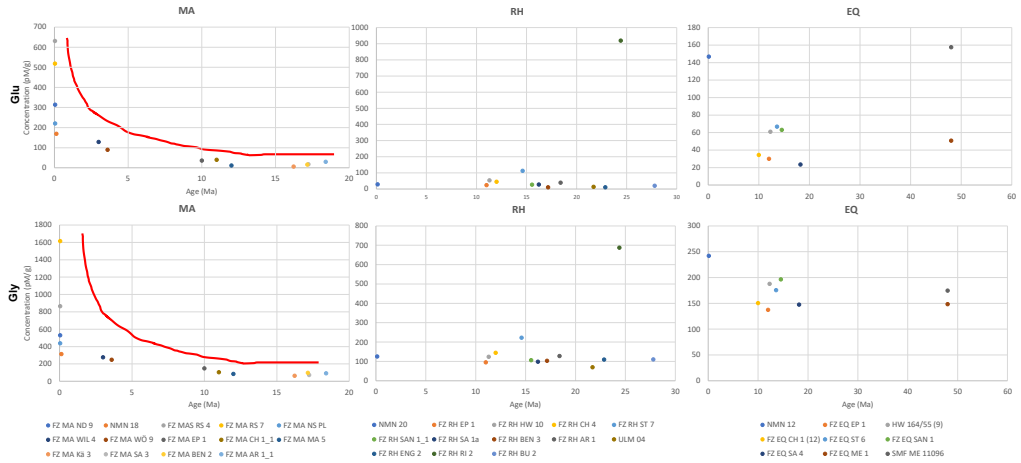

Figure 5.9. Scatter plots of MA, RH and EQ samples for some significant AAs versus the age of sample. Two AAs are reported as example: glutamic acid (first line) and glycine (second line). The data of MA showed a decreasing in AAs content according to the increasing of time (red lines). The only exception was FZ MA JAV bulk, but it could be influenced by the site of provenance.

5.2.3. Conclusions and further perspectives

The method here presented allowed the AAs detection in all the modern and fossil samples analyzed, using a low amount (~1 mg) of enamel powder.

The results contributed to clarify the AAs distribution in modern samples, from different species and with different diets, and to build a reference database. Moreover, the data revealed the AAs preservation in fossils dated 48 Ma, showing the possible survival of organic fraction in deep-times.

This method opens new prospects of research for reconstruction of the past and investigation of the trophic ecology of modern and fossil taxa.

Further analysis on a wide group of both modern and fossil samples will be performed in the future. Firstly, the investigation of more modern samples from the same species could improve the robustness of the data implementing the reference database. Secondly, more experiments on different individuals from the same species and the same site could be useful to valuate intra-cohort variations. In particular, the investigation of more mastodons could be crucial to evaluate the decreasing of some AAs according to time. Moreover, the evaluation of FAAs on the same samples could reveal their possible relation with peptide hydrolysis and their diagenetic loss overtime.

5.3. References

[1] B. Demarchi, *Amino Acids and Proteins in fossil Biominerals*. 2020.

[2] G. Wu, "Amino acids: metabolism, functions, and nutrition," *Amino Acids*, vol. 37, no. 1, pp. 1–17, 2009, doi: 10.1007/s00726-009-0269-0.

[3] G. Wu *et al.*, "Dietary requirements of 'nutritionally non-essential amino acids' by animals and humans," *Amino Acids*, vol. 44, no. 4, pp. 1107–1113, 2013, doi: 10.1007/s00726-012-1444-2.

[4] G. Wu, "Functional amino acids in growth, reproduction, and health," *Adv. Nutr.*, vol. 1, no. 4, pp. 31–37, 2010, doi: 10.3945/an.110.1008.1.

[5] M. Jágr, P. Ergang, S. Pataridis, M. Kolrosová, M. Bartoš, and I. Mikšík, "Proteomic analysis of dentin–enamel junction and adjacent protein-containing enamel matrix layer of healthy human molar teeth," *Eur. J. Oral Sci.*, vol. 127, no. 2, pp. 112–121, 2019, doi: 10.1111/eos.12594.

[6] G. A. Castiblanco, D. Rutishauser, L. L. Ilag, S. Martignon, J. E. Castellanos, and W. Mejía, "Identification of proteins from human permanent erupted enamel," *Eur. J. Oral Sci.*, vol. 123, no. 6, pp. 390–395, 2015, doi: 10.1111/eos.12214.

[7] C. Froment *et al.*, "Analysis of 5000 year-old human teeth using optimized large-scale and targeted proteomics approaches for detection of sex-specific peptides," *J. Proteomics*, 2020, doi: 10.1016/j.jprot.2019.103548.

[8] A. Gismondi *et al.*, "A multidisciplinary approach for investigating dietary and medicinal habits of the Medieval population of Santa Severa (7th-15th centuries, Rome, Italy)," *PLoS One*, vol. 15, no. 1, pp. 1–30, 2020, doi: 10.1371/journal.pone.0227433.

[9] D. R. Green, F. Schulte, K. H. Lee, M. K. Pugach, M. Hardt, and F. B. Bidlack, "Mapping the tooth enamel proteome and amelogenin phosphorylation onto mineralizing porcine tooth crowns," *Front. Physiol.*, vol. 10, no. JUL, pp. 1–16, 2019, doi: 10.3389/fphys.2019.00925.

[10] M. Buckley, S. Fraser, J. Herman, N. D. Melton, J. Mulville, and A. H. Pálsdóttir, "Species identification of archaeological marine mammals using collagen fingerprinting," *J. Archaeol. Sci.*, vol. 41, 2014, doi: 10.1016/j.jas.2013.08.021.

[11] K. Weber *et al.*, "Diagenetic stability of non-traditional stable isotope systems (Ca, Sr, Mg, Zn) in teeth – An in-vitro alteration experiment of biogenic apatite in isotopically enriched tracer solution," *Chem. Geol.*, vol. 572, p. 120196, 2021, doi: 10.1016/j.chemgeo.2021.120196.

[12] E. Cappellini *et al.*, "Early Pleistocene enamel proteome sequences from Dmanisi resolve Stephanorhinus phylogeny performed analyses and data interpretation," *Bienvenido Martínez-Navarro*, vol. 574, no. 7776, pp. 103–107, 2020, doi: 10.6084/m9.figshare.7212746.

[13] M. R. Dickinson, A. M. Lister, and K. E. H. Penkman, "A new method for enamel amino acid racemization dating: A closed system approach," *Quat. Geochronol.*, vol. 50, pp. 29–46, 2019, doi: 10.1016/j.quageo.2018.11.005.

[14] J. Hendy, "Ancient protein analysis in archaeology," *Sci. Adv.*, vol. 7, no. 3, pp. 1–12, 2021, doi: 10.1126/sciadv.abb9314.

[15] J. L. Bada, X. S. Wang, and H. Hamilton, "Preservation of key biomolecules in the fossil record: Current knowledge and future challenges," *Philos. Trans. R. Soc. B Biol. Sci.*, vol. 354, no. 1379, pp. 77–87, 1999, doi: 10.1098/rstb.1999.0361.

[16] B. Demarchi, K. Rogers, D. A. Fa, C. J. Finlayson, N. Milner, and K. E. H. Penkman, "Intra-crystalline protein diagenesis (IcPD) in Patella vulgata. Part I: Isolation and testing of the closed system," *Quat. Geochronol.*, vol. 16, pp. 144–157, 2013, doi: 10.1016/j.quageo.2012.03.016.

[17] B. Demarchi *et al.*, "An integrated approach to the taxonomic identification of prehistoric shell ornaments.", *PLoS ONE*, vol. 9, no. 6, e99839, 2014.

[18] F. Welker *et al.*, "Enamel Proteome shows that Gigantopithecus was an early diverging pongine.," *Nature*, vol. 576, no. 7786, pp. 262–265, 2020, doi: 10.1038/s41586-019-1728-8.Enamel.

[19] J. L. Bada, “Amino acid racemization dating of fossil bones.,” *Annu. Rev. Earth Planet. Sci. Vol. 13*, no. 1948, pp. 241–268, 1985, doi: 10.1146/annurev.ea.13.050185.001325.

[20] M. Krummen, A. W. Hilkert, D. Juchelka, H.-J. Schlüter, and R. Pesch, “A new concept for isotope ratio monitoring liquid chromatography/mass spectrometry,” *Rapid Commun. Mass Spectrom.*, 2004, doi: 10.1002/rcm.1620.

[21] S. Palaniswamy, “Determination of amino acid composition of cell culture media and protein hydrosylate standard,” *Agil. Technol. Appl. Note*, 2017.

[22] W. G. Armstrong and L. B. H. Tarlo, “Amino-acid components in fossil calcified tissues,” *Nature*, vol. 210, no. 5035, pp. 481–482, 1966, doi: 10.1038/210481a0.

[23] J. N. Leichliter *et al.*, “Nitrogen isotopes in tooth enamel record diet and trophic level enrichment: Results from a controlled feeding experiment,” *Chem. Geol.*, vol. 563, 2021, doi: 10.1016/j.chemgeo.2020.120047.

[24] A. R. Doberenz, M. F. Miller, and R. W. G. Wyckoff, “An analysis of fossil enamel protein,” *Calcif. Tissue Res.*, vol. 3, no. 1, pp. 93–95, 1969, doi: 10.1007/BF02058649.

CHAPTER 6

AN ELECTRO-IMMUNOCHEMICAL NON-DESTRUCTIVE METHOD FOR BINDER IDENTIFICATION

6.1. Electrochemical biosensors

Electrochemistry is the science that analyses and describes the material transformations on the atomic scale through variations of electronic charge, controlled by current devices. These transformations are redox reactions, thus electrochemistry consists in controlling redox reactions with a current or with a voltage [1].

According to the type of signal measured, electrochemical methods can be classified in different groups. Firstly, they can be divided in methods in which electrode reactions are not considered and method in which they are considered. The second ones are the most used and they can additionally be divided in reactions at the equilibrium or reactions at polarized electrode. Within these two groups, the main types are respectively potentiometric and amperometric (voltammetry) methods. The first one is based on the measurement of the potential different between working, counter and reference electrodes at the equilibrium. The second one considers the change in the oxidation state of the electroactive species, which is directly proportional to the analyte concentration. The current output measured is obtained applying an overpotential to the working electrode from an external potential source. Amperometry in a voltammetry in which the current is measured at a constant potential. There are different amperometric methods according to the type of electrode used or to the method used for potential application [2]–[4].

Electrochemical biosensor was defined by the international union of pure and analytical chemistry (IUPAC) as "*an analytical device that quantitatively or semi-quantitatively senses analyte through biological recognition which is integrated inside the device and contacts directly with the electrochemical transducer*" [2]. Indeed, electrochemical biosensors are constituted by a bio-receptor, which is a bio-recognition element, and a transducer, able to transform the output in a current signal.

In comparison to other analytical methods, electrochemical biosensors allow to achieve fast, precise, low cost and portable equipment and for this reason they have been applied in different fields, such as medical or environmental fields [3], [5]. Traditional electrochemical methods required, as other techniques, a high number of electrodes and connectors, benchtop potentiostat to control the parameters and computers. However, in

last years the new technologies have allowed a miniaturization of all the components previously cited [3]. In particular, screen-printed electrodes (SPEs) started to substitute the traditional electrochemical sensors, thanks to their lower cost and simplest use in situ too. They have been applied in different fields (*e.g.*, medical field, agronomy) and their surfaces were treated in different ways. In fact, the inks used for printing define the selectivity and sensitivity of the electrode, but the surfaces can be modified by the addition of different substances such as metals, enzymes, antibodies, polymers, with a consequent enhancement of electrodes performance [2], [3], [5]–[7].

The combination of immunochemical and electrochemical technologies has been tested in different fields, thanks to the combination between the high specificity of the antigen-antibody reaction with the high sensitivity and low detection limits of electrochemistry [5]. As for the other immunosensors, electro-immunosensors could be divided according to the approach used. The simplest method is a label-free system, in which a capture antibody is immobilized on the electrode and then the capture specific antibody recognizes the analyte. On the contrary, a competitive configuration is based on the competition between labeled and unlabeled analytes for antibody and it usually involved only one antibody. Finally, in sandwich method a capture-specific antibody is immobilized on the electrode surface and then the analyte is bonded over the antibody. Then a secondary antibody reacts with the immobilized analyte.

6.2. Gellan gel

Gellan is a high molecular weight polysaccharide, used as gelling agent in different fields. It is produced by *Pseudomonas elodea* and it is linear anionic heteropolysaccharide, composed by the repetition of (1,3)-β-D-Glucose, (1,4)-β-D-Glucuronic acid, (1,4)- β-D-Glucose and (1,4)-α-L-Rhamnose units (Figure 6.1.) [8].

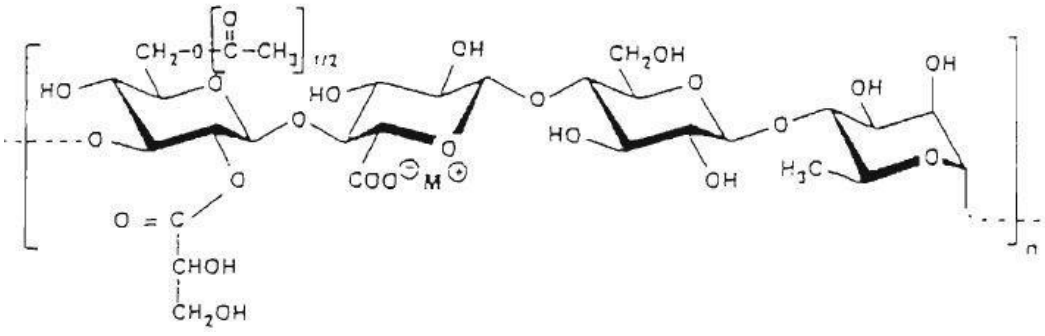

Figure 6.1: Gellan repetitive unit [8].

It is able to form hydrogels with temperature dependent sol-gel transition. In more detail, it forms hard and rigid gel with a slow syneresis rate. When heated, it arranges in a double-helix and, thanks to cations, it creates supramolecular aggregates. Gellan hydrogel structure depends on concentration, temperature, aqueous environment and cation type (monovalent or divalent) used to obtain the aggregation. Indeed, the double helix binds with another one through saline bridges and hydrogen bonds. The presence of monovalent or divalent cations increases the number of possible bonds, making the gel more heating resistant and enriching the gelification ability. This is possible due to the salt presence, which increases the ionic force [8].

The use of monovalent cations, as Na^+ from sodium chloride, allows the coordination of two molecules of water and two residues, one for helix. On the contrary, the use of divalent cations, as Ca^{2+} from calcium acetate, limits the coordination to two residues of the closest helix [8].

In addition to this, it is transparent, homogeneous and stable to pH variations. Because of its pH stability, it has been used in cultural heritage field as cleaning method on paper [9], [10].

6.3. Development of a portable prototype for characterization of binders through a Gellan gel-electro-immunochemical combination

The use of different proteins in paintings as binders and as adhesive is widely known. The preference for one of them was usually connected to the artistic technique or to the environment or to the period. For these reasons a deep studying of them is fundamental

in cultural heritage investigation in order to characterize artworks and artist work contest. Protein identification is a fundamental tool not only to understand the painting technique, but to plan restauration and conservation procedure too [11], [12].

Chromatographic techniques, such as gas chromatography mass spectrometry (GC-MS) and high-performance liquid chromatography (HPLC), are the most suitable for the complete chemical characterization, based on the quantitative determination of binders amino acid sequence [13]–[15]. However, they required a micro-sample and present identification problems in case of mixtures [14]. Fourier-transform infrared (FTIR) spectroscopy could be another useful approach to determine the polymers used, due to their distinctive vibrational features in the infrared [13], [16], [17]. The application of ATR on cross section allows a mapping of different binders used in the different layers, but it requires a sampling as for chromatographic methods. In last years, non-invasive reflection FTIR are preferred for an *in situ* investigation without sampling [18]. However, the signals present distortions due to the combination of specular and diffuse reflection, and to the overlapping of pigments peaks. Immunochemical portable chemiluminescence (CL) sensors have been developed to have an assay which is sensitive, thanks to the antigen-antibody high specific reaction, and easy to use *in situ*, thanks to their small dimension [19], [20].

According to these, there is the necessity to develop portable and sensitive methods, which are also safety for the operators, the artworks and the environment. Recent works presented *in situ* extraction methods, minimally invasive for the artworks [11], [21]. One research developed trypsin functionalized cellulose acetate sheets for *in situ* protein digestion [21]. The method was based on the adhesion properties of some fungal proteins, able to create homogenous layers on sheets, on which trypsin was immobilized [21]. Manfredi and colleagues presented an ethyl-vinyl acetate (EVA) film functionalized with strong cation/ion exchange and C_8 resins for proteins extraction from different artworks surfaces [11]. Despite the *in situ* step for extraction or digestion, the proteomic analysis required a second step with a complex and time consuming laboratory procedure.

In the light of the previous considerations, this work proposes a new biosensor based on the combination of biocompatible Gellan gel and electrochemical sensors, in order to

extract and identify painting binders through the contact between gel and painting and between gel and electrodes. It is faster than traditional extractive methods and less invasive, thanks to the migration of protein through the gel impacting electrodes previously functionalized with a primary and secondary antibody.

Gellan gel was preferred thanks to its properties, such as its stability with temperature and pH changes, flexibility due to boiling point at about 100°C, clearness, compatibility with other polymers and easy disposal thanks to its solubility in water [8]. An electro-immunoassay was chosen due to antigen-antibody high specific reaction, and higher sensitive detection through electrochemical revelation than traditional immunochemical methods. The use of screen-printed electrodes (SPEs) allowed to develop a portable, flexible and low-cost biosensor. Ovalbumin (OVA) was selected as first protein to investigate, because of its widely used as binders in paintings. Thanks to this approach protein digestion is not required, this new biosensor provides binder identification with a single analysis replicable on different artwork points and directly *in situ* without additional laboratories analysis.

The analyses were performed firstly on paper in order to develop a standard protocol on a simple substratum with known OVA concentrations and then on mock-ups paintings with different pigment layers and binders, to evaluate the gel ability to extract protein without painting damage. The results proved the mock-ups integrity after gel application and the ability of the sensors to detect OVA both on paper and mock-ups, in presence of other proteins too. Moreover, the data showed the possibility to stock the sensors in the fridge for more than one month before the use. The presented method could be a useful portable method for restorers for *in situ* identification of binders.

This project was realized in collaboration with the University of Roma Tor Vergata, especially with Prof.ssa Laura Micheli and Prof.ssa Claudia Mazzuca.

6.3.1. Materials and methods

6.3.1.1. Samples

A solution of OVA (1 mg/mL, Sigma Aldrich) was prepared in MilliQ water and calcium acetate ($(CH_3COO)_2Ca$, 0.04% w/w, Sigma Aldrich). Then standard dilutions were prepared in the following concentrations: 0 µg/mL, 0.01 µg/mL, 0.05 µg/mL, 0.1 µg/mL, 0.5 µg/mL, 1 µg/mL, 5 µg/mL, 10 µg/mL.

Squares (2.5x2.5 cm) of Whatman® paper were cut, uniformly covered with OVA standard solutions (1 mL) and then dried in the oven (30°C, 1 h) (Figure 6.2). These samples were used for the calibration curve and all the steps.

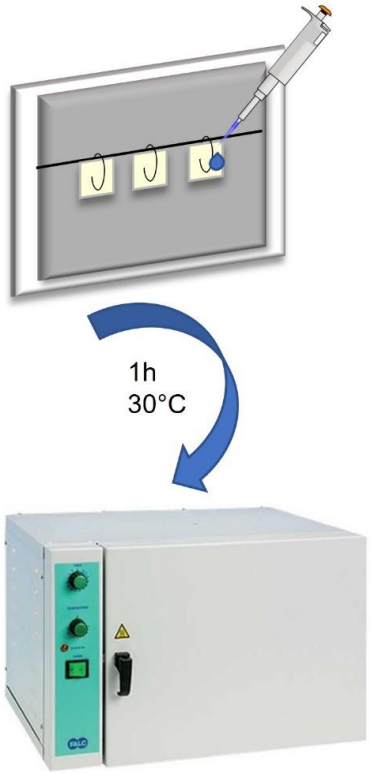

Figure 6.2. Preparation of the paper: addition of the OVA standard solutions and oven for drying.

Standard mock-ups with different binders were used as a real case study, the details of the mock-ups composition are reported in Table 6.1. For the evaluation of possible gel residues or damages on the surface, mock-ups with different compositions were tested.

Table 6.1. Description of the mock-ups layers.

Samples	Structure
B1	Lead white + oil
B2	Lead white + egg
B3	Lead white + glue
2L2	Layer 1 (under the layer 2): red ochre+casein Layer 2 (exposed layer): lead white + egg

6.3.1.2. Gellan gel preparation

The Gellan gel was prepared following the procedure reported in [22]. Calcium acetate powder ($(CH_3COO)_2Ca$, 0,04 % w/w, Sigma-Aldrich, St.Louis, USA) and Gellan gum (2 % w/w, KELCOGEL® CGLA product by CP Kelco, Atlanta Georgia, USA) were dissolved in MilliQ water and then heated in a microwave at 600 W (Mars Microwave, CEM Corporation, Matthews, NC, USA) until it was boiling. Then it was transferred in a petri dish and it was left to cool at room temperature. When it was solid, squares of gel (2x2 cm) were cut.

6.3.1.3. Electrodes preparation

Screen-printed electrodes (SPEs) were home printed at the Laboratory of Analytical Chemistry of the University of Roma "Tor Vergata". They were composed by a working and a counter electrode in graphite and a silver reference electrode. The diameter of the working electrode was 0.3 cm resulting in a geometric area of 0.07 cm^2. The SPEs were pre-treated before their use in order to reduce impurities and homogenize the surface of

the working electrode. The pre-treatment consisted in the addition of 80 µL of phosphate saline buffer (PBS, 0.05 M) and potassium chloride (KCl, 0.1 M, pH 7.4, Sigma-Aldrich, St.Louis, USA). Then an anodic potential of +1.7 V was applied for 180 seconds (chronoamperometry measurement). All the electrochemical measurements were performed by a µAutolab III potentiostat/galvanostat (Metrohm Autolab, Utrecht, The Netherlands).

After this, they were functionalized with 6 µL of anti-rabbit IgG antibody produced in goat (secondary antibody, 10 µg/mL, 0.68 mg/mL stock concentration, 12-348, Sigma-Aldrich Co., St. Louis, MO) in sodium carbonate (Na_2CO_3, 50 mM, pH 9.6, Sigma-Aldrich, St.Louis, USA) overnight at 4°C. The SPEs were rinsed with 45 µL of PBS (15 mM, pH 7.4) and then treated with 6 µL of a blocking solution with PVA 1 % in Na_2CO_3 (50 mM, pH 9.6) for 15 minutes. They were washed again with 45 µL of PBS and coated with 6 µL of anti-chicken ovalbumin antibody 1:7500 v/v (primary antibody, 1.0 mg/mL stock concentration, ab181688, AbCam, Cambridge, UK) in Na_2CO_3 (50 mM, pH 9.6) for 30 minutes in the dark at 4°C. After one washing with 45 µL of PBS, they were treated again with 6 µL of the blocking solution (PVA 1% in Na_2CO_3) for 15 minutes. At the end they were washed one last time with 45 µL of PBS.

6.3.1.4. Protocol for analysis

The first step of the protocol was the extraction of the protein through the application of the gel for 5 minutes on the sample (paper or mock-up) under low pressure. Then the gel was removed and turned of 180° to put the electrode in contact with the gel surface previously in contact with the sample. The immunosensor was left in contact with the gel for 10 minutes (Figure 6.3). The SPE was removed and rinsed one time with 45 µL of PBS (15 mM, pH 7.4) and tween 0.1 % and then two times with 45 µL of PBS to remove tween residues.

Before the analysis, 80 µL of potassium ferrocyanide solution ($K_3Fe(CN)_6$ 3 mM + KCl 10 mM) were added on the SPEs. The analysis was done with a scan rate square wave voltammetry (SWV) (Table 6.2). SWV is a voltammetry in which a square-wave potential waveform is superimposed on an underlying linearly varying potential ramp or staircase

ramp. The current is sampled just before the end of the forward-going pulse and of the backward-going pulse [23].

Table 6.2. Parameters applied in the SWV analysis.

Pre-treatment	
Depositional potential (V)	-0.1
Time (s)	30
Potentials	
Starting potential (V)	-0.1
Ending potential (V)	0.4
Step (V)	0.003

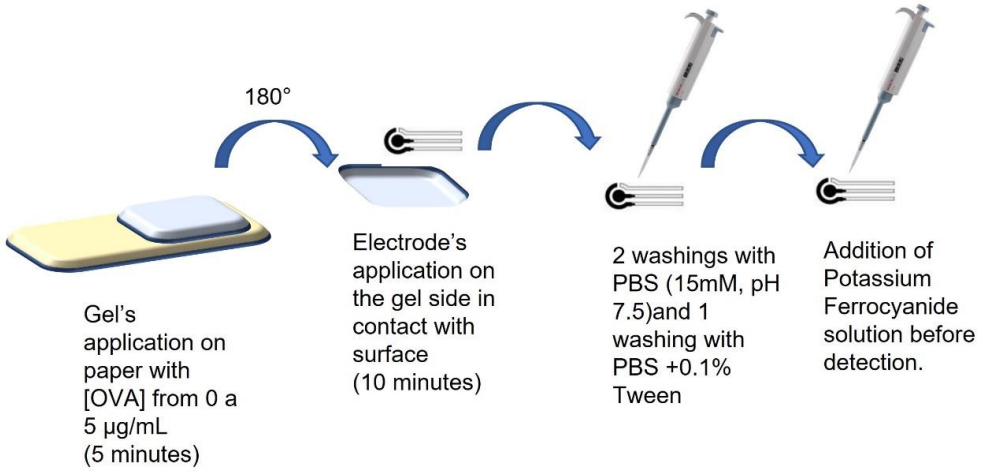

Figure 6.3. Steps for protein extraction and SPEs analysis. The Gellan gel was applied on the surface (paper or mock-up) for 5 minutes. Then it was turned and put in contact with the SPE for 10 minutes. After washings, it was analyzed in SWV.

6.3.1.5. Gellan gel analysis

To evaluate the possible removal of pigment from the mock-ups, a gel extraction was conducted after the application for 15 and 60 minutes on different surfaces. Each gel was weighed before and after the application. According to their weight, they were soaked in Falcon tubes with MilliQ water and left under stirring for 1 hour and 30 minutes. Then they were centrifuged for 15 minutes at 3200 rpm and the supernatant was transferred in new Falcon tubes. FTIR spectra of the extracts were acquired with a Thermo Scientific Nicolet™ iS50 spectrometer (Thermo Scientific Inc., Madison, WI) equipped with an attenuated total reflectance (ATR) (4000–525 cm^{-1} region) at a resolution of 4 cm^{-1}. A total of 64 scans were collected for each sample. The extracted solution was dried on aluminum foil and then put directly in contact with the crystal.

6.3.1.6. Residues analysis

To evaluate the possible Gellan gel residues on the surface of the mock-ups, they were documented before, after gel application and after 72 hours with a stereo-microscope Leica® MZ6 connected to a Canon® power shot 550 digital camera and with an Olympus BX51M optical microscope (Olympus Corporation, Tokyo, Japan) connected to an Olympus DP70 digital camera. Moreover, FTIR spectra were acquired before and after the application of the gel on mock-ups with a Thermo Scientific Nicolet™ iN10 MX imaging microscope (Thermo Fisher Scientific, Waltham, MA, USA) with a mercury-cadmium-telluride (MCT) detector cooled by liquid nitrogen. The analyses were performed using a slide-on ATR objective, equipped with a conical germanium crystal (4000-675 cm^{-1}) at a spectral resolution of 4 cm^{-1}. Backgrounds were acquired keeping the slide-on inserted and the ATR objected not in contract with the sample surface.

6.3.2. Results and discussion

6.3.2.1. Assay set-up

Antibodies dilutions, blocking solution concentration, washing steps and incubation time have been evaluated to improve the efficiency in the antigen-antibody recognition and binding, thus improving the assay performances. Moreover, different methods for the extraction of proteins from the paint models, were tested. In detail paper was used to

optimize the extraction reducing the times of application of the gel on the surface and increasing the efficiency of the system in terms of limit of detection (LOD) and reproducibility.

Preparation and assessment of the electrodes

The setting of the experimental conditions was initially carried out evaluating the antibodies concentrations. The immobilization of antibodies on SPEs was the most critical step, since the antibodies concentrations could influence the performance of the electrochemical sensor. All the tests for the optimization have been performed on paper squares treated with OVA solutions (0, 0.5, 1, 2.5, 5, 10 µg/mL). The Gellan gel was applied for 10 minutes on the paper, then the gel was removed and the SPE was applied on the gel for 5 minutes. Preliminary tests conducted on SPEs treated with different concentrations of the primary anti-OVA antibody, 1:2500 (v/v), 1:5000 (v/v) and 1:7500 (v/v), did not show a linear correlation between the current values and the OVA concentrations. In fact, the current signal should decrease with the increasing of the OVA concentration, due to the formation of an immunocomplex antigen-antibody which covers the SPE surface, reducing the SPE area available for the redox reaction of ferrocyanide and thus reducing the signal.

To overcome this interaction problem, a pre-coating on the SPEs with a secondary antibody was tested in order to promote the binding of the heavy chain of the OVA antibody to the secondary antibody; therefore, the variable region of the primary antibody was available for the antigen binding. Two concentrations of the anti-rabbit antibody were tested, 10 µg/mL and 10 ng/mL, to functionalize the SPEs through an overnight incubation in the dark at 4°C. After the pre-coating with the two different anti-rabbit antibody concentrations, the SPEs were washed with PBS, treated with a blocking solution (PVA 1 % in Na_2CO_3), to reduce the not specific signal, and washed again with PBS. Two different concentrations of anti-OVA, 1:5000 (v/v) and 1:7500 (v/v), were applied for SPEs coating. After an incubation of 30 minutes in the dark at 4°C, the SPEs were washed with PBS, treated again with the blocking solution and washed with PBS. Initially, the best results in terms of LOD and reproducibility were obtained with the combination of anti-rabbit 10 ng/mL and anti-OVA 1:7500 (v/v). However, after the

addition of 3 washings before the analysis (1 washing with PBS and tween 0.1 % solution and 2 washings with PBS), an increasing of the performance was observed with the combination of anti-rabbit 10 µg/mL and anti-OVA 1:7500 (v/v). In all tests, the nonspecific adsorption was avoided thanks to an incubation of 15 minutes with a blocking solution (PVA 1% in 50 mM Na_2CO_3 pH 9.6), after each antibodies incubations. Moreover, after each incubation, an additional washing step with PBS was conducted to remove the excess of the antibody or blocking solution.

Gel application

In order to avoid invasive interaction between the gel and the painted surface, particular attention was devoted to the application procedure and time of the gel on the surface. To this aim, preliminary investigations were performed on paper samples treated with OVA solutions (0, 0.01, 0.05, 1, 0.5, 1, 5, 10 µg/mL) to maximize the electrochemical sensor signal before the application on paintings (Table 6.3 and Figure 6.4.). For the optimization of this step SPEs were pre-coated with anti-rabbit 10 ng/mL and anti-OVA 1:7500 v/v, which was the protocol initially selected according to the SPEs pre-treatment tests.

Table 6.3. Description of the different times and methods for gel and SPEs application on paper.

Description	**Abbreviation**	**Total time (min.)**
1. Gel in contact with the sample for 10’ 2. Addition of the SPE on gel for 5’	10’+5’	15
1. Gel in contact with the sample for 10’ 2. Removal of the gel 3. Addition of the SPE on the gel for 5’	10’+5’ no sample	15
1. Gel in contact with the sample for 5’	5’+5’+5’	15

2. Removal of the gel, live it on the bench for 5’ 3. Addition of the SPE on the gel for 5’		
1. Gel in contact with the sample for 5’ 2. Removal of the gel 3. Turn it of 180° 4. Addition of the SPE on the same side of the gel previously in contact with sample for 10’	5’+10’ no sample same side	15

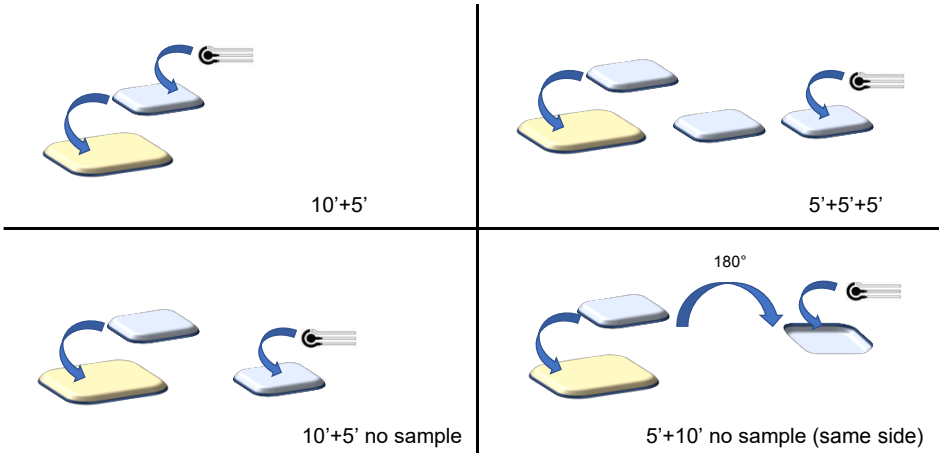

Figure 6.4. Schematic representation of times and methods tested for the application of the gel and the SPEs. The first one was abbreviated as 10’+5’, the second one as 10’+5’ no sample, the third one as 5’+5’+5’, the last one as 5’+10’ no sample (same side).

The first test consisted in the application of the gel on paper samples for 10 minutes, then the SPE was added on the gel for 5 minutes. The second test was performed applying the gel on the paper for 10 minutes. After this time, the gel was removed from the sample and the SPE was applied on the gel for 5 minutes. These two tests were conducted with the

aim to reduce the time of contact between the gel and the sample. However, the results obtained were similar to the original one obtained with 15 minutes of application of gel and SPE together on the sample. This was probably due to the excess of protein adsorbed by the gel with a long time of application, resulting in the release of the protein on the sample surface. Therefore, a third test was performed in order to reduce the time of contact between the gel and the sample. It consisted in the application of the gel on the sample for only 5 minutes, then the gel was removed and leave on the bench for 5 minutes. After this, the SPE was added on the gel for 5 minutes. However, it was not possible to obtain current values. This was due to the time of diffusion of the protein in the gel for capillarity. In fact, the protein is adsorbed by the gel and then it is diffused in the gel structure, before to reach the opposite side of the gel. To avoid this diffusion problem and to maintain short times of contact between sample and gel, the fourth test was performed adding the SPEs on the same side of the gel previously in contact with the sample, immediately after the removal of the gel from the paper. This last approach allowed to obtain the best performance in terms of current signals, data reproducibility and short time of contact with the sample. It was selected for the final protocol in combination with the selected antibodies concentrations.

Assay performance

The full protocol (SPEs treatment and gel application time/way) was used to obtain a calibration curve (Figure 6.5). Paper squares were wet with OVA solutions (0, 0.01, 0.05, 0.1, 0.5, 1, 5, 10 µg/mL). The SPEs were pre-coated with anti-rabbit antibody 10 µg/mL in Na_2CO_3 overnight at 4°C in the dark. Then they were washed with PBS, covered with the blocking solution for 15 minutes, washed again and incubated with the anti-OVA antibody 1:7500 v/v for 30 minutes at 4°C in the dark. Then the washings and the blocking step were repeated. The gel was applied on the paper samples for 5 minutes, then it was removed and turned of 180° and the SPE was applied on the same side of the gel previously in contact with the sample. After 10 minutes, the SPE was removed and washed 1 time with tween 1 % and 2 times with PBS, before the current signal measurement.

The curve was obtained applying the logistic function with 3 parameters:

$$y = \frac{(a)}{1 + (x|x_0)^b}$$

For each concentration three replicates were performed and the current values were normalized as follow:

$$I\% = \left(\frac{I - I_{min}}{I_{max} - I_{min}}\right) \times 100$$

Where I corresponds to the faradic current value relative to the different protein concentration, I_{max} corresponds to the maximum registered during the analysis and I_{min} corresponds to the minimum value registered during the analysis. The normalization allowed to remove the errors due to the electrode (*i.e.*, printing).

In Figure 6.5 it is possible to see that increasing the OVA concentration, the signal decreased. Thus, in presence of OVA an immunocomplex antigen-antibody covers the SPE surface, reducing the SPE area available for the redox reaction of ferrocyanide. On the contrary, in absence of the protein the surface does not change. Thus, higher is the protein concentration on the electrode, lower is the current signal. The highest value, here reported as 100 %, corresponds to the blank, which was an electrode pretreated with antibodies but without protein.

From the results obtained, it was possible to evaluate the LOD, which was 0.005 μg/mL, linear range 0.5-0.14 μg/mL (calculated between 10 % and 80 % of the curve), and RSD 1%.

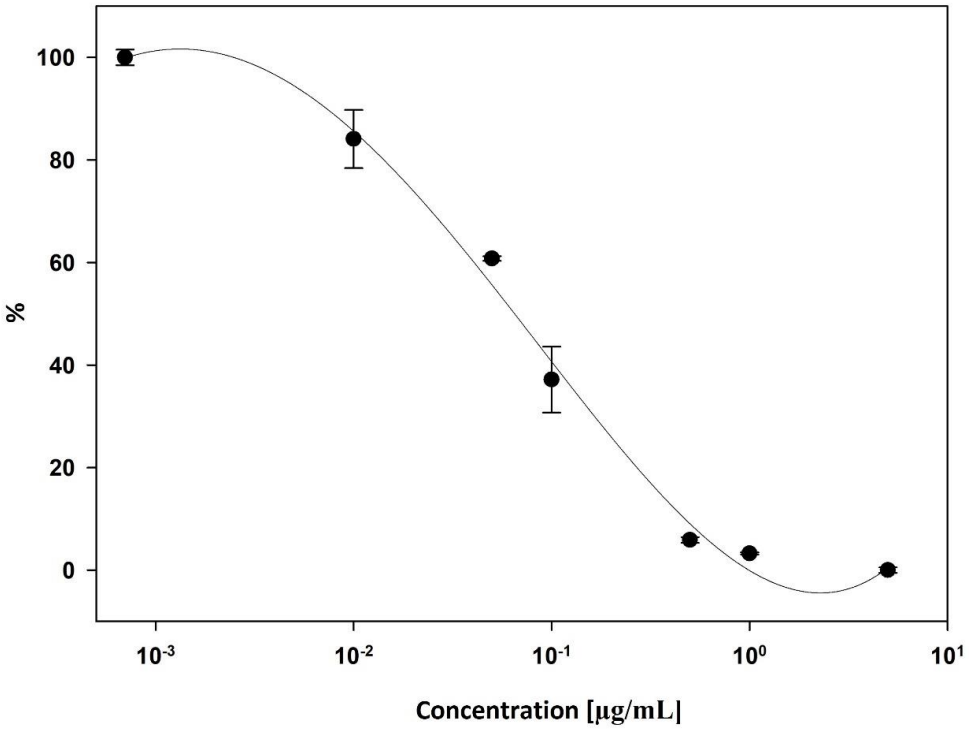

Figure 6.5. Calibration curve obtained using paper wet with standard OVA solutions. The data were normalized and reported as current percentage.

Cross-reactivity

To evaluate the specificity of the immunosensor, the biosensor was tested using different single proteins solutions (casein, collagen, bovine serum albumin (BSA), OVA) in a concentration of 0.1 µg/mL, which was the inflection point of the calibration curve of OVA and thus clearly detectable by the system.

A first test was conducted applying the electrodes on the gel for 5 minutes and then measuring directly the current. The current values were normalized with the same function previously used for the calibration curve, considering the maximum of current (no protein) as 100 %. Despite the quite good difference between the percentage of OVA and the other proteins, the RSD was high for the not specific proteins (Figure 6.6.a).

The possible interference of aspecific signal due to excess of non-bonded protein and gel residues on the working electrode was evaluated. To this purpose, to improve the reproducibility and reduce the error, three washings were added before the analysis: one washing with tween and two washings with PBS. The addition of this washing step allowed to remove the residues on the SPEs, revealing only the contribution due to the protein bonded with the antibody. For the other proteins percentages of current close to the maximum, thus equal or close to 100 %, were obtained, with a reduction of the RSD too (Figure 6.6). These results confirmed that there was no detectable binding between the antibody and other proteins. Moreover, without the washings the OVA percentage was ~ 50 %, while with the addition of the washings its percentage was ~ 40 %. This means that the interference due to gel residues on the SPE was reduced thanks to the washings and current value decreased also demonstrating an improvement in sensitivity for the detection of OVA (Figure 6.6.b.). The results confirmed that the immunosensor was selective for the target protein (OVA) and not for the other proteins, allowing a sensitive and selective identification of OVA.

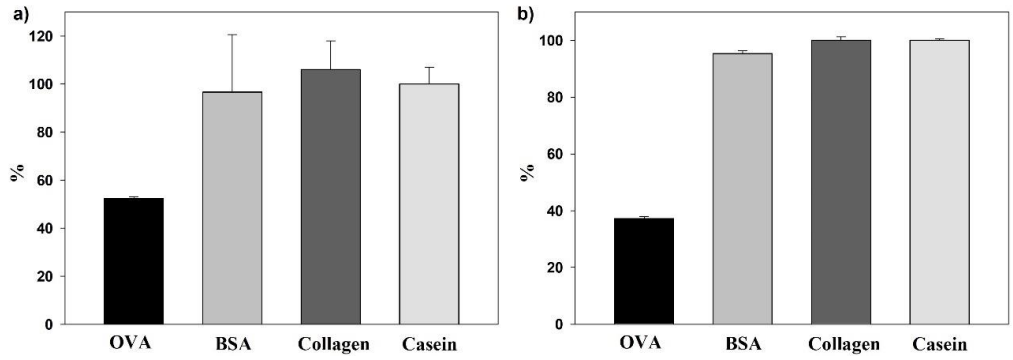

Figure 6.6. Histograms represent the current values of the different proteins without the addition of the washings (a) and with the addition of the washings before the measure (b).

Immunosensor stability

The final aim of the work was the development of fast and easy to use biosensor, that the restorers could use *in situ* in order to evaluate the best approach. For this purpose, the evaluation of immunosensors storage for some months was tested to consider the feasibility of the method. The SPEs were treated as explained in Material and methods

and, after the last blocking step, they were stored in a humid chamber in the dark at 4°C. The measurements were conducted with standard concentrations of OVA in the day of preparation and after 14, 30 and 60 days. Normalizing according to the day 0, thus considering the day 0 as 100 % of current intensity, the day 60 showed the 65 % revealing a decreasing of the 37 % (Figure 6.7). Despite the minimal reduction of efficiency of the system, the results showed the possibility to obtain reliable data after 60 days.

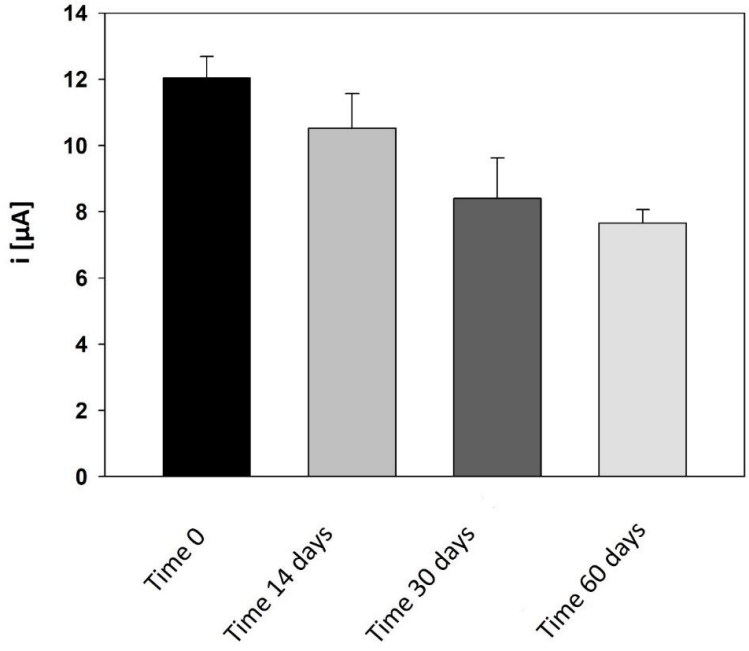

Figure 6.7. Histogram with current intensities detected in different times after the preparation (Time 0): 14, 30 and 60 days. They showed a decreasing of the 37 % after 60 days.

6.3.2.2. Effects of gel on paintings

It was important to evaluate two possible effects: pigments removal and gel residues on the surface.

To this aim, stereomicroscope and optical images were acquired before and after gel application and micro FTIR-ATR analysis was performed pre- and post-gel application.

Regarding pigments removal, gel was treated to extract eventual residues and then analyzed with macro FTIR-ATR, but no residues were detected in the gels.

The assessment was conducted on different mock-ups with different binders (egg, glue, oil, casein) and different pigments (gypsum, lead white, red ochre, azurite) and no residues were detected on the surfaces both from microscopic images and IR spectra (Figure 6.8.). The sample reported was a double layer mock-up, composed by a first layer of glue and red ochre covered by a second layer of lead white and egg. The FTIR spectra before and after the application of the gel did not show changes in the signal and no peaks ascribable to Gellan gel were detected.

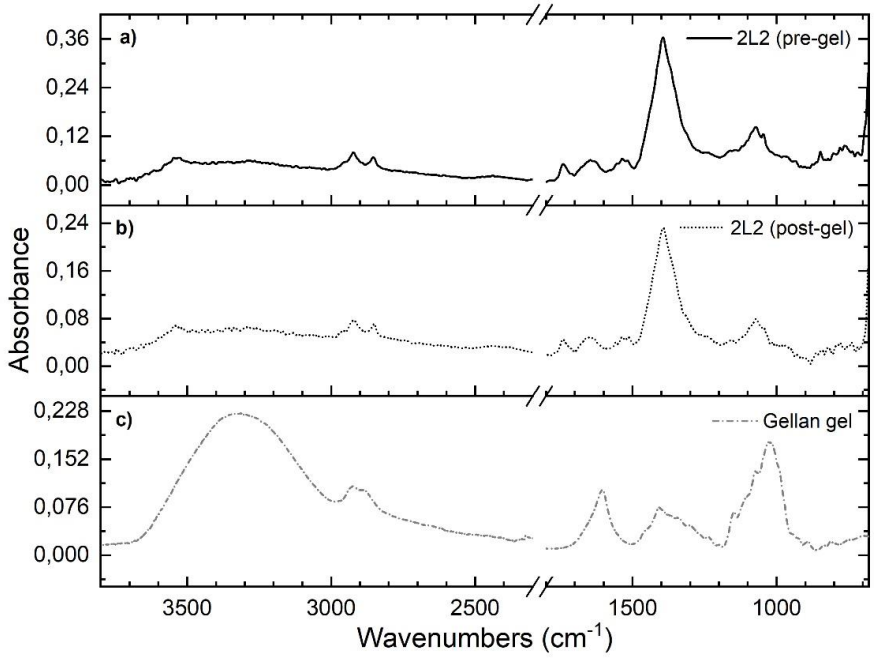

Figure 6.8. FTIR-ATR spectra acquired a) before and b) after gel application, and c) Gellan gel reference spectrum.

These results proved that the gel did not damage the surface of the painting with these times of application. Therefore, the full protocol with the Gellan gel extraction and the biosensor application was tested on some mock-ups.

6.3.2.3. Paint samples

The immunochemical biosensor developed was finally applied on painted surfaces, characterized by the use of different type of binder and pigments. In past studies, Gellan gel has been used as cleaning method, thus it is demonstrated its ability to adsorb environmental contaminants [9,22]. In this case, the aim of the work was the binder detection and thus the possible presence of contaminants entrapped into the gel or their interaction with the SPE had have to be considered and reduced to avoid problems in the detection. In order to correct the possible effects due to the surface contaminants, the current value of a blank was subtracted to the mock-ups results. The blank was obtained for each mock-up by a SPEs without the primary antibody and thus subjected only to the effect of gel and not specific materials.

The current values obtained after the blank subtraction were lower for mock-ups with egg as binders and higher for the mock-ups with other proteins, demonstrating the specificity of the biosensor on the mock-ups too. The data were then interpolated with the calibration curve to obtained protein concentrations for each sample (Table 6.4).

It is possible to notice that high concentrations of OVA were detected in the samples with egg as binder (2L2 layer 2 and B2), while proteins were not detected in samples with oil and glue. The value of the casein was detected in an area of sample 2L2 in which the underlayer (layer 1) was visible. However, the measurement could be affected by OVA residues from the overpainting (layer 2). The results confirmed the sensitivity and specificity of the immunosensor, revealing the possible real application of the method on paintings for binder identification.

Table 6.4. The table shows the concentration values of OVA detected on the different mock-ups with different binders and corrected with a blank.

Sample	**Concentration (ng/mL ± σ)**
2L2 (layer 2: egg)	20,5 ± 0,8 (layer 2)
(layer 1: casein)	1 ± 0,5 (layer 1)
B1 (oil)	n.d.
B2 (egg)	15 ± 2
B3 (glue)	n.d.

6.3.3. Conclusions and further perspectives

The developed biosensor allowed the non-invasive extraction of the binder and the identification of OVA used as binder in painting. This was possible thanks to the combination of a Gellan gel extraction and electro-immunochemical detection.

The extraction with the Gellan gel allowed to preserve artworks integrity. It was proved that it did not remove pigments and it did not release residues. The combination of the selectivity of immunological reaction and high sensitivity achievable by electrochemical detection permit to develop an efficient system.

Moreover, the possibility to store them in the fridge was an additional value which allows a real future application of this method *in situ* and a possible industrial production of the biosensors.

The results obtained open the door to future multiplex-systems for a simultaneous detection of different binders. It is worth mentioning the relevance in simultaneous detection of proteins in cultural heritage materials. This method could be useful thanks to the low time-consumption and to the possibility to do more analysis on the same painting in different points without sampling it.

6.4. References

[1] C. Lefrou, P. Fabry, and J.-C. Poignet, *Electrochemistry - The Basics, with Examples*. 2009.

[2] E. Y. Jomma and S. Ding, "Recent Advances on Electrochemical Enzyme Biosensors," pp. 5–21, 2016.

[3] A. G. Ferrari, S. J. Rowley-neale, and C. E. Banks, "Talanta Open Screen-printed electrodes : Transitioning the laboratory in-to-the field," vol. 3, no. December 2020, 2021, doi: 10.1016/j.talo.2021.100032.

[4] A. Ivaska and J. Bobacka, "Electroanalytical Techniques," in *Contemporary Electroanalytical Chemistry*, vol. 3, no. Pt 1, A. Ivaska, A. Lewenstam, and R. Sara, Eds. 2005, pp. 309–316.

[5] O. Dom, M. J. A. Mart, O. D. Renedo, M. A. Alonso-Lomillo, and M. J. A. Martínez, "Recent developments in the field of screen-printed electrodes and their related applications," *Talanta*, vol. 73, no. 2, pp. 202–219, 2007, doi: 10.1016/j.talanta.2007.03.050.

[6] E. Martínez-Periñán, C. Gutiérrez-Sánchez, T. García-Mendiola, and E. Lorenzo, "Electrochemiluminescence Biosensors Using Screen-Printed Electrodes," *Biosensors*, vol. 10, no. 118, pp. 1–39, 2020, doi: 10.3390/bios10090118.

[7] K. Torres-rivero, A. Florido, and J. Bastos-arrieta, "Recent Trends in the Improvement of the Electrochemical Response of Screen-Printed Electrodes by Their Modification with Shaped Metal Nanoparticles," 2021.

[8] I. Giavasis, L. M. Harvey, and B. McNeil, "Gellan gum," *Crit. Rev. Biotechnol.*, vol. 20, no. 3, pp. 177–211, 2000, doi: 10.1080/07388550008984169.

[9] L. Micheli, C. Mazzuca, E. Cervelli, and A. Palleschi, "New Strategy for the Cleaning of Paper Artworks : A Smart Combination of Gels and Biosensors," vol. 2014, 2014.

[10] H. Li *et al.*, "Gellan Gum Hydrogel as an Aqueous Treatment Method for Xuan

Paper Die Anwendung von Gellan Gum zur wässrigen Behandlung von Xuan-Papier," *Restaurator*, vol. 42, no. 1, pp. 37–54, 2021, doi: 10.1515/res-2020-0010.

[11] M. Manfredi *et al.*, "Method for Noninvasive Analysis of Proteins and Small Molecules from Ancient Objects," *Anal. Chem.*, vol. 89, no. 6, pp. 3310–3317, 2017, doi: 10.1021/acs.analchem.6b03722.

[12] E. Barberis *et al.*, "Towards the non-invasive proteomic analysis of cultural heritage objects," *Microchem. J.*, vol. 139, pp. 450–457, 2018, doi: 10.1016/j.microc.2018.03.033.

[13] R. Mazzeo, *Analytical chemistry for cultural heritage*. 2017.

[14] G. Leo, L. Cartechini, P. Pucci, A. Sgamellotti, G. Marino, and L. Birolo, "Proteomic strategies for the identification of proteinaceous binders in paintings," *Anal. Bioanal. Chem.*, vol. 395, no. 7, pp. 2269–2280, 2009, doi: 10.1007/s00216-009-3185-y.

[15] S. Dallongeville, N. Garnier, C. Rolando, and C. Tokarski, "Proteins in Art , Archaeology , and Paleontology : From Detection to Identi fi cation," 2016, doi: 10.1021/acs.chemrev.5b00037.

[16] E. Joseph, S. Prati, G. Sciutto, M. Ioele, P. Santopadre, and R. Mazzeo, "Performance evaluation of mapping and linear imaging FTIR microspectroscopy for the characterisation of paint cross sections," *Anal. Bioanal. Chem.*, vol. 396, no. 2, pp. 899–910, 2010, doi: 10.1007/s00216-009-3269-8.

[17] Y. M. Issa, G. Abdel-Maksoud, M. Ibrahim, and M. Magdy, "A combination of analytical methods to evaluate the effect of humidity aging on the painting materials of icon models," *Vib. Spectrosc.*, vol. 107, no. September 2019, p. 103010, 2020, doi: 10.1016/j.vibspec.2019.103010.

[18] D. Mancini, A. Percot, L. Bellot-Gurlet, P. Colomban, and P. Carnazza, "On-site contactless surface analysis of modern paintings from Galleria Nazionale (Rome) by reflectance FTIR and Raman spectroscopies," *Talanta*, vol. 227, no. January, p. 122159, 2021, doi: 10.1016/j.talanta.2021.122159.

[19] M. Zangheri *et al.*, "A portable device for on site detection of chicken ovalbumin in artworks by chemiluminescent immunochemical contact imaging," *Microchem. J.*, vol. 124, pp. 247–255, 2016, doi: 10.1016/j.microc.2015.08.026.

[20] G. Sciutto *et al.*, "Miniaturized Biosensors to Preserve and Monitor Cultural Heritage: from Medical to Conservation Diagnosis," *Angew. Chemie - Int. Ed.*, vol. 57, no. 25, pp. 7385–7389, 2018, doi: 10.1002/anie.201713298.

[21] P. Cicatiello, G. Ntasi, M. Rossi, G. Marino, P. Giardina, and L. Birolo, "Minimally Invasive and Portable Method for the Identification of Proteins in Ancient Paintings," *Anal. Chem.*, vol. 90, no. 17, pp. 10128–10133, 2018, doi: 10.1021/acs.analchem.8b01718.

[22] L. Micheli *et al.*, "Interdisciplinary approach to develop a disposable real time monitoring tool for the cleaning of graphic artworks. Application on 'le Nozze di Psiche,'" *Microchem. J.*, vol. 138, pp. 369–378, 2018, doi: 10.1016/j.microc.2018.01.022.

[23] J. M. Pingarrón *et al.*, "Terminology of electrochemical methods of analysis (IUPAC Recommendations 2019)," *Pure Appl. Chem.*, vol. 92, no. 4, pp. 641–694, 2020, doi: 10.1515/pac-2018-0109.

CHAPTER 7

CONCLUSIONS

The present research has been focused on the development of new immunochemical and spectroscopic methods for the investigation and characterization of proteins in ancient remains and paintings, trying to fill the gaps in the present knowledge.

Regarding the ancient remains, the combination between LA-ICP-MS and a new CL immunochemical imaging, allowed to clarify and demonstrate for the first time the mutual relation between variations in element mass fraction and collagen preservation. The diagenetic proxies considered in this study support the idea that post-burial collagen degradation is linked with the alteration of the bone in-vivo element composition. In particular, the diagenetic markers REE and U uptake seems to show a strong negative correlation with the presence of collagen. However, post-burial history might result in different elemental contents and collagen preservations. This work shows that the combination of in-situ CL immunochemical imaging, for the first time applied on archaeological samples, and elemental analyses may help to unravel bone diagenesis history and understand the link between the primary organic content and the alteration of the mineral phase.

Due to the higher resistance of teeth to diagenesis than bones, a CL immunochemical protocol for proteins detection and localization in tooth cross-sections was also developed in this work. The optimization of the experimental settings allowed the successful localization of collagen and amelogenin X in teeth. In detail, the collagen was homogenously localized in the dentin, while amelogenin X was localized only in the DEJ area. For this reason, an extraction protocol was developed on enamel tooth powder. The developed method proved the effective encapsulation of the protein in HA crystals with a consequent reduction of protein availability to the Ab-Ag reaction on the cross-section surface. Implementing the method also for amelogenin Y, this approach could be a turning point for a fast sex determination, using only 1 mg of powder and thus saving the sample.

In order to preserve bone integrity as much as possible, low cost and low-time consuming prescreening acquired higher importance for archaeologists in order to select samples according to their conservation and collagen presence. In this study we proposed bone prescreening with a new microNIR spectrometer prototype, which is completely non-invasive, combined with appropriate data processing. The results showed a good prospect

towards the knowledge of collagen content, thanks to the good separation of samples according to their collagen content. These results could be the starting point for the creation of a predictive model applying on the data a PLS, able to quantify the collagen content of bones preserving them. The model could be created using standard samples and/or real bones with known collagen content. This prescreening could save bone integrity and could allow to select bones for further destructive analyses.

Moreover, the new NIR-HSI method developed provided an efficient mapping of collagen distribution, abetting an intra- and inter-sample comparison, fully exploiting the potentialities of the NDI data processing translated into chemical maps or into box and whisker plots, leading to a qualitative and semi-quantitative evaluation of the relative collagen content distribution. The approach is fast and completely non-invasive, helping to identify interesting areas within the same specimen on which to conduct further analyses, reducing size and number of samples, and saving money, time and bone integrity. The results demonstrate that the high collagen content in old bones may be often restricted to a few areas, clearly indicating the importance of an adequate screening method to avoid incorrect evaluations and to maximize the ratio between information gain and sample destruction. Further research is now in progress to develop linear and non-linear multivariate regression models to extract quantitative data from the NDI-HSI chemical images.

The method developed for the AA investigation in modern and fossil teeth allowed the AAs detection in all the samples analyzed, using only 1 mg of enamel powder. The results contributed to clarify the AAs distribution in modern samples, from different species and with different diets, and to build a reference database. Moreover, the data revealed the AAs preservation in fossils dated 48 Ma, showing the possible survival of organic fraction in deep-times. This method opens new prospects of research for reconstruction of the past and investigation of the trophic ecology of modern and fossil taxa. Further analysis on a wide group of both modern and fossil samples will be performed in the future to improve the robustness of the data. Moreover, the evaluation of FAAs on the same samples could reveal their possible relation with peptide hydrolysis and their diagenetic loss overtime.

Regarding painting binders, the developed biosensor allowed the non-invasive extraction of the binder and the identification of ovalbumin used as binder in paintings. This was possible thanks to the combination of a Gellan gel extraction, which preserves artwork integrity, and electro-immunochemical detection. The combination of the selectivity of immunological reaction and high sensitivity achievable by electrochemical detection permit to develop an efficient system. The use of SPEs allowed to obtain a compact, portable and easy to use system. Moreover, the possibility to store the sensors in the fridge was an additional value which allows a real future application of this method *in situ* and a possible industrial production of the biosensors. This method will be the starting point for future multiplex-systems for a simultaneous detection of different binders.

Acknowledgments

The present works have been mainly performed in the M2ADL – Microchemistry & Microscopy Art Diagnostic Laboratory (University of Bologna, Ravenna Campus). I thank my supervisor Prof. Rocco Mazzeo and my co-supervisors, Prof.ssa Silvia Prati and Prof.ssa Giorgia Sciutto for the opportunity. I thank all the colleagues for the great work environment that we have created.

This research has been carried out with the collaboration of different research groups in Italy and Europe. I thank the following research groups:

- Analytic and Bioanalytic Laboratory of Prof. Aldo Roda, with special thanks to Dr.ssa Martina Zangheri, Prof.ssa Mara Mirasoli and Prof. Massimo Guardigli (University of Bologna)
- Bones Lab group of Prof. Stefano Benazzi, special thanks to Dr.ssa Sara Silvestrini and Dr. Federico Lugli (University of Bologna, Ravenna Campus)
- The Department of Pharmacy of the University of Genova, special thanks to Dr. Paolo Oliveri
- Organic Isotope Geochemistry group of Dr. Alfredo Martínez-García (Max Planck Institute for Chemistry, Mainz, Germany), special thanks to Dr. Martínez-García for the opportunity and to all technicians and the PhD students for their support
- Prof. Thomas Tütken, from the Johannes Gutenberg University of Mainz
- Analytic Chemistry group of Prof.ssa Laura Micheli (University of Roma Tor Vergata), thanks to all the PhD and Master students, especially to Dr.ssa Cecilia Lisarelli
- Laboratory of Physical Chemistry of Prof. Antonio Palleschi, special thanks to Prof.ssa Claudia Mazzuca (University of Roma Tor Vergata)